The Influence of Slurry Formulation on the Multi-Scale Structure and Functional Properties of Spray Dried Detergent Powders

by

Amin Farshchi

Submitted in accordance with the requirements for the degree of

Doctor of Philosophy

The University of Leeds

The School of Chemical and Process Engineering

March 2018

"The candidate confirms that the work submitted is his own and that appropriate credit has been given where reference has been made to the work of others."

Acknowledgements

First and foremost, I want to thank my supervisors Prof. Andrew Bayly and Dr. Ali Hassanpour. Prof. Bayly, it has been an honour to be your first PhD student at the University of Leeds. I would like to thank you for encouraging my research and allowing me to grow as a research scientist. Dr. Hassanpour, I greatly appreciate your academic supervision and personal support throughout my research.

I would like to express my sincere gratitude to Mr. Joel Caragay, Mrs. Clare Philbrick, Mr. Paul Gould, Dr. Hossam Tantawy, Dr. Jeremie Gummel and Dr. Eric Robles at Procter and Gamble (Newcastle, UK). I appreciate all their contributions and ideas.

I would like to thank Dr. Amin Sadeghpour from Empa-Swiss Federal Laboratories for Materials Science and Technology and Prof. Michael Rappolt from School of Food Science & Nutrition, University of Leeds, for their guides and constructive feedback on SAXS data.

I would like to thank Mr. Stuart Micklethwaite and Dr. John Harrington for their technical support at Leeds Electron Microscopy and Spectroscopy Centre (LEMAS).

I gratefully acknowledge the funding sources that made my PhD work possible. I was funded by Advanced Manufacturing Supply Chain Initiative (AMSCI). The financial support from Procter and Gamble is also greatly appreciated.

I would like to express my special thanks to my friend Jabbar Gardy for his sincere support throughout my research.

Lastly, I would like to thank my family for all the support and love. For my parents who always supported me throughout my education. And most of all for my loving and supportive wife; my gratitude to her is beyond the words.

Abstract

Globally, spray drying is the most commonly used process by which detergent slurries can be transformed into low-density and free-flowing powders. The structure and formulation of these granules have a profound effect on the functional properties, *e.g.*, flow behaviour, storage stability and dissolution rate, of the final product. Nevertheless, little is known about the structure and functional properties of the spray-dried powders due to the lack of scientific works in the public domain. In this thesis, four simple model formulations based on linear alkyl benzene sulphonate (NaLAS) and sodium sulphate were used to probe the influence of initial slurry water content and binder, SiO_2:Na_2O molar ratio of sodium silicate, on the structure. Moreover, flow behaviour and water sorption characteristics were chosen to be investigated as the findings of these studied can provide a better understanding of the influence of slurry formulation on the granule structure.

The complex multiscale structure of these granules was characterized using a complementary range of techniques including scanning electron microscopy (SEM), image analysis, x-ray micro-tomography, wide angle and small angle x-ray scattering (WAXS, SAXS). A complex composite structure is revealed due to the multiphase nature of the starting slurry and its evolution during the drying process. The structure revealed can be viewed as a continuous matrix consisting of NaLAS, sodium sulphate and binder in which large, dense, crystals of sodium sulphate are embedded. These were initially undissolved in the slurry and are consequently reduced in number in the product made from higher water content slurry. Air is also dispersed in this matrix at two length scales, large vacuoles, at sizes of the order of the particle diameter which are the result of 'puffing' *i.e.* water boiling, and micro-scale porosity which evolved during the crystallisation of the drying matrix.

The matrix is a composite structure of binder, dried surfactant liquid crystalline phase and sub-micron scale crystallites of sodium sulphate. Changes in the initial composition, water content or binder, of this phase are seen to change both the sulphate polymorphs present and the *d*-spacing

of the NaLAS phase. Morphology and surface characteristics are also seen to change with the high initial moisture content particles producing more irregular structure and a rougher surface. The SAXS data were further analysed by reconstructing electron density profiles (EDP) of the one-dimensional repeat of bilayer stacking by Fourier analysis, and the parameters of lamellar *d*-spacing, bilayer thickness (d_{HH}) and water layer thickness (d_W) were determined. The relative humidity was found to be a critical factor determining the number of coexisting lamellar polymorphs. The greater the RH value, the fewer is the number of lamellar polymorphs. The presence of binders is another factor, due to its hygroscopic properties, controlling the short-range order structures of self-assembled surfactants. To investigate the influence of relative humidity on the microstructural evolution and moisture sorption behaviour of spray-dried detergent powders, the samples were stored at various relative humidity. The moisture sorption isotherms of the powders were gravimetrically determined using a dynamic vapour sorption (DVS) technique. The extent of moisture uptake in these samples was found to be determined by the solid state of sodium silicate.

The powder flowability was investigated using a Schulze ring shear tester. The initial water content of the slurries was found to have a profound effect on the flowability of the resulting spray-dried powders. The powders produced from high-water content showed a better flow behaviour. This was attributed to the influence of water content on the matrix composition. The chemical composition of the detergent powders was also probed using Raman confocal microscopy techniques. The powders containing lower surface concentration of surfactant had a better flowability. Sodium silicates significantly improved the flow behaviour of the particles. The silicate is thought to form a glassy continuum linking sulphate crystals and surfactant domains, which consequently increases the apparent granule strength, and hence improves the flow behaviour.

Table of Contents

List of Figures

List of Tables

Chapter 1 Introduction

Spray drying is one of the most commonly used processes for the manufacture of laundry detergent powders. The functional properties, *e.g.*, dissolution rate, storage stability and flowability, of these products are primarily governed by their structure. Improvement of these functional properties requires a better fundamental understanding of the granular structure. This consequently leads to an appropriate selection of slurry formulation and operating conditions.

Complex structured spray-dried detergent powders are difficult to study because of the presence of many ingredients. In this work, four simple model formulations are used to study. This allows for a better understating of what role each of the ingredient plays within the structure of resulting granules. The objective of this study was also to examine the relationship between the structure and a number of functional properties, *e.g.*, storage stability, flow behaviour.

This chapter present the aim and objectives of this research. This also includes a brief background in the manufacture of detergent powders.

Background

Laundry detergent is a type of cleaning agent mainly containing one or more surfactant and other specific ingredients which result in the removal of dirt and/or pigmented soils from textile substrates during the washing process. Spray drying was long recognised as a conventional technology for the production of laundry detergents until 1987. However, fast growing developments in textile fibres and washing machines led to the diversity of the products over recent decades. Nowadays, although liquid laundry detergent dominates the washing products market in North America and, to a lesser extent, South East Asia, powdered detergents still comprise the largest share of the world detergent market. Procter and Gamble and Unilever, along with Germany's Henkel are three major detergent manufacturer supplying about 50% of the global market for powder detergents. From a detergency standpoint, household powdered detergents can be classified into two main categories: heavy-duty detergents and specialty detergents. Heavy-duty detergents are products developed to meet the needs of all types of

household fabrics at all wash temperatures and all levels of water hardness. The category *specialty detergents*, however; include those products which are particularly formulated to be used for specific fabrics such as wool, easy-care and coloured fabrics (Jakobi and Löhr, 1987).

Several methods are utilised for the manufacture of powdered detergents, which predominantly include spray-drying and granulation processes. In the latter case which is also known as non-tower granulation process, the primary ingredients as fine particles can be fluidized by fast-rotating stirrers while a binder solution containing an anionic surfactant is sprayed on the moving particles. This gives rise to the formation of relatively compact agglomerates which may undergo further drying steps in a fluidized-bed dryer. The liquid binder sprayed on the powder blends is used as a versatile functional ingredient in detergent granulation. In other words, a liquid binder not only serve to form material bridges between primary particles, but also it is intentionally added as a prominent functional component of the detergent formulation to achieve the desired properties of the resulting granules. Therefore, compared with many other industries, much larger quantities of binder solutions might be required to produce agglomerates of superior performance. (Boerefijn et al., 2007a). However, in non-tower granulation processes the quantity of water in binder solutions is restricted to a certain concentration (14 wt%) (Smulders and Rähse, 2000).

In the current study, laundry detergents are produced by spray-drying process. Spray drying of detergent slurries, is the core technology in many detergent manufacturer. In general, this process is one of the most suitable techniques whereby a homogeneous slurry of thermally stable and chemically compatible components can be transformed into low-density powders of a controlled particle size. The first stage for the manufacture of spray-dried powders, is the preparation of detergent slurries having an appropriate and manageable viscosity for the atomization step. The slurry feed is prepared by mixing solid and liquid ingredients in a continuous mixing/blending vessel, also known as crutcher. Water is added at this step as a key versatile ingredient as it influences the slurry characteristics such as its rheology as well as the structure of the spray-dried powder. The slurry is then transferred into the dryer tower, and atomised using a series of nozzles. The tower powders can be subsequently supplemented with other ingredients, which are thermally

sensitive, such as enzymes and fragrances. In spray drying process, larger quantities of liquid phase can be incorporated into the initial mixture, as compared with the granulation process, leading to formation of fairly homogeneous powders from a homogeneously mixed slurry. This process can then alleviate the concerns on the homogeneity of the distribution of detergent components in final products (Parikh, 2009).

The characteristics of the detergent finished product are critical factors determining the performance and hence consumer acceptance. These characteristics mainly include physical properties such as bulk density, flowability, caking tendencies and solubility, which are a direct consequence of the powder structure and the intrinsic characteristics of the added ingredients (Boerefijn et al., 2007b, Galante and Dillan, 1981). From the structural point of view, although there exist some previous works on the structure of detergent agglomerates manufactured by non-tower agglomeration processes, there has been no systematic work on the structure of spray-dried detergent powders, and how it is influenced by the slurry formulation. The slurry can be characterised as a multi-component colloidal dispersion in which crystals of inorganic salts along with self-assembled structures of surfactants are dispersed within a continuous liquid phase which is super saturated with respect to inorganic salts (Stewart et al., 2009). It has been demonstrated that spray-drying process tends to produce hollow, low-density and porous granular products due to the rapid removal of water. It is therefore hypothesised that the evaporation of water from the continuous aqueous phase may cause the dispersed phases to come into closer proximity, and consequently become concentrated within a porous solid matrix. Figure **1.1** illustrates a schematic of a hypothesis representing the distribution of inorganic crystals and self-assembled structures of surfactant molecules within a droplet being dried in a spray dryer and its corresponding dried particle. Inorganic crystals can exist as different physical forms, *i.e.*, polymorphs. Also, various ordered nano-structures of amphiphilic molecules can be identified. The amount and size of the aforementioned dispersed phases and more particularly their spatial arrangements may have a profound effect on the functional properties of the final product.

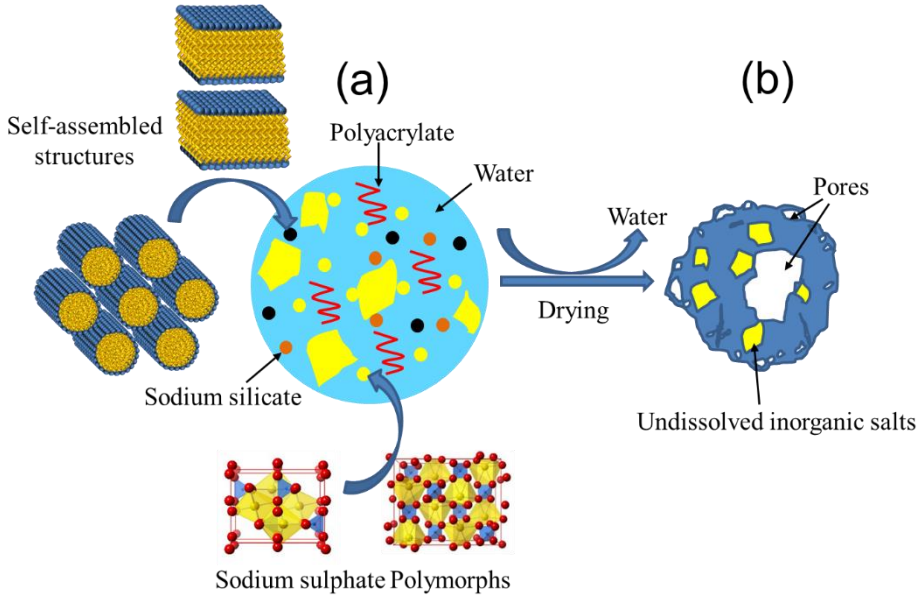

Figure 1.1 A schematic representation of hypothesis for the structure of a droplet produced from a typical detergent slurry (a), showing the dispersion of self-assembled structures of surfactant molecules (NaLAS) along with different polymorphs of sodium sulphate and other functional ingredients, *e.g.*, builders, within a supersaturated aqueous phase, and its corresponding dried particle after drying process (b).

1.1 Aim and objectives

The structure of spray-dried detergent powders may have a significant effect on their functional properties such as dissolution rate and water sorption properties (Boerefijn et al., 2007a). A deeper understanding of the structure and its influence on the functional properties allows for a better selection of process and formulation variables. Therefore, the overall objective of this study was to provide a better fundamental understanding of the structure of spray-dried detergent powders. In particular this research aims to understand how different ingredients interact with each other and how this interaction influences the morphology and microstructure of spray-dried detergent powder. Since the complex and multi-component structure of detergent powders is difficult to study, four simple model formulation was used to be investigated. Typically, the role of water as a key versatile ingredient, is particularly highlighted in the structure and functional properties. Furthermore, the relationship between the structure and a number of functional properties of these powders are investigated. Powder flowability is of great industrial interest because it plays a significant role in the handling and processing operations such as storage and transportation. The

structure formed by the ingredients in detergent granules can be reflected in the mechanical behaviour and consequently impact the powder flow behaviour. Therefore, the focus will also be on demonstrating that structure in detergent granules is a key parameter in the understanding of powder flow behaviour. Water vapour sorption behaviour is another topic of great interest in detergent powders, which can be studied to probe the influence of the structure and the addition of hygroscopic ingredients on the capacity of water sorption of detergent powders. For these purposes a number of experimental works were designed and a series of state-of-the-art techniques were utilised which are presented in the following chapters.

1.2 Structure of the thesis

Chapter 2 – Literature review

This chapter provides some information regarding the ingredients as well as the manufacture of spray-dried detergent powders. This chapter also introducesthe state-of-the-art techniques which are relevant to the characterization of spray-dried powders.

Chapter 3 – The structure of spray-dried detergent powders

This chapter particularly focuses on the structure of spray-dried detergent powders. The complex multiscale structure of spray dried granules is characterized using a complementary range of techniques including scanning electron microscopy (SEM), image analysis, x-ray micro-tomography, wide angle and small angle x-ray scattering (WAXS, SAXS). The multiscale influence of formulation on structure highlights the challenge in predictive design of these detergent products.

Chapter 4 – Liquid crystalline phases of Linear Alkylbenzene sulphonate

This chapter describes, in more detail, the phase behaviour of self-assembled structures of surfactant molecules in detergent powders. Detailed information was obtained from the x-ray diffraction results, through the electron density calculations by Fourier reconstruction approach.

Moreover, extended information about hydrocarbon chain conformational order of surfactant molecules were provided using infrared spectroscopy measurements.

Chapter 5 – Evolution of surface microstructure and moisture sorption characteristics

This chapter deals with the effect of relative humidity on the microstructural evolution and moisture sorption behaviour of spray-dried detergent powders. The moisture sorption isotherms of the detergent powders are determined and the ability of various mathematical models for prediction of experimental data are evaluated. Furthermore, the effect of water sorption as a function of relative humidity, on the microstructural evolution of the detergent powder are examined using a series of techniques including x-ray diffraction measurements and microscopic observations.

Chapter 6 – The role of inorganics on the surface microstructure and flowability

In this chapter the influence of the initial water content of the slurry and the addition of inorganic binders on the powder flowability is investigated using a Schulze ring shear tester. The role of initial water content on the surface microstructure and chemical composition of resulting granules is highlighted in this chapter. The surface microstructural properties and chemical composition of spray-dried powders is probed using SEM, confocal Raman microscopy and x-ray microtomography techniques. The link between these properties and powder flowability is then investigated.

Chapter 7 – Conclusions

The overall conclusion of this work is presented in this chapter. This also includes some recommendations and ideas for future studies.

Chapter 2 Literature review

A laundry detergent powder is a formulated mixture of ingredients which predominantly include surfactants, builders, bleaches, and fillers. Globally, detergent powders are mainly manufactured either by spray drying or by mechanical granulation. Spray drying is the most widely used process by which slurry droplets can be transformed into low-density and free-flowing powders. The spray-dried detergent powders contain most of the thermally stable functional ingredients inside their individual granules. This characteristic minimize segregation effects during downstream processing, handling, transportation and storage. These granules are also ideal in that they tend to possess a hollow or porous structure and hence high surface area, which in turn, can provide the benefit of fast dissolution (Zoller and Sosis, 2008). Typically, bulk densities of these powders fall in the range of 300-550 g/L (Smulders and Rähse, 2000). The bulk density of powdered detergents is of significant interest since it ensures the appropriate filling volume in cartoon packing. Both the bulk density and surface area can vary depending on the slurry formulation and process parameters.

The spray-dried base powder commonly contains the thermally stable ingredients, *e.g.*, surfactant and builders, and comprise 30-90 wt% of the finished products. Other additives which cannot be processed during the spray drying, such as enzymes, bleaches, foam regulators and fragrances are subsequently added in post-tower operations. The finished product is commercially available in cartoons. Individual sachets containing smaller quantities of detergents are also available to provide low cost and convenient single-serve portions (Boerefijn et al., 2007b, Zoller and Sosis, 2008).

2.1 Spray-dried powder ingredients

The spray-dried detergent powder is also referred to as “blown powder”. The key ingredients of these powders include those components which are thermally stable and chemically compatible during the spray drying and slurry preparation respectively. Therefore, the blown powder is

mainly composed of anionic surfactants, builders, inorganic salts and polymers (Zoller and Sosis, 2008).

2.1.1 Anionic surfactants

In general, surfactants possess both hydrophilic and hydrophobic sites within their molecules which enable them to adsorb onto the air-water interface in aqueous systems, with their hydrophilic head groups, while their hydrophobic moieties protruding to the air side. As a consequence, these surface active materials tend to lower the surface tension by disrupting the bonding of water molecules, thereby emulsifying dirt and soils, *e.g.*, hydrocarbon oils and greases on fabrics (Herman de Groot et al., 1995, Smulders and Rähse, 2000). Three mechanisms have been proposed for surfactants, which account for the removal of dirt and soils from the fabrics. These mechanisms include roll-up, emulsification and solubilisation. Regarding the rolling-up mechanism, the surfactant gives rise to increase the contact angle between the oily dirt and the fibre, thereby rolling up the oily dirt from the fibres. Upon the adsorption of surfactant molecules onto the oil/water interface, the electrostatic repulsion forces between the head groups and fibres, enhances this separation. Emulsification is the key functional property of surfactant molecules in laundry detergent products. This process include the adsorption of surfactant molecules onto the oily dirt which leads to the formation of a protective micelle, thereby preventing the emulsified dirt from being re-deposited by providing steric and/or electrostatic repulsion (Bajpai and Tyagi, 2007). The emulsified particles are subsequently removed by rinsing. The solubilisation mechanism usually involves the transfer of insoluble materials, e.g., crystalline solids, or liquids into the micelles. Therefore, the formation of micellar structure has been suggested to be a critical elements determining the efficiency of solubilisation. The hydrophobic parts of most surfactants are relatively similar, comprised of a long-chain alkyl moiety which can be linear, branched, or aromatic. Hence, surfactants are commonly classified according to their polar head groups.

Anionic surfactants are widely used in most surfactant-based detergent formulations. Laundry detergent slurry predominantly contains sodium salt of linear alkyl benzene sulfonate (LAS)

which is commercially available as an aqueous paste or powder (Figure **2.1**). Other negatively charged surfactants include fatty alcohol sulphate, alpha-olefinsulphonate, alpha-sulpho-methylester and soap. LAS is synthetically manufactured by sulphonating linear alkylbenzene with sulphur trioxide in sulfuric acid. Sulphonation of benzene is an electrophilic substitution reaction in which a hydrogen atom of the aromatic ring, in the ortho or para positions, is replaced by a sulphonic acid group. The length of the alkyl chain varies between 10 and 14 carbon atoms. However, commercial LAS with a molecular weight of 340 g/mol, and an alkylate chain length distribution of C_{11}, C_{12} and C_{13} has been suggested to exhibit a superior performance in terms of laundry washing. HLAS is commonly neutralised prior to slurry preparation, with concentrated sodium hydroxide or sodium carbonate, which results in the formation of a waxy and hygroscopic solid phase known as LAS paste which mainly contains liquid crystalline phases of the surfactant molecules. The neutralisation of LAS is of great importance because any remainder of acid can deteriorate the colour and perfume (Boerefijn et al., 2007b).

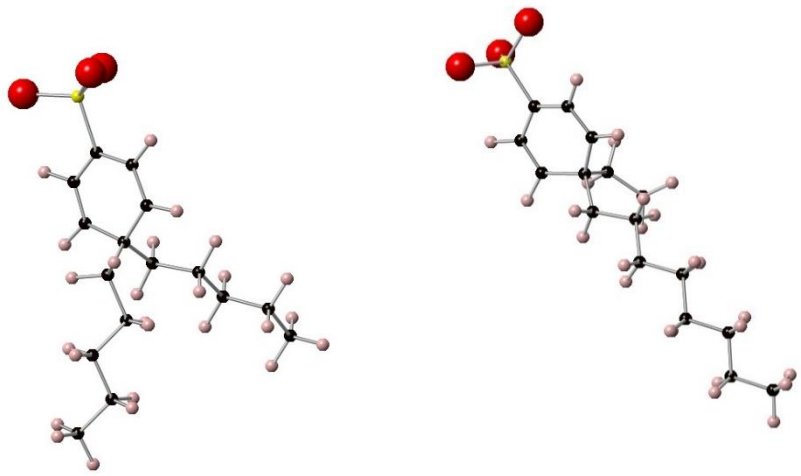

Figure 2.1 Schematic representation of two positional isomers of linear sodium alkylbenzene sulphonate (NaLAS) with different alkyl chain length (Stewart et al., 2009).

It has been demonstrated that amphiphilic molecules in the presence of water, have a tendency to arrange themselves into various ordered nanostructures (1, 2 and 3 dimensional self-assemblies) depending on the concentration and molecular shape (Figure **2.2**). For example the formation of

micellar structures is favoured at concentrations equal to or greater than critical micellar concentration (CMC), while higher concentrations may give rise to the formation of disk-like or rod-like micelles and particularly liquid crystalline phases (Kulkarni et al., 2011). The shape of surfactant molecule can play a decisive role in determining the structural features of the self-assembled phases. The dimensionless packing parameter can be used to describe the shape of a surfactant molecule. The molecular packing parameter is defined as $p = v/al$, where v and l are the volume and extended length of the surfactant tail and a is the surface area of the hydrophilic head group. The ratio v/l is not dominated by the chain length of most surfactants considered in this study, and equals to 21 and 42 $Å^2$ for double-chained lipids and single-chained lipids respectively. Therefore, the arrangement of these structures is mainly governed by the head-groups. Surfactant molecules containing a single hydrocarbon chain and very large head-group area (p<1/3), promote the formation of micellar aggregates. If p≈1, the overall shape of surfactant molecule resembles a cylinder which therefore triggers the formation of a planar bilayer (lamellar phase) with zero curvature, while truncated-cone-shaped surfactants possessing a relatively larger head-group (1/2<p<1), cause the planar lamellar phase curve slightly towards the tail region, leading to the formation of vesicles (Israelachvili, 2011).

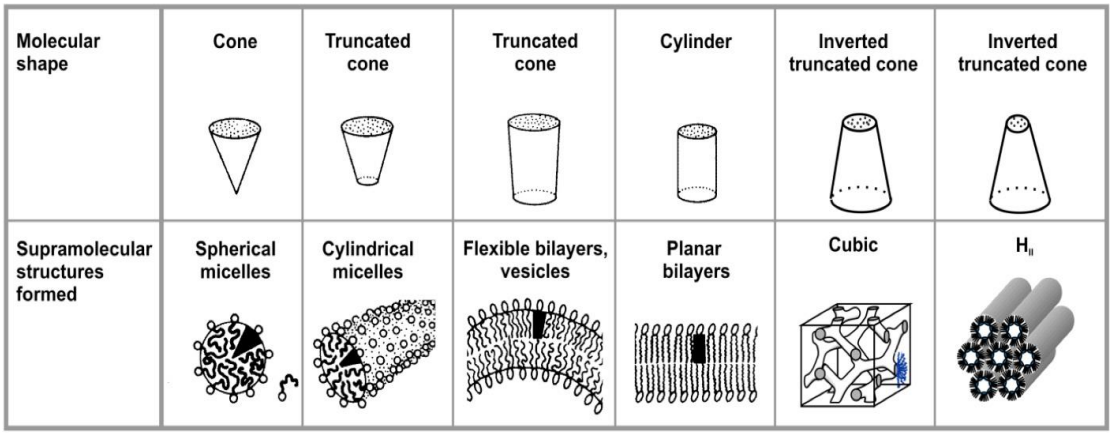

Figure 2.2 . Molecular shape and their corresponding self-assembled structures (Garidel et al., 2015, Israelachvili, 2011).

As mentioned earlier, a commercial NaLAS consists of various isomers and homologues with different alkyl chain lengths (range from C_{11} to C_{14}). The reason for this can be explained by the possibility of substitution of benzene ring in any position of alkyl chain except the terminal methyl groups (Alexandridis et al., 1998, Ma et al., 2006). Therefore, these amphiphilic molecules with varied alkyl chain lengths may adopt various ordered self-assembled structures, whether they are hexagonal or lamellar phases, by altering the molecular packing parameter (Israelachvili, 2011), and consequently this influences their properties, *e.g.*, the rheology of the fluids. It has been suggested that NaLAS isomers possessing a benzene ring substituted in the middle of hydrocarbon chain, trigger the formation of lamellar phases, while positional isomers with a benzene ring at the extremities of the hydrocarbon chain, but not at the terminal $-CH_3$, promote the formation of micellar aggregates (Poulos et al., 2016, Stewart et al., 2009).

2.1.2 Inorganic salts

Sodium silicates, also referred to as "water-glass", are widely used in detergent products because of their good buffering capacity. Also, they can soften water by exchanging sodium ions for divalent cations, and hence augment the detergency performance of anionic surfactants (Smulders and Rähse, 2000). However, these alkaline ingredients not only augment the detergency performance of anionic surfactants, *e.g.*, NaLAS, but also act as binders between different components. (Keeley, 1983) suggested that sodium silicates can serve as a binder to form detergent agglomerates from dry detergent components and that they provide reinforcement to the matrix, and hence the structure of finished product. Concentrated sodium silicate solutions are defined as a colloidal dispersion of silicate anion species, and characterized by a SiO_2:Na_2O molar ratio from 1.8 to 3.8. Varying the molar ratio gives rise to solutions having different characteristics, *e.g.*, rheological and binding characteristics (Roggendorf et al., 2001, Tognonvi et al., 2010, Yang et al., 2008b). In the current study, the aqueous sodium silicate solutions have a composition characterised by molar SiO_2:Na_2O ratios of 1.6 and 2.35. These are typical commercial sodium silicate solution ratios which are used for the manufacture of detergent

powders. In such a system, a dispersion of monomer, dimer, cyclic trimer and polysilicates are supposed to be in a chemical equilibrium (Yang et al., 2008a). It has been confirmed that concentrated sodium silicate solutions with SiO_2:Na_2O ratios > 2 contain mainly polymeric ions. The polysilicates are considered to possess a highly polymerised dense structure with various populations of surficial functional groups, *e.g.*, silanol (Si-OH), siloxide (SiO-) and siloxane (Si-O-Si) (Böschel et al., 2003). Upon drying of the concentrated sodium silicate solutions, the removal of water gives rise to decreasing the volume of interstitial solution until the aggregates are forced into close contact and form a transparent, solid and amorphous structure (Roggendorf et al., 2001).

2.1.3 Builders

The main role of builders is to augment the detergency performance of the surfactants by removal of divalent ions, e.g., calcium and magnesium, and prohibiting them from interacting with surfactants and soils. Additionally, builders are considered as a source of alkalinity which prevents the removed soil from re-deposition. With respect to the nature of builders, three mechanisms have been proposed for the removal of calcium and magnesium ions from the wash solution. For example, the salts of sodium carbonate or sodium orthophosphate have a tendency to interact with calcium and magnesium ions which gives rise the formation of the precipitates of calcium and magnesium salts. The resulting precipitates may subsequently form mineral scales in washing machine. On the other hand, divalent cations can be sequestered and form a stable water-soluble complex in the presence of adequate sodium triphosphate, which hinders redeposition of soils on the fabrics. Ion exchangers such as zeolites and sodium disilicate are water-insoluble builders which are capable of exchanging ions for calcium and magnesium. Sodium aluminium silicate, also known as Zeolite-A having a porous and crystalline structure, considerably exchange mobile ions of sodium for calcium and to a lesser extent magnesium ions. Owing to its poor exchanging for magnesium ions, Zeolite A is predominantly applied in conjunction with co-builders such as polycarboxylates.

2.2 Manufacturing processes

2.2.1 Slurry preparation

The objective of this stage is to produce a reasonably uniform detergent slurry in terms of physical properties, *e.g.*, viscosity and aeration level, and chemical composition to ensure efficient atomization. This can be achieved by mixing the ingredients using a continuous or batch mixer, also known as a crutcher (Figure **2.3**). Powder and liquid ingredients, which are not heat sensitive, are drawn off from silos and tanks, weighed in separate scales and then transferred into the mixers. The neutralized LAS is added to the composition which typically form the largest single added component in the formulation. The water content of the slurry is maintained as low as possible to minimize the drying load, though it should be such that the slurry can be efficiently atomized. The detergent slurry is subsequently transferred into a stirred storage tank where the slurry ages, and it is continuously pumped to downstream stages (Zoller and Sosis, 2008).

The structure of the slurry plays a significant role in the properties of the resulting blown powder. Typically, the structure is governed by the formation of liquid crystalline phases of LAS. The interaction between the self-assembled structures of surfactant molecules and other functional ingredient, *e.g.*, polymers and co-surfactants, may give rise to the formation of supra-molecular structures which consequently influence the shear-thinning behaviour of the slurry, and hence the morphological properties of the granule morphology. The crystallization of inorganic salts, *e.g.*, sodium sulphate, is also of significant importance. The extent to which this occurs during the aging stage, may have significant effect on the structure and flow behaviour of the resulting blown powder (Galante and Dillan, 1981, Zoller and Sosis, 2008). In this respect, the water content not only plays a crucial role in the dissolution of inorganic salts, but also determines the state of crystal hydrates within the slurry, allowing a good control over the structure formation of granules. Moreover, the slurry water content is known to allow for easy control of the particle size distribution and the bulk density of the product (Huntington, 2004).

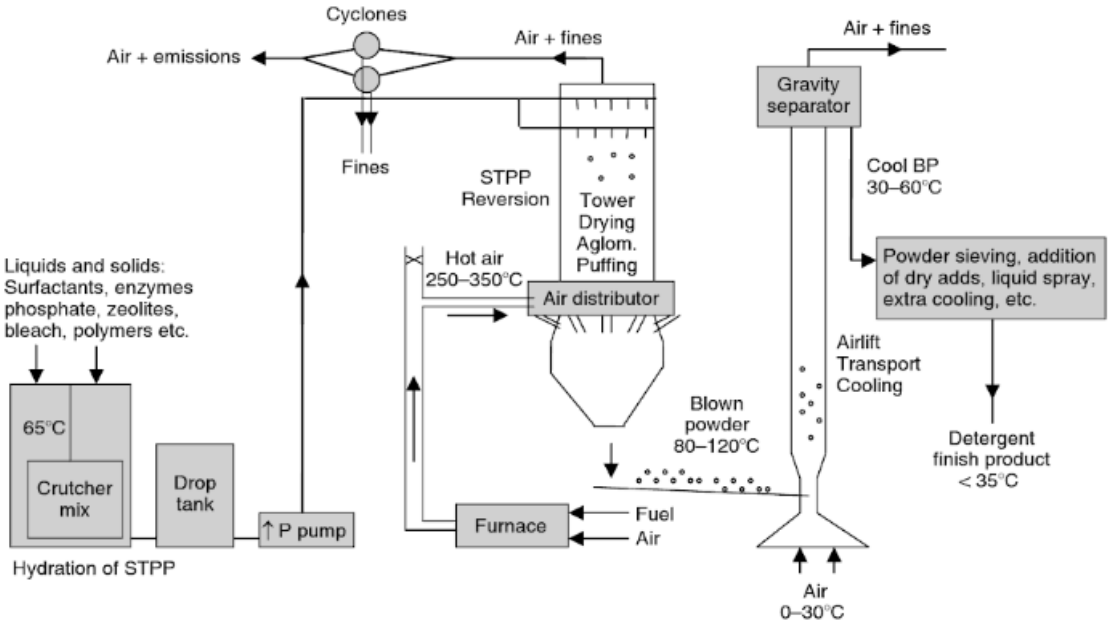

Figure 2.3 Schematic of a typical unit for the production of spray-dried detergent powders (Zoller and Sosis, 2008).

2.2.2 Pumping and atomization

From the storage tank, also known as a drop tank, the slurry is pumped to the atomization nozzles. However, prior to pumping a filtration process is carried out to keep the slurry as homogeneous as possible such that it does not contain any lumps to cause blockage in atomization nozzles. The slurry is then transported by means of high-pressure pumps, *e.g.*, positive displacement pumps to the spray tower where atomization is carried out using a number of high-pressure nozzles. The objective of this stage is to produce a spray of fine droplets by discharging the slurry through an orifice under pressure of 50 to 90 bar (Huntington, 2004, Zoller and Sosis, 2008).

2.2.3 Drying

The blown powders are commonly produced using counter-current spray drying towers with a swirling air flow. The hot air with a temperature of ~ 300 °C is injected at the bottom of the chamber, while the slurry enters the coldest zone of the tower. One of the advantages of this design is to minimize the energy consumption (Francia et al., 2016a). It has been demonstrated that increased inlet air temperature results in a reduction in bulk density of the blown powder.

This is explained by the classical mechanism of the drying. During drying in spray dryer, water initially evaporates from the air- droplet interface. As the drying progresses, the evaporation front recedes towards the centre of the particle, leading to the formation of a rigid skin which consequently decreases the evaporation rate. At this stage, also known as "falling-rate" period, the evaporation rate depends on the diffusion of water molecules through the capillaries and imperfections. This concomitantly occurs with a progressive increase of the interior temperature of the particle which eventually gives rise to the expansion and puffing of water vapour, and thus decreases the density of the structure (Huntington, 2004). However, overheating of the blown powder may cause discoloration and poor product quality (Zoller and Sosis, 2008).

2.2.4 Performance and functional properties

2.2.4.1 Bulk density

Bulk density is of great importance because the consumer expects that the mass indicated on the carton to fill the package volume entirely. Moreover, the consumer typically measures the detergent by volume into the washing machine dispenser drawer. As previously mentioned, the bulk density of the blown powder falls in the range of ~ 300 – 550 kg/L. This property considerably depends upon the inlet air temperatures, density of the added ingredients, and water content of the slurry. Also, the slurry aeration level is an additional factor influencing the bulk density. The level of aeration can be modified by mechanical or chemical means. The greater the aeration of the slurry, the lower is the bulk density of the blown powder.

2.2.4.2 Flow behaviour

The flow characteristics of these powders play an important role in their handling and processing operations, *e.g*., feeding, mixing.

Typically, spray-dried powders can become cohesive during the discharge from silos and hoppers, and develop arching and ratholing in the worst-case scenarios, which consequently result in the stoppage of the process. On the contrary, a free flowing powder can ensure a reliable and consistent feed from hoppers and feeders into downstream processes (Muir, 2007). These flow

problems are mainly governed by physicochemical properties of powders which include particle size and morphology, particle size distribution, surface microstructure and moisture content (Schubert, 1987). The slurry formulation have a clear impact on the aforementioned properties. For example, NaLAS is added in relatively large quantities to the slurry formulation and consequently is responsible for the physical properties and many performance related characteristics of the formulation such as caking tendency and dissolution rate. Sodium sulphate is usually added as a filler. The amount of added inorganic salts such as sodium sulphate can alter the mechanical properties and hence the flow behaviour of the blown powder. Additionally, the structure of the blown powder can be influenced, to large extent, by the water content of the slurry, since water plays a key role in dissolving the inorganic salts. Consequently, this may potentially impact the mechanical properties and flow behaviour of detergent powders.

2.2.4.3 Caking and moisture sorption

Much like many other chemical, pharmaceutical and food products, detergent powders are known to have a tendency to cake and agglomerate during the storage at humid conditions (Thakur et al., 2014). This uncontrolled agglomeration can be detrimental to consumer acceptance. Several mechanisms have been proposed which account for the initiation of caking process, including van der Waals forces, electrostatic forces, liquid bridge forces, surface roughness and plastic deformation (Zafar et al., 2017). At high levels of relative humidity the stickiness and caking of powders have been shown to be largely associated with the formation of liquid bridges formed between the powder granules (Peleg, 1977). The formation of liquid bridges decreases the surface viscosity, thereby increasing the molecular mobility and this consequently induces a number of determinative physico-chemical reactions leading to crystallisation, stickiness and hence caking (Shrestha et al., 2007). Nevertheless, the mechanism of caking is largely governed by the intermolecular structure of the components within the powders. Spray-dried detergent powders contain a complex mixture of amorphous and crystalline ingredients. Amorphous components are considered as non-equilibrated glassy solids which remain stable, below the glass transition relative humidity (RH), for long periods of time, due to the high viscosity (Aguilera et al., 1995).

With increasing the equilibrium moisture content, as a function of the relative humidity of the surrounding air, the glassy solid undergoes a transition to rubbery phase as a consequence of water plasticisation. This allows the less viscose liquid-like material to flow and therefore increase the susceptibility of the powder surfaces to stickiness (Carter and Schmidt, 2012). Crystalline materials have less tendency to adsorb water at low relative humidity conditions. However, as relative humidity exceeds the deliquescence relative humidity, a liquid phase is formed on the crystal surface which is capable of dissolving water-soluble components. This surface dissolution can subsequently induces a variety of physical changes leading to the sintering and hence stickiness and caking (Ahlneck and Zografi, 1990). Therefore, the solid state and hygroscopic properties of the added ingredients can significantly influence the moisture sorption, and hence caking of the blown powder during storage or transport to the customer.

2.2.4.4 Solubility

From the consumer point of view the rapid dissolution is a key quality attribute for the detergent powders. Typically, for handwash consumers the granules are expected to be dissolved quickly without leaving residues on the fabrics. The dissolution of detergent powders is primarily determined by the formulation and component interactions. In general, crystalline components have a lower dissolution rate as compared with amorphous components (Boerefijn et al., 2007b, Zoller and Sosis, 2008). Additionally, different crystalline forms differ in solubility and dissolution rate. For example, metastable polymorphs tend to have a higher solubility and a faster dissolution rate than stable polymorphs (Parikh, 2009). The speed of dissolution also depends on granule size and granule size distribution. The smaller the particle, the greater is the surface area. Therefore, the dissolution rate will increase as the particle size decreases. Porosity and surface area are also key properties affecting the dissolution process. It is known that the penetration of dissolving liquid into porous materials is associated with capillary action. Therefore, the increased volume fraction of intra-granule pores in spray-dried detergent powders results in the enhanced capillary rise, thereby increasing the effective surface area for the wetting and, hence dissolution process (Forny et al., 2011).

2.2.4.5 Granule size distribution and morphology

The granule size and morphology are two other noteworthy properties which significantly impact both functional properties and visual appearance of detergent powders. Typically, the volume weighted mean diameter of detergent granules falls into a range of ~ 400-500 μm. In general, the larger the mean granule size, the lower is the bulk density. The granule size and its distribution are also key factors controlling the dissolution of detergent powders. One may take into account the surface roughness and morphological properties as the key parameters. However, asperities are washed away quickly from the granule surface. Therefore, it is the granule size which mainly governs the dissolution rate. It is well known that the specific surface area increases with decreasing the mean granule size, leading to an increase in the dissolution rate. Granule size distribution is also known to have a great impact on the powder flowability. While the flowabilty of fine particles is mainly influenced by the inter-particle forces, *e.g.*, van der Waals forces, gravitational forces become the dominant factors in the case of coarse particles (Li et al., 2004a). Monitoring and control of the granule size and its distribution can be typically achieved by controlling the operating conditions. A lower slurry water content, lower slurry temperatures, lower tower loading and higher inlet air temperatures gives rise to the formation of smaller granules. The opposite conditions can be used to produce coarser granules. Agglomeration is another important factor which not only alters the morphological properties, but also increases the mean granule size. Agglomeration is a physical phenomenon whereby primary granules collide and stick to each other, leading to the formation of lager porous secondary granules (Palzer, 2005). There are several ways to conduct and control agglomeration in spray dryer towers. The agglomeration process can be carried out by using a multi-level nozzle tower where the formation of agglomerates can be explained by the collisions between semi-dried particles of different spray cones, if nozzles partially overlap each other. Typical morphologies of the agglomerates of detergent granules obtained from a spray drying tower can be seen in Figure **2.4**.

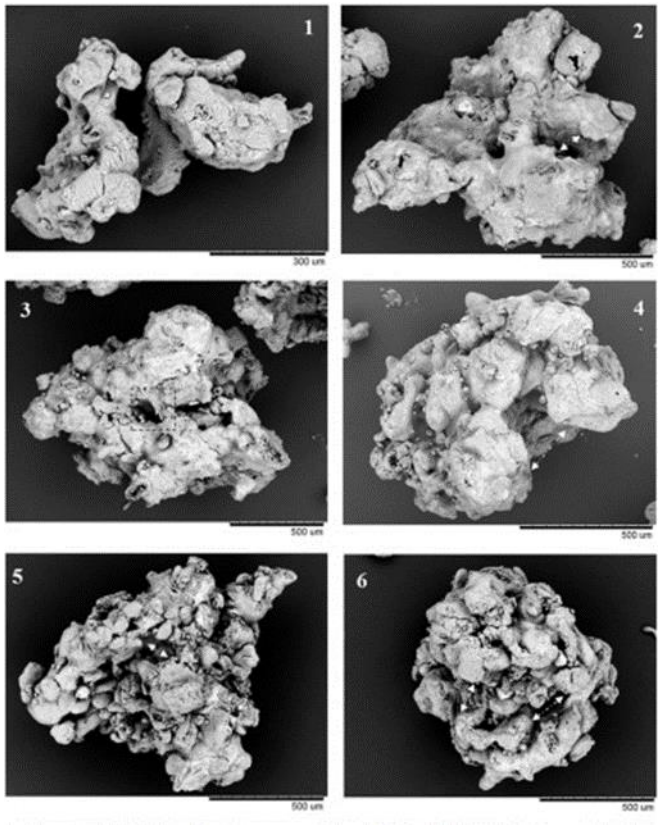

Figure 2.4 SEM micrographs illustrating the morphology of detergent granules agglomerated in a counter-current spray drying tower. (1) Shows medium-sized agglomerate (355-450 µm). Panels 2-6 show coarser agglomerates (850-1180 µm) (Francia et al., 2016b).

2.3 Granule structure

Most of the earlier works have dealt with the structure of detergent powders produced by non-tower agglomeration processes. From the structural point of view, these detergent agglomerates have been shown to be composed of three different phases including inorganic crystallites or solid phase, liquid-like or soft solid matrix and the entrapped air. Boerefijn et al., (2007) proposed a brick-and-mortar system for the structure of detergent agglomerates in which the bricks, *e.g.*, crystalline particles of inorganic salts, are randomly distributed within a soft percolating matrix. Size and/or volume of these phases has a significant impact on the granule structure. **Figure 2.5**illustrates cross-sectional views of typical detergent agglomerates and their corresponding schematic structures.

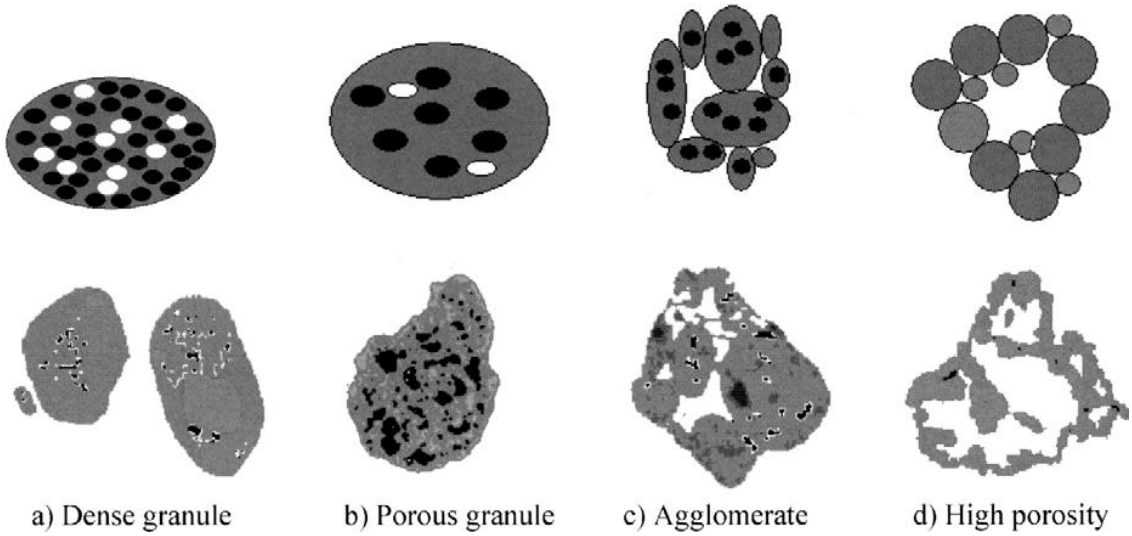

Figure 2.5 X-ray tomography (cross sectional view) showing examples of different structures of detergent powders obtained from non-tower agglomeration process, along with their corresponding schematics (Boerefijn et al., 2007b).

The volume fraction of the aforementioned phases is mainly determined by the process conditions as well as the amounts of solid and liquid ingredients. Typically, the entrapped air and porosity is formed during the mixing process where a neutralization reaction occurs due to an interaction between LAS and alkaline ingredients, *e.g.*, sodium carbonate, of the powder blend, leading to the liberation of carbon dioxide and water molecules. The neutralization reaction is accompanied by the increasing viscosity of moist sinter bridges arising from the addition of binder. This gives rise to the formation of relatively loose and porous agglomerates which may undergo further drying steps in a fluidized-bed dryer.

The structure of spray-dried detergent powders, however, has not been reported in the public literature, though there exist some studies conducted on the colloidal systems of detergent slurries (Liaw et al., 2003, Stewart et al., 2011). A detergent slurry can be composed of a continuous aqueous phase supersaturated with respect to inorganic salts, in which liquid crystalline phases of surfactants along with inorganic materials are suspended (Stewart et al., 2009). Upon spray drying, the liquid phase can be transformed into a continuous dried matrix which binds the solids together. The solid matrix phase may include dehydrated liquid-crystal phase of surfactant molecules and sub-micron scale crystallites of inorganic materials. Beside these phases, porosity

has been demonstrated to be one of the most frequently encountered characteristic in spray-dried powders. Therefore, spray-dried detergent powders are considered to possess a complex structure composed of three different phases including remaining undissolved inorganic crystallites, soft solid matrix and the entrapped air.

In general, even if a sufficiently homogeneous slurry can be produced, the slurry components are likely to be redistributed in different ways along a droplet radius depending on the physico-chemical properties of the slurry. This may have a profound effect on the structure and hence functional properties of spray-dried powders. For example, while the accumulation of surfactants may impart a continuous skin to the outer surface of particles and consequently increase the susceptibility of the particles to stickiness, some ingredients with fast crystallization kinetics may immediately crystallize on the surface and improve the flow behaviour. In the case of spray-dried detergent powders, the distribution of inorganic crystals, *e.g.*, sodium sulphate, whether they are preferentially distributed on the surface or there is a random homogeneous distribution of the crystallite within the matrix, typically consisting of LAS, may affect dissolution properties of the granules. The porous phase within spray-dried detergent powders can be of significant interest. Spray-dried powders normally possess a porous structure composed of gas-filled void space and micropore , which the latter case might be either closed (without any connection to the exterior) or open to the particle surface (Rouquerol et al., 1999). Particle' porosity has been demonstrated to be an decisive factor that can influence the functional properties of spray-dried granules, by lowering their bulk density, or by enhancing the dissolution rate of dried particles (Ansari and Stepanek, 2008, Juppo and Yliruusi, 1994). Therefore, the amount and size of the constitutive phases in a detergent granule, and more particularly their spatial arrangements, might have a profound effect on handling and functional properties of bulk detergent powders.

2.4 Techniques to characterise granule structure

2.4.1 X-ray tomography

X-ray computed tomography, also known as x-ray CT, was primarily introduced and developed in the early 1970s for medical applications which use x-ray images for non-invasive visualization of 3D structures of the internal organs and tissues (Jameson, 2014). For these purposes x-ray beams are emitted from an x-ray source, passed through the patient's body, and eventually captured using a detector behind the patient. During this process, x-rays pass through materials of different densities and thicknesses, leading to contrast within the overall x-ray radiograph. This contrast in radiographs can be explained by the Beer-Lambert law which relates the x-ray absorption to the linear attenuation coefficient as well as the thickness of a material, which are responsible for the image contrast. The linear attenuation coefficient, μ, is an intrinsic property which is dependent on the density of a material and its effective atomic number as well as incident photon energy. (Kelkar et al., 2015). In the 1990s, advances in detector technology allowed the feasibility of more compact x-ray-CT systems. The advances in detector technology particularly include the conversion of x-rays to visible light photons using a scintillator, which are then detected by a charge-coupled device (CCD) or an optical microscope. This led to the introduction of laboratory-based microscopic computed tomography (Micro-CT).

Since then, micro-CT systems are being successfully used in numerous non-medical fields, including geology, archaeology and chemical engineering (Tsotsas and Mujumdar, 2011, Wang et al., 2015). Over the last decade the use of x-ray computed tomography has grown significantly for the characterization of porous materials. Despite the capability of various characterization techniques, *e.g.*, scanning electron microscopy (SEM), mercury porosimetry and gas pycnometry, for the analysis of the structure of porous materials, a combination of these techniques is required. Micro-CT can serve as a versatile non-destructive technique which can provide comprehensive data (Ho and Hutmacher, 2006). In the case of detergent granules, detailed information on the granule structure allows for an effective assessment of the influence of formulation and operating

conditions on the internal structure and functionality, *e.g*., surface area and pore size distribution. The structure can be characterized in two specific scales. The granule size and shape factor are analysed on a macroscale level. The presence of large pores and vacuoles is also investigated at this level. The microscale is the scale of the spatial distribution crystallites as well as gaseous phase or pores within the solid phase.

2.4.1.1 Macrostructures

Analysis of the spray-dried powders on the macroscale, *e.g*., granule size, morphology, hollowness, and shape factor is important for understating their performance, *e.g*., flow behaviour and bulk density. These parameters are routinely achieved using most commercially available micro-CT systems, having spatial resolutions of 6-30 μm (Jerram and Higgins, 2007). For this purpose a large number of radiographs at different viewing angles are collected by the x-ray detectors, resulting in a series of overlapping projections of the imaging objects. 3D volume of a complete sample is then established by computer reconstruction. The solid phase, can be readily distinguished from the interstitial spaces or gaseous phase due to their high difference in linear attenuation coefficient (Tsotsas and Mujumdar, 2011). Despite the industrial importance of spray drying process, rather few studies have applied X-ray CT to visualize the internal structure and morphology of spray-dried granules. Most recently, Both et al. (2018) used x-ray tomography to investigate the influence of different drying temperatures and different compositions of a two binary solution containing food hydrocolloids, on the morphological properties of the final dried particle produced using a single droplet drying method. The authors clearly showed the critical role of polymeric components on the shape and degree of hollowness, using an X-ray micro-CT. Similarly, Gamble et al. (2016) applied X-ray micro-CT to obtain detailed information on the polymeric stabilized spray-dried dispersion particles. They analysed these particles using this approach and quantified the wall thickness, void volume and hence solid volume fraction of the particles.

In the case of detergent powders, Van Dalen et al., (2011) studied the structure of detergent powders produced from non-tower agglomeration process, using a combination of several image

analysis measurement techniques including x-ray micro-CT, Fourier Transform Infrared microscopy and Scanning Electron Microscopy (SEM). However, the study was mainly focused on the capability of correlative microscopy combined with other image analysis techniques to characterize the structure of detergent powders. The detergent granules were embedded within a resin and their morphological properties were characterized using an X-ray micro-CT technique. The application of other complementary characterization techniques, e.g., SEM and FTIR imaging, on the same location of the embedded detergent granules can provide further information about the chemical composition and microstructure. Figure **2.6** shows a good combination of X-ray micro-CT and scanning electron microscopy with energy dispersive X-ray analysis (SEM-EDX), which can be effectively applied to characterize the structure of spray-dried detergent granules in a similar way.

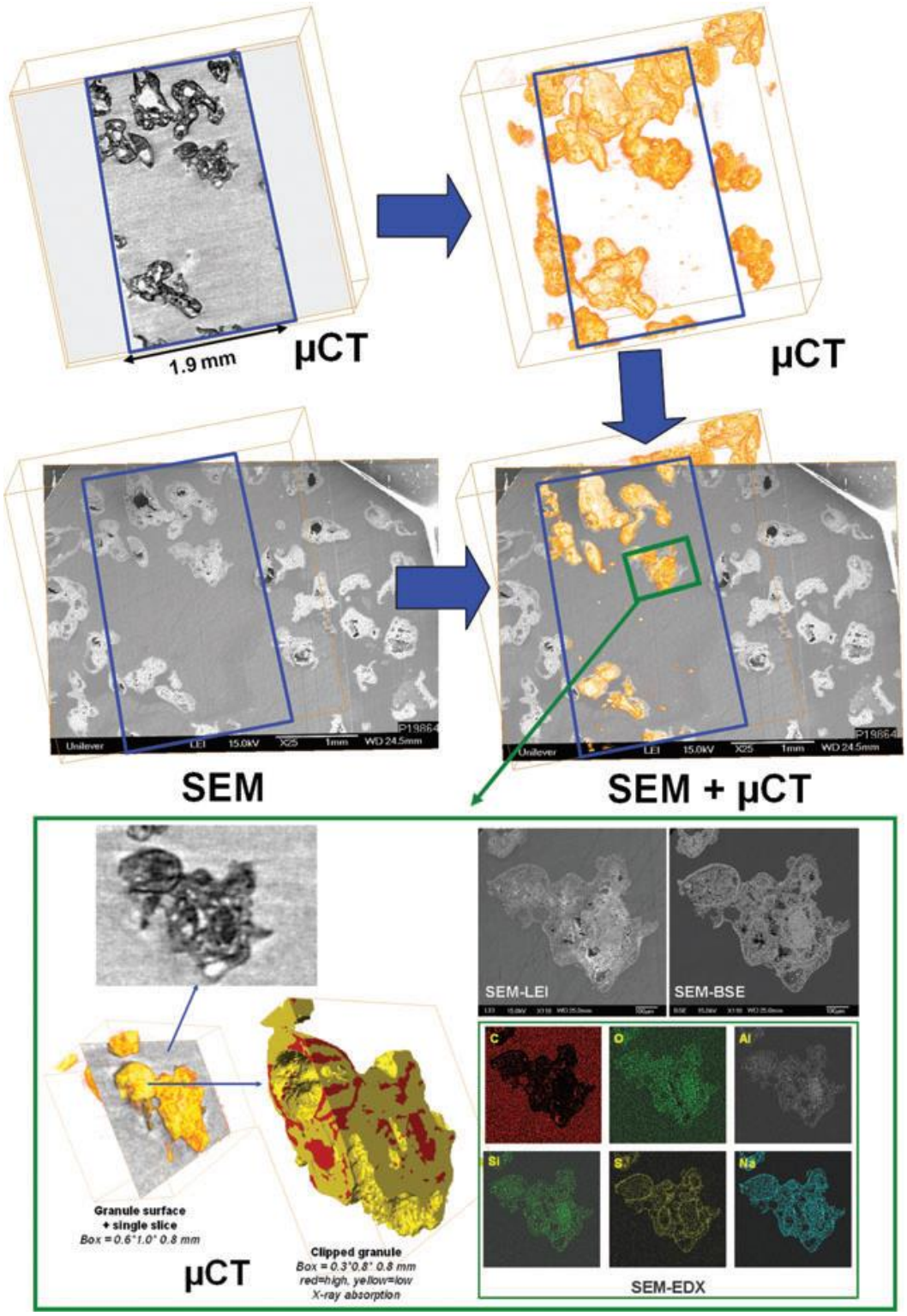

Figure 2.6 Correlating X-ray micro-CT with SEM-EDX (Van Dalen et al., 2011)

2.4.1.2 Microstructures

At the microstructural level, the quantification of small pores and crystallites is of significant interest. The gaseous phase, *i.e.*, pores, can be readily distinguished from the solid texture due to

its significantly lower linear attenuation coefficient. Analysis of the porosity is important, since it is a key characteristic affecting the performance, *e.g.*, bulk density, water sorption, and dissolution rate, of the spray-dried powders. Farber et al. (2003) used X-ray micro-CT technique to investigate the internal microstructure and porosity of pharmaceutical granules, and suggested that more detailed information such as pore shape, pore connectivity and spatial distribution can be obtained from x-ray micro-CT as compared with the mercury porosimetry, though the minimum pore size was limited by the resolution of the instrument.

For heterogeneous materials such as spray-dried detergent powders, having density variations within their structure, it is interesting that their multi-components structure to be quantified by measuring size, shape, and spatial arrangement of the solid constitutive components. Typically, crystals of inorganic salts can be distinguished from the granule matrix, depending on the linear attenuation coefficient, μ, of materials distributed within the solid phase. The greater the difference in the linear attenuation coefficient, μ, the higher is the contrast between the solid components (Barrera-Medrano et al., 2007). Data volumes obtained from the x-ray microtomography are grayscale images in which only one value is assigned to each voxel for opacity according to the attenuation coefficient. Therefore, the linear attenuation coefficient, μ, determines the threshold contrast visibility for the separation of the object within the matrix. Voxels in an perfect crystals possess a narrow range of μ values, while there is a much wider range for imperfect crystals and those included and finely distributed within the matrix (Jerram and Higgins, 2007). In this case, the acquisition of 3D images requires a higher resolution and accuracy. A synchrotron source can fulfil these requirements, since x-ray beams are almost monochromatic, parallel and coherent. The parallel beam geometry results in more exact reconstruction compared with cone or fan beam geometries. The coherent x-ray flux not only reduces the required acquisition time, but also improves signal-to-noise ratio. However, the main advantage of synchrotron-based CT system is that they rely on monochromatic x-ray sources, which therefore minimize the preferential absorption of low-energy photons by materials, and hence artifacts which appear as cupping, streaks and dark bands (Carmignato et al., 2018).

2.4.2 Scanning electron microscopy (SEM)

Scanning electron microscopy is one of the most commonly used techniques for the visualization of microstructures with high resolution and contrast. In scanning electron microscopy, images can be obtained in different detection modes, mainly including secondary electron (SE), back-scattered electron (BSE) and dispersive x-ray spectroscopy (EDX)(Jensen, 2012). The secondary electron detector is widely used to analyse particle size, shape and surface morphology. This relies on the detection of low-energy electrons which are produced as the consequence of inelastic scattering interactions between orbital electrons of the atoms in the specimen and primary beam electrons. As low-energy electrons are mainly emitted from a few nanometres from the specimen surface, they provide valuable information on surface topography. However, back-scattered imaging relies on the detection of high-energy electrons emitted from below the specimen surface. The signals are produced as the consequence of elastic interactions reflecting back the incident electrons from the specimen. The interactions of primary electrons with heavy elements having high atomic number results in a stronger elastic scatter as compared with light elements, which consequently leads to the projection of brighter areas and hence image contrast (Zhao and Darwin, 1990). Therefore, back-scattered electron contain valuable information on the composition of the different phases. The intensity of BSE signals is also highly related to the abundance of elements in a specimen. The darker contrast of BSE image indicates a higher electron density region. This allows larger contrast differences between crystals and their backgrounds. Figure **2.7**a shows a secondary electron image of a typical composite material containing different elements (Macaluso et al., 2016). Figure **2.7**b shows the corresponding micrograph in a, but obtained from a back-scattered electron (BSE) detector, illustrating variations in density between the sample components.

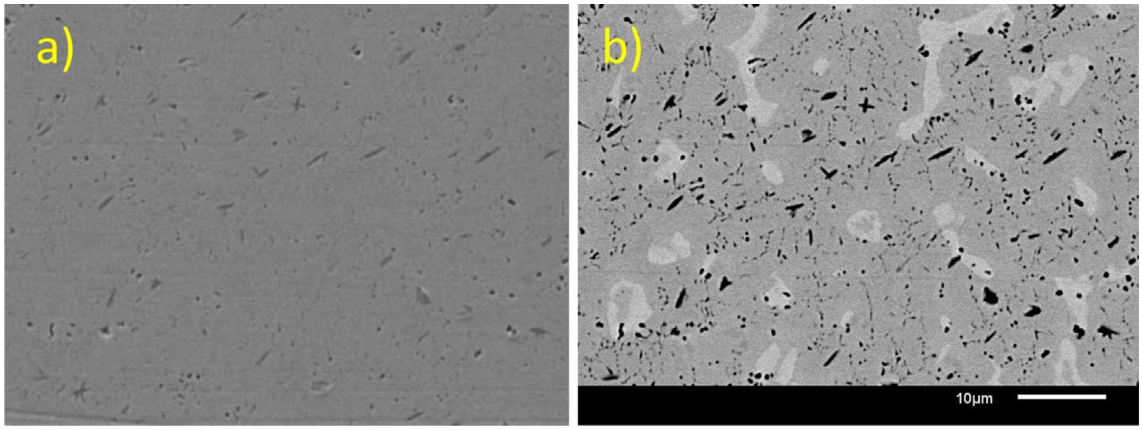

Figure 2.7 (a) Secondary and (b) backscattered micrographs of a composite material (Macaluso et al., 2016). The brighter regions in BSE micrograph correspond to compositions of lower electron density.

Scanning electron microscopy (SEM) in conjunction with energy dispersive x-ray spectroscopy (EDX) is an ideal analytical technique to characterize the surface composition of spray-dried powders. In EDX technique, the atoms of the specimen are bombarded by high-energy electrons, leading to the ejection of inner-shell electrons of the atoms, which are then replaced by the outer-shell electrons. This electron replacement between the shells having different energy level, results in the emission of x-ray photons. The energies of the emitted x-rays are unique to the elements which generate them, allowing the elemental analysis of materials (Scoutaris et al., 2014). Preparing highly polished cross sections of granular products followed by EDX-SEM analysis can provides valuable information on the internal distribution of chemical components. The cross sections can be produced by microtome sectioning of resin embedded granules using a diamond knife. This technique also allows the visualisation of granule internal structures at higher magnifications and contrast compared with laboratory-based x-ray Micro-CT systems. Figure **2.8** shows a cross-sectional view of a typical detergent granule produced from non-tower agglomeration process.

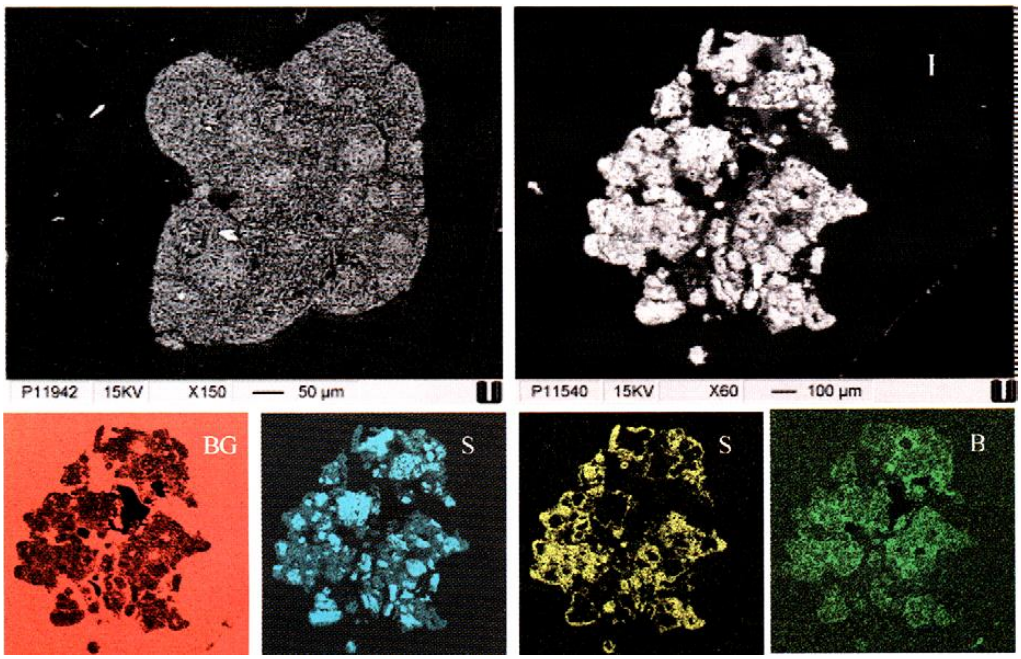

Figure 2.8 A SEM micrograph taken from a cross-sectional view of a detergent granule, in secondary electron (SE) mode (Top-left) and back-scattered electron mode (BSE) (Top-right), and its corresponding SEM-EDX images illustrating the elemental distribution of the detergent components (Van Dalen et al., 2011).

2.5 Concluding remarks

Spray drying is the most commonly used process whereby a homogeneous detergent slurry can be transformed into porous and free-flowing detergent powders. The powders are multi-component granules mainly containing LAS, organic salts and builders. The formulation and structure, *e.g.*, porosity, crystal polymorphs, and spatial arrangement of these components, have a great impact on the functional properties of the resulting powders. Typically, the water slurry content can play a significant role in governing the morphology and structure by dissolving the primary components during the slurry preparation and creating gas phases, *i.e.*, porosity, upon spray drying process. The extent of porosity not only determines the bulk density, but also governs the water sorption properties and dissolution rate of the granular products.

Despite the important role of the structure, few studies have been carried out on the structure of powdered detergents, and those that have been conducted have focused on the structure of detergent powders produced by non-tower agglomeration processes. Therefore, until recently

little is known about the structure of spray-dried detergent powders, and no systematic work has been carried out to study the relationship between the structure and functional properties.

Much like many other spray-dried products, detergent powders have a complex structure. This complex and multi-component structure cannot be described with a singular analytical approach, and a comprehensive multi-scale approach is required. This can be achieved by a combination of state-of-the-art instrumentation and appropriate methodology and techniques, which allows for a fundamental understanding of the relationship between the structure and functional properties of spray-dried detergent powders.

Chapter 3 The structure of spray-dried detergent powders

This chapter is particularly focused to develop a better fundamental understanding of the relationship between the slurry formulation and structure of these powders, which is considerably important for a particle design. Four simple model formulations based on sodium salt of linear alkyl benzene sulphonate (NaLAS) and sodium sulphate were used to probe the influence of initial slurry water content and binder, sodium silicate with molar ratios of 1.6 and 2.35 SiO_2:Na_2O, on the structure. In terms of the morphological properties, both external and internal morphologies of the resulting detergent powders were examined using several techniques including SEM and X-ray microtomography. The internal microstructures, e.g., cross sections of particle wall, were further investigated by microtome sectioning technique. A second point investigated was nano-structures, *e.g.,* self-assembled nano-structures of surfactant molecules and polymorphs of inorganic salts. To this purpose, small-angle x-ray scattering (SAXS) was used as an excellent technique to probe the phase behaviour of self-assmbled structures of NaLAS molecules. Also, the existence of polymorphs of sodium sulphate was examined at smaller length scales using a wide-angle x-ray scattering (WAXS) technique.

3.1 Material and methods

3.1.1 Materials

Four model formulations of detergent granules were produced with a pilot-scale co-current spray dryer at Procter & Gamble. The main features of the detergent spray drying tower include tower diameter 1200 mm, total height 3477 mm, air capacity 2-25 kg/h and water evaporation rate 2-25 kg/h. The tower was equipped with two fluid co-current nozzle atomization, and integrated fluid bed. Typical process conditions were used and these were kept consistent between formulations. Detergent slurries with a temperature of 85°C were introduced into the spray dryer operating under the following conditions: inlet air temperature 280°C, exhaust temperature 100 °C, nozzle

pressure 0.5-3.0 bar. All spray-dried powders contained the sodium salt of NaLAS, with a molecular weight of 340 g/mol, and sodium sulphate. However, their formulation varied depending on either the initial water content (30 or 63 wt%) of the slurry or the addition of sodium silicate with molar-ratios of 1.6 and 2.35 SiO_2:Na_2O. The details of four compositions are shown in Table 3.1. The abbreviations used to identify the formulations are used throughout this thesis: **LW**: low-water content slurry; **HW**: high-water content slurry; **LW+1.6 R**: low-water content slurry containing 1.6 SiO_2:Na_2O R; **LW+2.35 R**: low-water content slurry containing 2.35 SiO_2:Na_2O R.

Table 3.1 Composition of the detergent slurry formulations

	Compositions of the detergent slurries (wt %)				
Description	Water	NaLAS	Sodium Sulphate	Sodium Silicate (1.6 R)	Sodium Silicate (2.35 R)
LW	30.0	13.6	56.4		
HW	63.0	7.2	29.8		
LW+1.6 R	28.0	14.0	49.3	8.6	
LW+2.35 R	28.0	14.0	47.2		10.8

Notes: (LW) low-water content slurry; (HW) high-water content slurry; (LW+1.6 R) low-water content slurry containing 1.6 SiO2:Na2O R; and (LW+2.35 R) low-water content slurry containing 2.35 SiO_2:Na_2O R.

As mentioned in the introduction, a detergent slurry can be considered as a multi-component colloidal system in which crystals of inorganic salts along with liquid crystalline phases of surfactant molecules are suspended in a continuous aqueous phase saturated with the inorganic salts. The amount of sodium sulphate remaining undissolved in the detergent slurries can be roughly estimated based on the solubility of sodium sulphate in water at 85°C; the solubility of sodium sulphate at this temperature is ~ 31.0 g in 100 g of water (Okorafor, 1999). Table **3.2** shows an estimated level of undissolved salts and the corresponding composition of the liquid

matrix. The both the amount and composition of the liquid matrix is governed by the water content of the slurries. The higher the concentration of water, the greater the amount of dissolved sodium sulphate, and hence, the higher the ratio of sodium sulphate to NaLAS within the liquid matrix. From Table **3.2**, it can be seen that the matrix of detergent slurries containing 63 wt% water, are estimated to possess the highest amount of dissolved sodium sulphate, and consequently the highest ratio of sodium sulphate to NaLAS "active matter". On the contrary, the detergent slurries containing a lower quantity of water, are likely to undergo a greater degree of phase separation *i.e.*, formation of remaining undissolved crystallites. The extent of phase separation as the results of the initial water content, can be consequently reflected within the matrix composition of resulting spray-dried powders. The influence of initial water content in phase composition is highlighted here since it is an important consideration in the discussion that will follow when interpreting the microscopic observation.

Table 3.2 Estimated composition of the phases in detergent slurries used

Description	Sodium sulphate in detergent slurries (wt %)		Estimated compositions of the continuous phase in detergent slurries (wt %)				
	Undissolved Sodium Sulphate	Dissolved Sodium Sulphate	Water	NaLAS	Sodium Sulphate	Sodium Silicate (1.6 R)	Sodium Silicate (2.35 R)
LW	47.1	9.3	56.7	25.7	17.6		
HW	10.3	19.5	70.2	8.0	21.8		
LW+1.6 R	40.6	8.7	47.2	23.6	14.6	14.5	
LW+2.35 R	38.5	8.7	45.5	22.8	14.1		17.6

Notes: (LW) low-water content slurry; (HW) high-water content slurry; (LW+1.6 R) low-water content slurry containing 1.6 SiO2:Na2O R; and (LW+2.35 R) low-water content slurry containing 2.35 SiO_2:Na_2O R.

3.1.2 Microscopic observations

The morphology of three representative sieve fractions, 150-180, 300-350 and 600-710 µm, was evaluated using scanning electron microscopy (SEM). Prior to SEM observation, the sample were sputter coated with an ultra-thin coating of gold to inhibit charging during SEM examination. A microtome sectioning technique was also utilised to examine the internal structure of the granules. Prior to microtoming the samples were embedded with an epoxy resin (Epofix cold mounting resin, Struers) in plastic moulds and cured over 24 hours. The blocks of resin containing samples were then polished using an ultra-microtome equipped with a diamond knife. The polished blocks were subsequently mounted and coated before microscopic observation. In order to determine the interconnectivity of pores in SEM micrographs, the pores were segmented using an interactive thresholding tool in Avizo software. The connected sets of objects were then labelled with the same colour, based on pixel connectivity, by the Lable image tool in Avizo. The processed image is presented using a cyclic colour map such that pores in close proximity are likely to be displayed in a different colour.

3.1.3 Shape characterization of particles by Malvern Morphologi G3

Particle size distribution and shape analysis were carried out using an imaging based system, the Malvern Morphologi G3 (Malvern Instrument, Malvern, UK). Prior to particle size measurements, representative samples were obtained using a sample splitter, these samples were then dispersed and distributed as a monolayer onto a sample stage using the automated dispersion unit. A dispersion pressure of 1.2 bar was chosen to avoid aggressive dispersions, and hence particle attrition. For the particle size measurements, particle imaging was carried out using 2.5× magnification lens (13µm–1000µm resolution range). Since the shape factor is a function of particle size, a sieve fraction, *i.e.*, 300-350 µm, which was a representative of the medium-size particles was chosen for the shape analysis. For the shape characterization, 5 times magnification (6.5µm - 420µm) was used. The 2-dimensional images of each particle were used to produce size and shape distributions of the sample. Amongst the shape parameters, circularity is sensitive to

both changes in overall shape and edge roughness. High sensitivity circularity, *HSC*, defined in eq. (1) below was chosen as a suitable shape parameter. HSC is an indicator of the closeness to a perfect circle and can be written as follows:

$$HSC = circularity^2 = 4\pi \times \frac{area}{perimeter^2} \qquad \text{Eq.(1)}$$

HSC values ranges between 0 (highly irregular) to 1 (perfect sphere). Further information can be found in Li et al. (2008) and Ulusoy and Kursun (2011).

3.1.4 Micro-computed tomography (Micro-CT) scanning

X-ray micro-tomography has proved to be a non-destructive and useful technique to provide detailed 3D visualisation of internal structures and morphologies of spray-dried powders (Gamble et al., 2016). In this study, the internal structure of spray-dried detergent powders were qualitatively examined using a Phoenix Nanotom CT scanner (GE Measurement and Control, US). This provides qualitative and quantitative analysis of the distribution of high density and low density phases within the powder.

Sieved size cuts of the sample powders were loaded in a plastic tube (internal diameter 2 mm, height 8.5 mm), which was subsequently mounted on a rotating stage between an X-ray source and X-ray detector. Samples were then scanned in the full range of 0–360°. A series of X-ray micrographs were obtained and three-dimensional volumes were reconstituted using the VGStudio software package. The original volume was cropped and a cube (1500×1500×1500 μm) was created for further image processing (Figure **3.1**). To improve the 3D data visualisation, a number of different image processing tools including filtration and segmentation, were applied to the X-ray micrograph data using the Avizo software package. A non-local mean algorithm was applied to the grey scale projections to reduce image noise. The segmentation of highly dense regions, corresponding to initially undissolved sodium sulphate particles, from the matrix was conducted using an interactive thresholding tool in Avizo. The resulting 3D rendered volume of

the segmented region was then used to determine the quantity of undissolved sodium sulphate and estimate the matrix composition. The true density of anhydrous sodium sulphate (2.66 g/cm^3) was used to determine the mass of the rendered volume corresponding to undissolved salts. The total mass of detergent powders within the volume of interest was estimated using from bulk and tapped density measurements (as presented in Table **3.4**). The segmentation of intra-particle pores, which are connected to neither interior nor exterior surfaces, from the particle matrix was conducted using an interactive Top-Hat thresholding tool and the resulting binary images were used for 3D-volume rendering and further analysis. An example of the 3D rendered intra-particle pores can be seen in Figure **3.1**b. The pore fraction (φ) was defined by the ratio of the volume of isolated pores space (V_V) to the mass of powders (M_P) within the 3D reconstructed cube.

$$\varphi = \frac{V_V}{M_P} \times 100 \qquad \text{Eq.(2)}$$

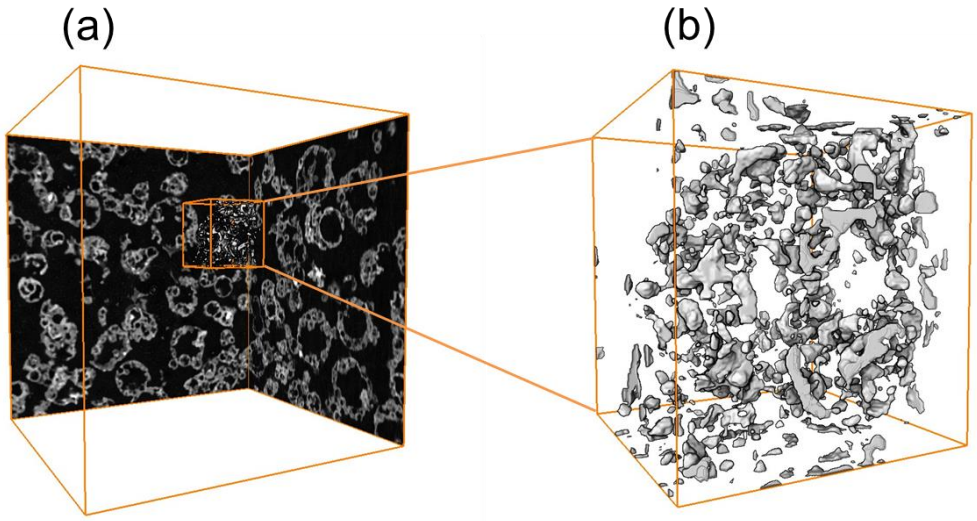

Figure 3.1 A filtered grey scale XRT image (pixel size: 2.5 µm) showing two sides of a cubic sub-volume (1500×1500×1500µm) obtained from the original scan (a), and an example of typical 3D rendered pores within an individual granule (b).

3.1.5 X-ray diffraction (XRD) measurements

The existence of polymorphs of anhydrous sodium sulphate was investigated by X-ray diffraction, XRD, (D8 Advance, Bruker Axs, Karlsruhe, Germany) using a Cu Kα X-ray source. The samples

were packed tightly in a sample holder with a 2mm indent. The scanning region of the diffraction angle was between 10 - 40° (2Θ). Small-angle x-ray scattering was conducted using a Xeuss 2.0 SAXS system (Xenocs, France). A Cu Ka X-ray source (λ=0.154 nm) and scatterless collimating slits were used during the experiments. The scattering vector modulus is defined in this work as $q = 4\pi/\lambda \sin(\theta)$, with 2θ being the scattering angle. The one-dimensional lattice spacing (*d*-spacing) was determined according to the Bragg equation, $d = 2\pi/q$. For lamellar phases of surfactant molecules this equals to the sum of the water and alkyl chain region dimensions (Figure **3.2**).

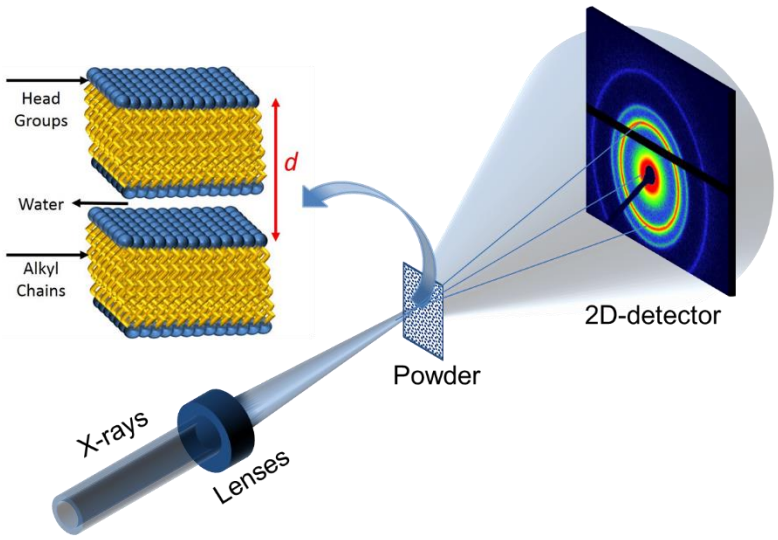

Figure 3.2 A typical schematic of a lamellar phase and SAXS measurement.

3.2 Results and discussion

3.2.1 Morphology and particle size distribution

The morphological characteristics of the spray-dried detergent powders were evaluated using scanning electron microscopy (SEM). As these characteristics are a function of particle size, three representative sieve fractions, 150-180 µm, 300-350 µm and 600-710 µm, were chosen to be examined under the microscope. From the scanning electron micrographs in the range of 150-180 µm (Figure **3.3**), it is evident that spray-dried detergent powders from low-water content slurries

are relatively spherical in shape and show smooth surfaces, though in the presence of sodium silicate, a small number of fine particles can be occasionally observed on the surfaces. The samples produced from high-water content slurries, however; were less spherical.

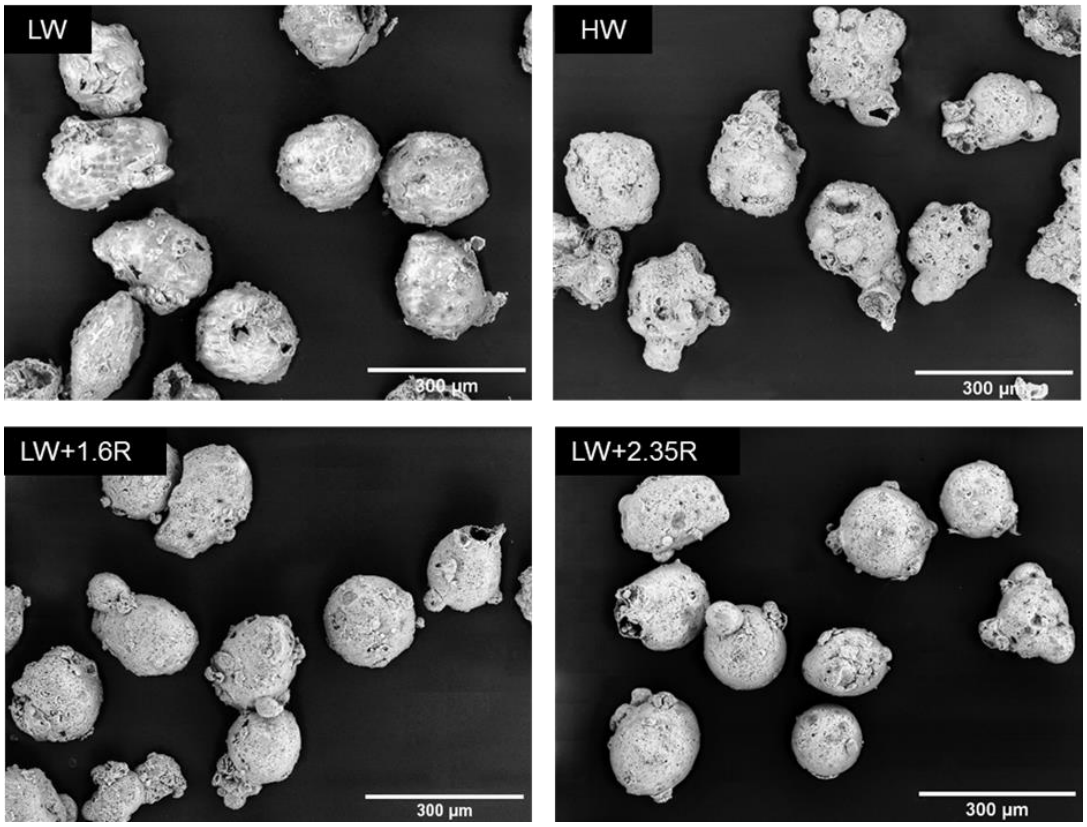

Figure 3.3 SEM micrographs of spray dried detergent powders (150-180 µm).

Considering the scanning electron micrographs in the range of 300 to 350 µm, which are fairly representatives of mean particle sizes, (Figure **3.4**), it can be seen that the influence of the slurry formulation on the morphological properties is more pronounced. Detergent slurries containing higher water content were found to have a blistered appearance. This morphological feature was expected, and can be explained by a rapid vaporization of water on one hand and pliable nature of the particle structure on the other hand. In general, several mechanisms have been proposed to the shape dynamics of a droplet being dried in a spray dryer, which mainly include solvent diffusion, internal flows, phase transition, skin formation and mechanical stability (Sadek et al., 2013). As the particle temperature reaches or exceeds the boiling temperature of the solvent during drying, internal bubbles are formed and expand due to the increased vapour pressure of

the droplet. The resulting bubbles, depending on the mechanical properties of the shell, may retain their shape and impart a blistered appearance to the droplet surface, or collapse and shrivel (Tsotsas and Mujumdar, 2011). Several previous studies have shown that a lower solid concentration results in the formation of a thin and pliable shell which cannot withstand the internal vapour pressure. In contrast, higher solid concentrations results in the formation of a rigid shell retaining the spherical shape of particles (Schiffter and Lee, 2007, Vicente et al., 2013). A cross-sectional view of these powders can provide some clues as to the origin of these external blisters. We shall discuss this point later in section 3.2.2. For detergent powder containing sodium silicate, the number of adhered fine particles on the surfaces was remarkably larger than those observed in the smaller sieve fraction, *i.e.*, 150-180 µm.

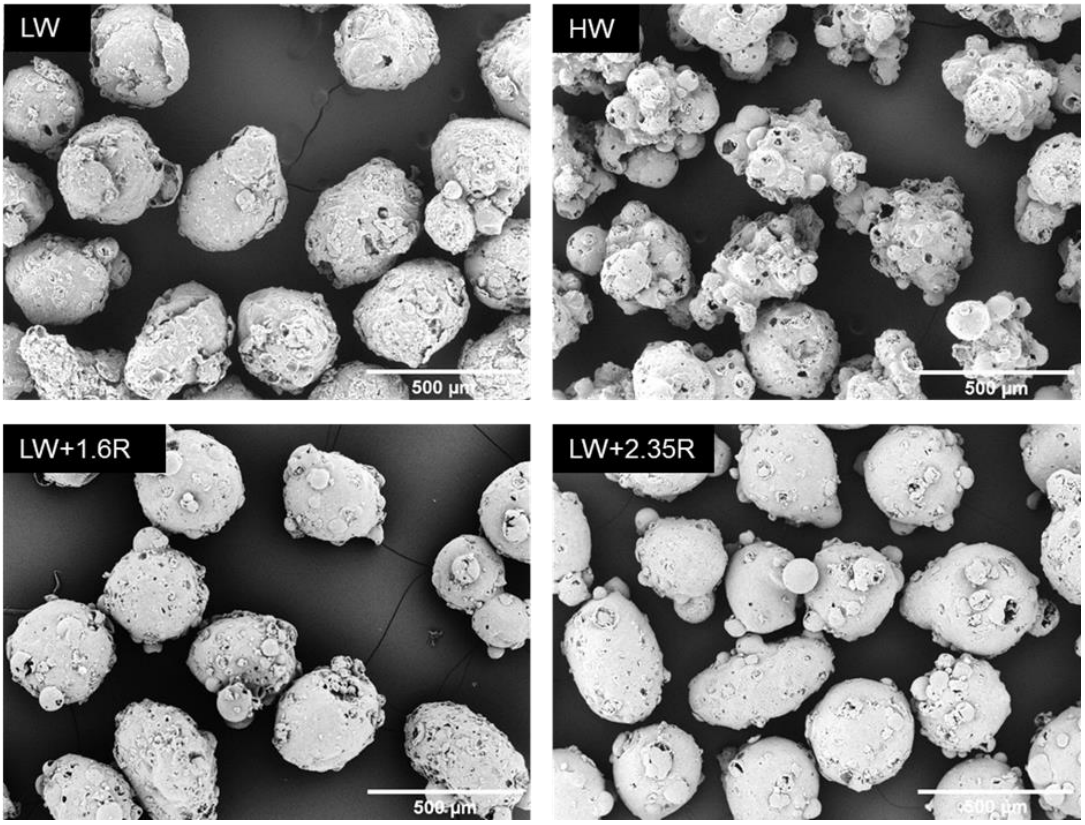

Figure 3.4 SEM micrographs of spray dried detergent powders (300-350 µm).

The external agglomeration was particularly, and to a larger extent, observed in the largest sieve sizes between 600 to 700 µm (Figure **3.5**c and d). In general, agglomeration can occur inside the spray dryer chamber mainly due to the collisions between fine particles, which are already dried,

and semi-dried particles having still wet surfaces which consequently lead to an increase in the roughness of host particles. It is known that the extent of agglomeration of spray-dried powders is determined by the surface composition and the moisture content of the outermost layers of drying droplets. During the spray drying process, as the evaporation progresses, the droplet surface viscosity rapidly increases with a concomitant increase in solute concentration, until reaching a critical value. This viscosity is often referred to as sticky-point viscosity (10^6-10^8 Pa.s) above which further agglomeration does not take place (Walton, 2002, Goula and Adamopoulos, 2008). Indeed, in a sufficiently rapid drying rate, the surface drop viscosity can fairly exceed the sticky-point, before colliding with fine particles, at which a glassy film is created onto the particle surface. Consequently, a faster drying rate, results in the formation of non-sticky particles which are less likely to undergo agglomeration. In this study, one possibility for this agglomeration tendency can be partially attributed to the presence of sodium silicate on the particle surface. Sodium silicates species are known to possess hygroscopic characteristics, and are capable of adsorbing water molecules around their silanol (Si-OH) functional groups (Asay and Kim, 2005, Leroch and Wendland, 2012). This characteristic can potentially increase the surface stickiness of the partially dried particles.

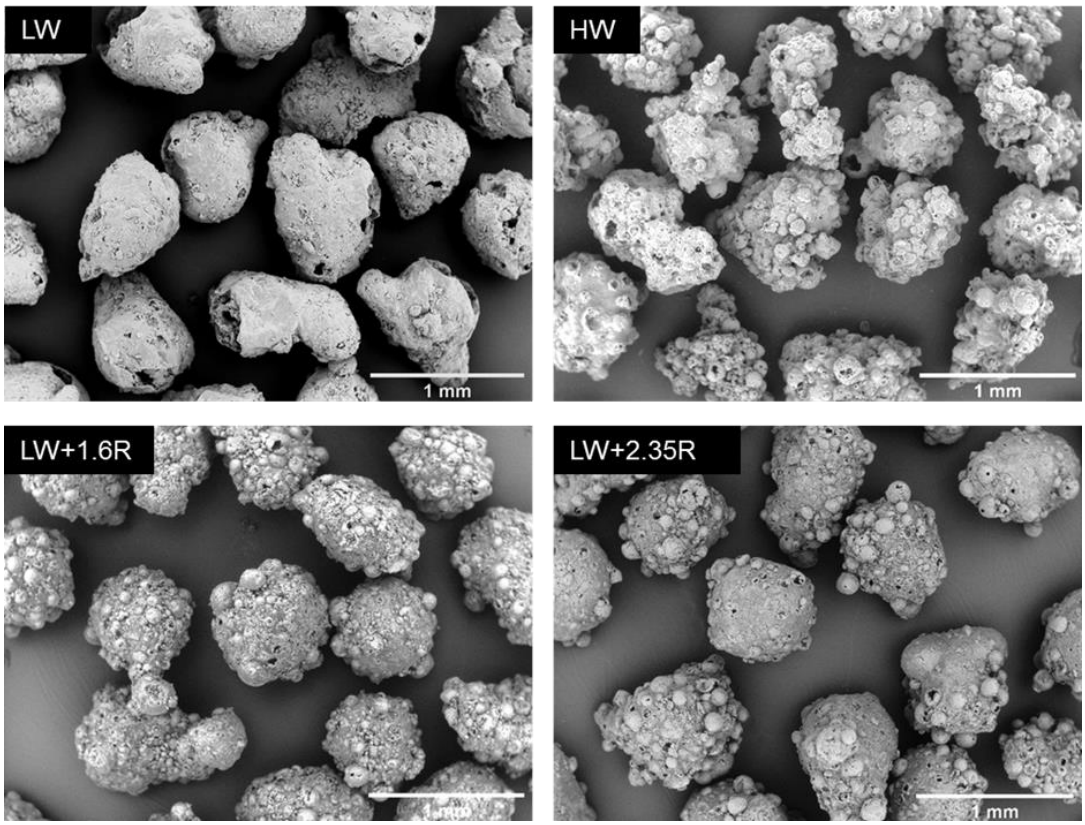

Figure 3.5 SEM micrographs of spray dried detergent powders (600-710 µm).

Particle size distribution of the detergent powders were conducted by using the Morphology G3. The typical volume-weighted particle size distributions are shown in Figure **3.6**. The 10th, 50th and 90th percentiles of volume converted circular equivalent (CE) diameter, and the mean values of volume converted High sensitivity circularity (*HSC*) are presented in Table **3.3**. The particle size measurements show that powders produced from high water-content slurries are significantly larger, d50 = 377 µm, than those produced from low-water content slurries, d50 = 270 µm. A possible explanation for this can be due the increased water content which leads to increasing build-up of internal gas pressure, consequently enhancing particle vacuolization and thus particle ballooning and puffing (Walton, 2002). Also, assuming a relatively smaller specific volume for high-water content slurries, which can be determined by knowing the density and volume fraction of each component in detergent slurries, the volume of the resulting sprayed-droplets are expected to be larger than those produced from low-water content slurries. Therefore, upon the removal of water from low-density droplets, the space occupied by the volume of water remains as voids,

leading to a formation of a larger porous structure. The addition of sodium silicate with the SiO_2:Na_2O molar ratios of 1.6 and 2.35 to low water-content slurries, however, did not result in a noticeable change in the median particle diameter d50 ~ 270 µm, although the volume percentage of larger particles in the range of 360-600 µm is slightly higher compared with those in the absence of sodium silicate. This is possibly due to the formation of agglomerates in the silicate-containing formulations (as was earlier shown in SEM micrographs).

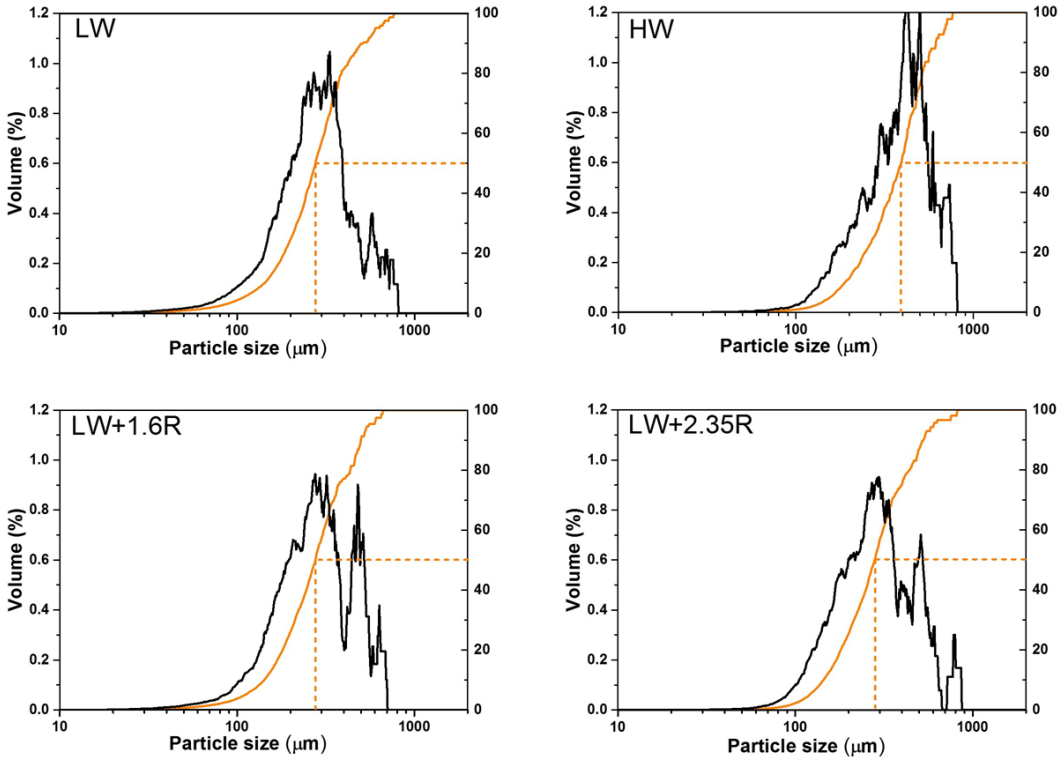

Figure 3.6 Volume-weighted particle size distributions of spray-dried powders as a function of detergent formulation. Each graph includes the probability distribution and the cumulative distribution.

The results of the SEM micrographs are also reflected in the High sensitivity circularity (*HSC*) distribution obtained from the Morphology G3. The volume based converted *HSC* of detergent powders (300-350 µm) is presented in Table **3.3**. The spray-dried detergent powders produced from high-water content slurries showed the lowest HSC value (*HSC* = 0.624). These results suggest that detergent slurries containing higher water content have led to the formation of

irregular particles with rougher edges. In contrast, low water-content slurries in the absence of sodium silicate, were found to have a tendency to produce particles with more spherical and smooth characteristics. However, interestingly the mean *HSC* value of detergent powders considerably decreased to 0.664 and 0.703 on addition of sodium silicate with the SiO_2:Na_2O molar ratios of 1.6 and 2.35 respectively. Therefore, it is the formation of agglomerates in the presence of sodium silicate that is mainly responsible for the observed upshift in particle sizes.

Table 3.3 The 10th, 50th and 90th of percentiles of volume converted circular equivalent (*CE*) diameter and mean values of volume converted high sensitivity circularity (*HSC*).

Description	volume converted circular equivalent (CE) diameter (μm)			HS circularity
	d10	d50	d90	
LW	141±2	270±1	504±8	0.760
HW	186±4	377±17	606±12	0.624
LW+1.6 R	143±7	273±4	518±17	0.664
LW+2.35 R	141±5	272±3	516±20	0.703

Notes: (LW) low-water content slurry; (HW) high-water content slurry; (LW+1.6 R) low-water content slurry containing 1.6 SiO_2:Na_2O R; and (LW+2.35 R) low-water content slurry containing 2.35 SiO_2:Na_2O R.

Considering the SEM micrographs in conjunction with the HSC values obtained from the image analysis, three distinct categories of particle morphology can be identified. The spray-dried detergent powders can be irregular in shape with a blistered appearance as a consequence of the increased water content of the slurries. At lower water content, however, the morphological properties of the resulting powders can be governed by the presence of other additives, i.e., sodium silicate,: 1) smooth characteristics in the absence of sodium silicates; 2) agglomerates with the addition of sodium silicate to the formulation.

3.2.2 Internal structures

At the macro-scale, the internal morphology, *e.g.*, degree of hollowness, shape and spatial distribution of remaining undissolved sodium sulphate, of the spray-dried powders was examined

using the x-ray microtomography technique. Since the morphology is a function of the particle size two sieve fractions, i.e., 300-350 μm and 500-600 μm, were chosen to be investigated. Figure **3.7** compares 3D reconstructed slices, ~ 70 μm thick, taken across the centre of typical particles. The dark areas inside the particles indicate the intra-particle spaces. The bright blue, almost white, internal bodies within the particle, correspond to more dense materials, *i.e.*, remaining undissolved sodium sulphate. For the smaller sieve cut, *i.e.*, 300 -350 μm, of the powders produced from low-water content slurries (LW and LW+1.6 R), one or more vacuoles, *i.e.*, relatively large intra-particle space, can be observed inside the particles. Some particles contain a large central vacuole accompanied by small-sized voids, *i.e.*, macro-pores, distributed throughout the wall. It was found that the presence of small voids on the particle wall is more particularly prevalent among spray-dried particles containing sodium silicate. The reconstructed tomographs also revealed the presence of a large number of chunks of remaining undissolved sodium sulphate (light blue regions). The initial size of these particles, prior to the slurry preparation, was measured using a laser light scattering technique. The volume-weighted mean diameter (d_{43}) of these particles was around ~ 230 μm, which is subject to change depending the initial water content of the slurries. These crystalline remnants are either non-homogeneously dispersed around the central vacuole or occupy most of the internal space of the granules as a big particle. Figure **3.8** illustrates the spatial distribution of these crystalline components within a single detergent granule. High-water content detergent slurries (HW), however resulted in the formation of foam-like structures. The presence of a large central vacuole is not a commonly encountered characteristic of these powders. Additionally, undissolved sodium sulphate crystallites are rarely observed within these granules. Returning to the estimated composition of the liquid matrices in Table **3.2**, it was shown that the high-water content slurries are expected to have the lowest quantities of undissolved sodium sulphate. The amount of these crystallites in spray-dried powders was calculated and presented in Table **3.4**.

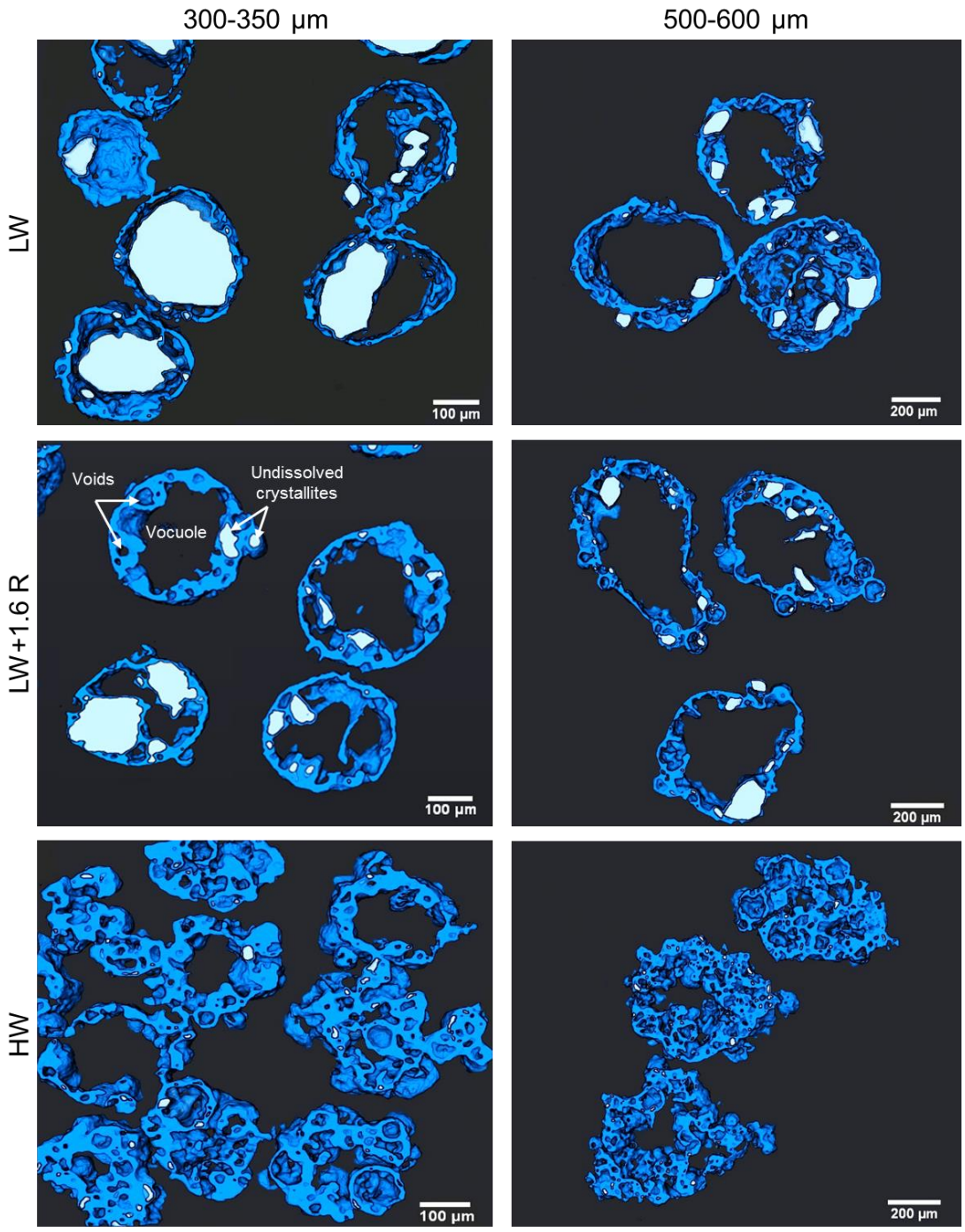

Figure 3.7 3D central cross sections (60-70 microns thick) of spray-dried detergent powders, with voxel resolution of 2.5×2.5×2.5 µm, from 300 – 350 µm, left hand column, and 500 – 600 µm, right hand column, sieve fractions. LW, HW and LW + 1.6 R formulations.

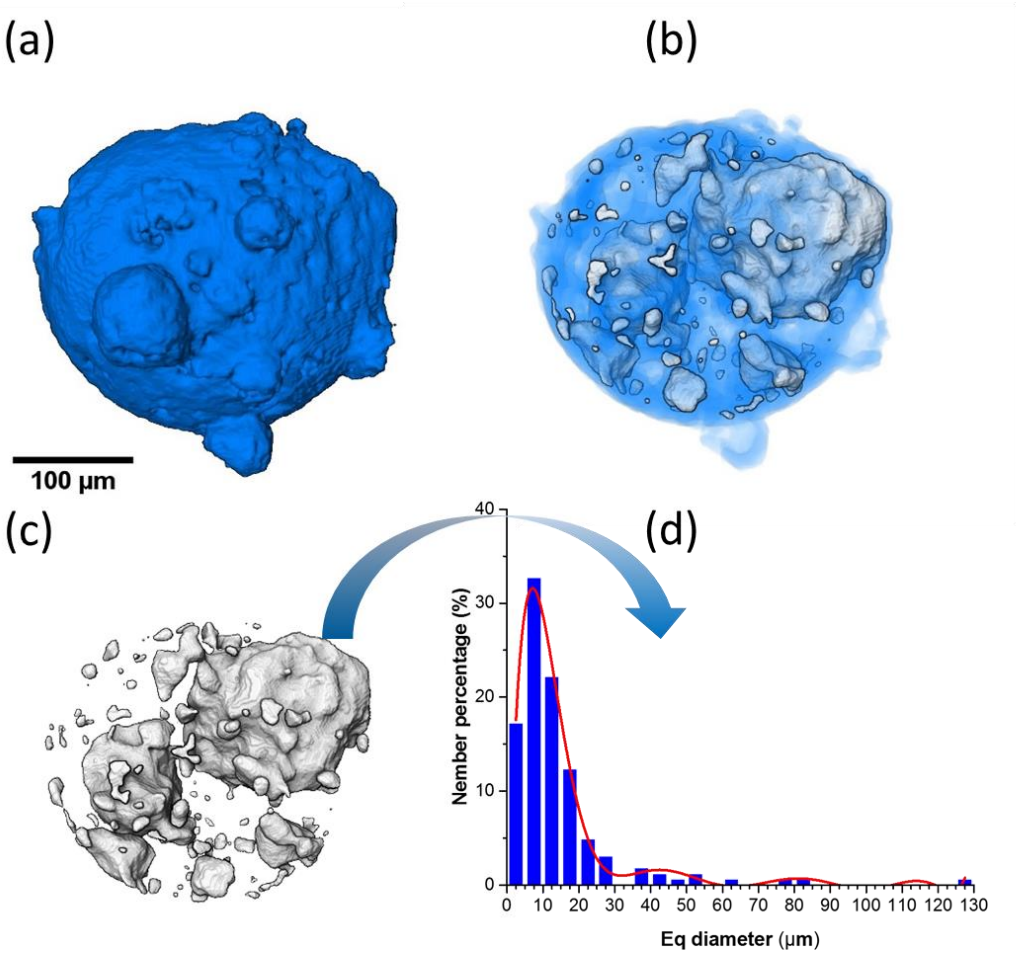

Figure 3.8 3D XRT image, voxel size: 1.74 µm, of a single detergent granule (equivalent diameter: 300.2 µm) produced from LW + 1.6 R slurry., a) – c) have increasing matrix transparency to show morphological properties and distribution of initially undissolved crystals of sodium sulphate; d) is number distribution of the undissolved material.

For the larger sieve fraction, 500 to 600 µm, it can be seen that the internal space is occupied by a large central vacuole around which most undissolved sodium sulphate crystallites are distributed within the wall. The presence of macro-pores throughout the wall, as a function of the addition of sodium silicate was similarly observed for the coarse particles. A possible explanation for this observation may be due to the skin forming properties of sodium silicates. It is known that the polymeric materials are capable of forming a skin layer on the air-droplet interface, thereby slowing down the diffusion of moisture from the interior of the particle due to the restricted heat and mass transfer (Walton, 2000). This can potentially increase the droplet temperature which consequently results in bubble nucleation. Upon further drying, a rapid vaporization of residual

moisture within the partially dried particle, giving rise to the expansion of internal bubbles within the particle matrix. On the other hand, as drying progresses, the rheological properties of the skin changes since it undergoes a transition from a sol to a glassy state. This in turn confers elastic properties to the droplet surface. The strength and mechanical properties of the developed skin will determine the stability of air bubbles against a pressure difference between the inside and the outside of a bubble surface (Both et al., 2018, Pauchard and Allain, 2003). Walton (2000) studied the morphology of sodium silicate particles produced from a single-droplet drying method, and found evidence for the formation of internal small bubbles within larger parent particles. This, according to the author, was attributed to the polymeric nature of sodium silicates (Walton, 2002). In aqueous sodium silicate solutions, also known as "water-glass", a dispersion of monomer, dimer, cyclic trimer and polysilicates are supposed to be in a chemical equilibrium (Yang et al., 2008a). Upon drying, the removal of water from the interstitial spaces, forces the colloidal aggregates into close proximity which eventually leads to the formation a transparent, solid and amorphous structure (Roggendorf et al., 2001). This phase transition can potentially alter the mechanical properties of the droplet being dried. Therefore, it can be inferred that it is a sol-colloidal glass transition that might have been responsible for the formation and stability of macro-pores.

The influence of the initial water content and sodium silicate on the formation of bubbles can be better elucidated by distinguishing the intra-particle pores which are not connected to the exterior and to the main central vacuole of the particle, as described in the materials and methods section. Figure **3.9** shows the distribution of equivalent diameter of the intra-particle pores obtained from the x-ray microtomography. The smallest mean pore diameter (32.28 μm) was observed in detergent powders produced from low-water content slurries in the absence of sodium silicate. It can be observed that pore sizes are mainly distributed in a narrow range of 5-30 μm. These samples also showed the lowest pore fraction (φ = 4.78%). With increasing the water content, a significant increase in volume of pores in a range of 30-60 μm was found which caused a shift of mean pore diameter to a larger value (46.45 μm) (Figure **3.9**b). Furthermore, the increased water

content noticeably increased the pore fraction to 22.81% in resulting detergent powders. Comparing Figure **3.9**a and c, it can be observed that the pore sizes were also affected by the addition of binders. The addition of sodium silicate with a molar-ratio (SiO_2:Na_2O) of 1.6 considerably changed the pore size distribution, where the average size increased to 42.91 µm. At higher SiO_2:Na_2O ratio the resulting detergent powders were found to have a relatively larger mean pore size (46.56 µm). These increases in mean pore diameter were concomitant with increases in pore fractions.

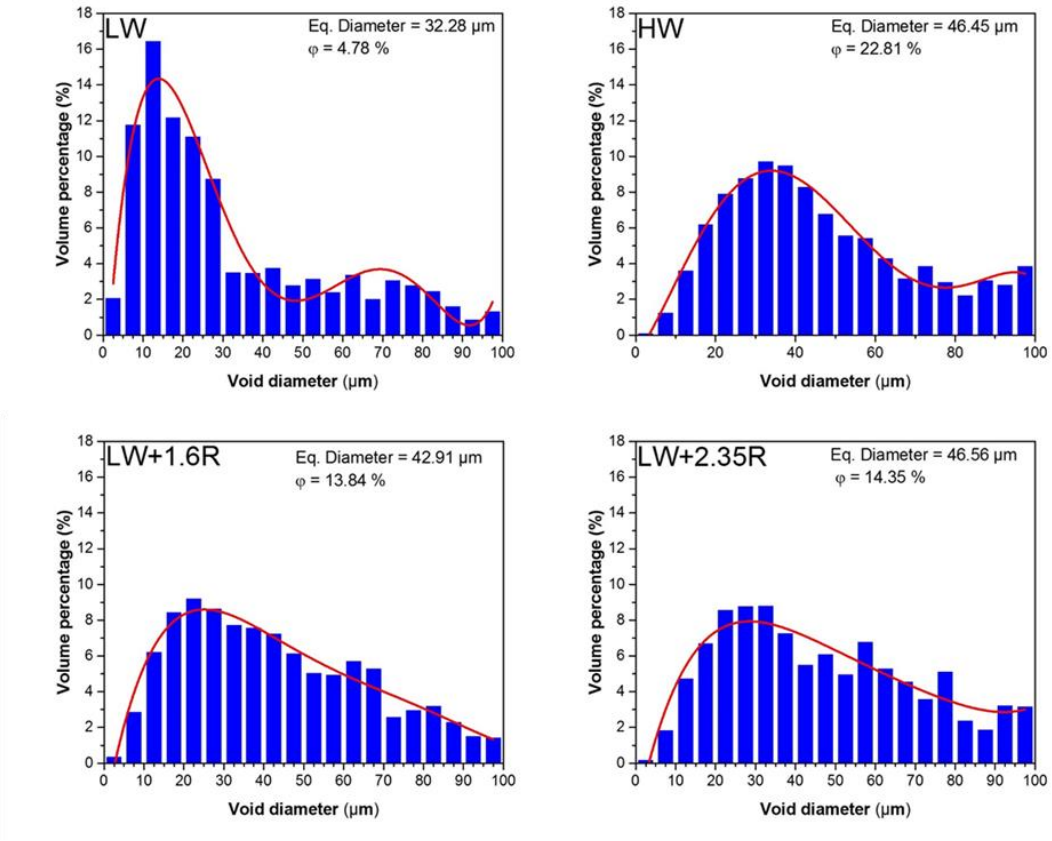

Figure 3.9 Pore size distribution in spray-dried detergent powders (300-350 µm) as a function of slurry formulation. The parameters of equivalent mean void diameter (Eq. Diameter) and pore fraction (φ) are summarised in the graphs.

The complex multi-component structure of spray-dried detergent powders can be better elucidated, at the micro/nano-scale, by scanning electron microscopy, SEM. To reveal the internal structure both fractured internal surfaces and microtome sectioned granules were analysed. Figure **3.10** shows the internal surface of a fractured LW granule. At a low magnification it can

be seen that the granule contains a large vacuole with several small voids distributed throughout the granule matrix. At a higher magnification (Figure **3.10**b) a porous matrix is observed, created as the matrix has dried and crystalized. In contrast, the granule shell appears to be compact with limited porosity. Figure **3.10**e shows the presence of prismatic nano-sized crystals of sodium sulphate distributed within a less crystalline continuum. The presence of these crystals was also evidenced by a back-scattered electron (BSE) detector (Figure **3.10**d) at which the intensity of BSE signals is highly related to the abundance of elements in a specimen. The brighter contrast of BSE image indicates a higher electron density region, where more electron scattering occurs, signifying the presence of sodium sulphate crystals.

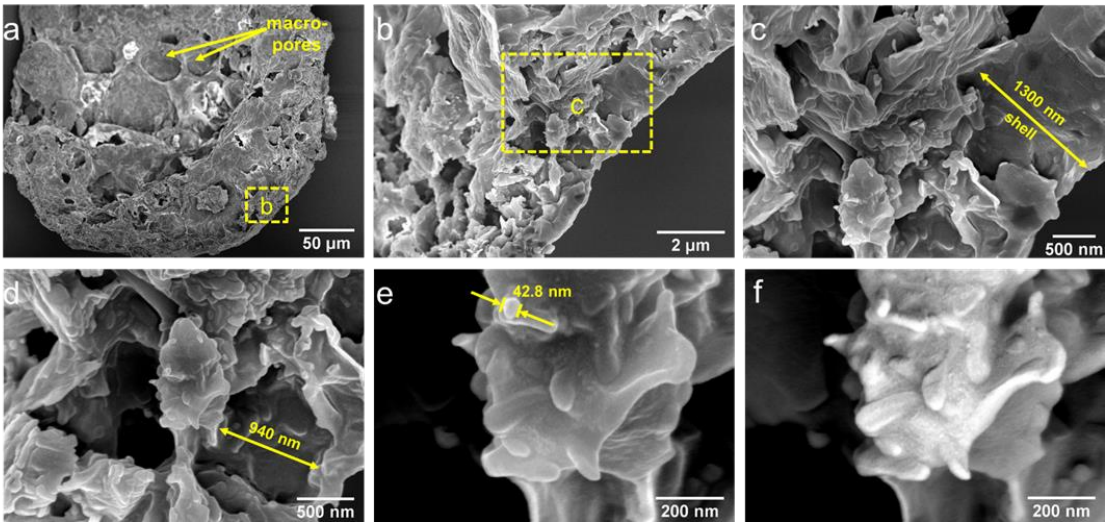

Figure 3.10 A SEM micrograph of the internal structure of a fractured detergent granule produced from low-water content slurry (LW) (a) shows a close up view of the matrix and granule wall (b), and its higher magnification image (c). The matrix micro-structure can be observed in (d) illustrating the morphology of the porous matrix, and nano-sized crystals of sodium sulphate can be observed at its higher magnification image (e), and the same region obtained from the backscattered electron detector (f).

SEM observations of cross-sections of embedded particles make a valuable contribution to a better understanding of the porous structure of the particles (Figure **3.11**). The porous microstructure in these images can be classified into three groups: 1) slit-shaped closed pores, 2) irregular inter-connected open pores,< 5 um diameter and 3) larger, irregular semi-open macro-pores, > 5 um diameter. In spray-dried powders produced from low-water content slurry, the matrix of the wall appears noticeably compact which mainly contain slit-shaped pores, though

some near spherical pores can be observed at the middle region of the wall, away from the shell. Interestingly, the addition of sodium silicate resulted in the formation of what looks to be relatively irregular macro-pores in the matrix. Detergent slurries with higher water content led to the formation of irregular open pores with some degree of interconnection within the wall of the particle. These irregular patterns might have been formed as a direct consequence of the movement and evaporation of the increased quantity of water leaving a complex flow pattern within the matrix upon drying. The extent of pore connectivity is also evident in corresponding coloured-labelled images, showing the sets of connected pores denoted by the same colour.

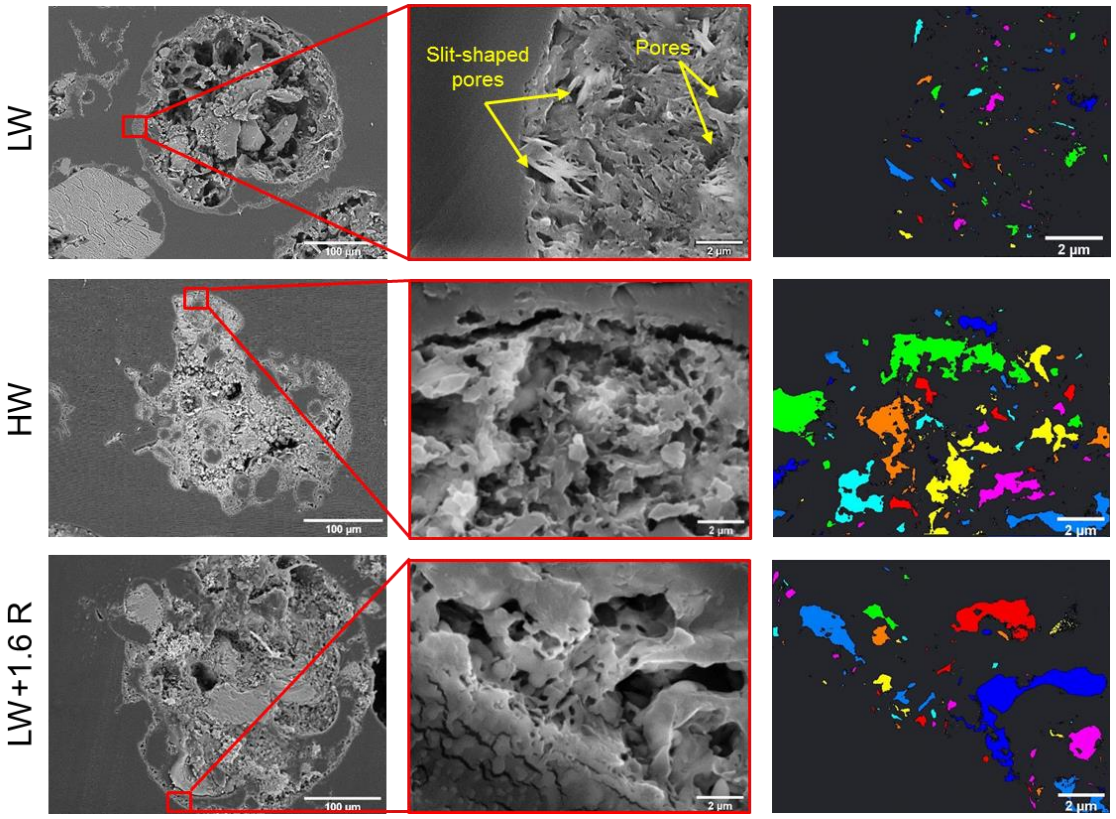

Figure 3.11 SEM micrograph of a microtome-polished cross-section of embedded detergent powders illustrating the matrix microstructures at high magnifications and the corresponding coloured image showing sets of connected pores labelled with the same colour, based on pixel connectivity, created by the Lable image tool in Avizo.

3.2.3 Surface characterization

The surface microstructure of spray-dried detergent powders was evaluated by SEM. The micrographs in Figure 3.12, indicates that the morphology of surfaces is considerably different.

In the case of detergent granules produced from low-water content slurries in the absence of sodium silicates, the surface appears to be covered with a continuous non-crystallne matrix containing with a few crystallites of sodium sulphate embedded in the surface (Figure 3.12b). The presence of these crystals is clearly evident in the corresponding backscattered electron micrographs (Figure 3.12 c). At higher magnification some shallow folds can be observed on the surface (Figure 3.12 d). In contrast, high-water content slurries gave rise to the formation of granules with a more crystalline surface. Figure 3.12 f, g and h illustrates that the surface morphology is mainly dominated by sub-micron sized crystals of various shape (pyramidal, dendritic and elongated). Even though both above-mentioned spray-dried powders have chemically and quantitatively similar components at the end of drying, the reason for the discrepancy in particle surface morphology can be explained by different matrix composition resulting from different initial quantities of water in detergent slurries. In this study, the matrix was considered as the particle structure excluding the remaining undissolved sodium sulphate. The approximate compositions of the resulting detergent powders are given in Table **3.4**. The amount of remaining undissolved sodium sulphate was obtained from the XRT technique (as mentioned earlier in the material and methods section). It can be seen that detergent powders produced from high-water content slurries exhibit the lowest quantity of undissolved sodium sulphate. Thus, the presence of a sufficient amount of water caused the formation of what looks considerably crystalline surface. In detergent powders produced from low-water content slurries containing sodium silicate some regions appear to be similar with their equivalents produced in the absence of sodium silicate. The surface of powders are still smooth in some regions (Figure 3.12 j), however; the SEM micrographs at higher resolution revealed the presence of some nano-sized crystals in some other regions (Figure 3.12 k and l).

Table 3.4 Composition of the resulting detergent powders

Description	Bulk density (g/cm^{-3})	Approximate compositions of the detergent powders (wt %)					
		Moisture	LAS	Dissolved Sodium Sulphate	Undissolved Sodium Sulphate	Sodium Silicate (1.6 R)	Sodium Silicate (2.35 R)
LW	0.472	0.5	19.5	15.26	65.24		
HW	0.267	1.0	19.5	57.3	23.2		
LW+1.6 R	0.544	2.0	19.5	11.9	56.6	12	
LW+2.35 R	0.536	1.2	19.5	14.3	51.2		15

Notes: Moisture contents were determined using a gravimetric method, *i.e.*, dynamic vapour sorption (DVS). The quantities of undissolved sodium sulphate were measured using x-ray microtomography.

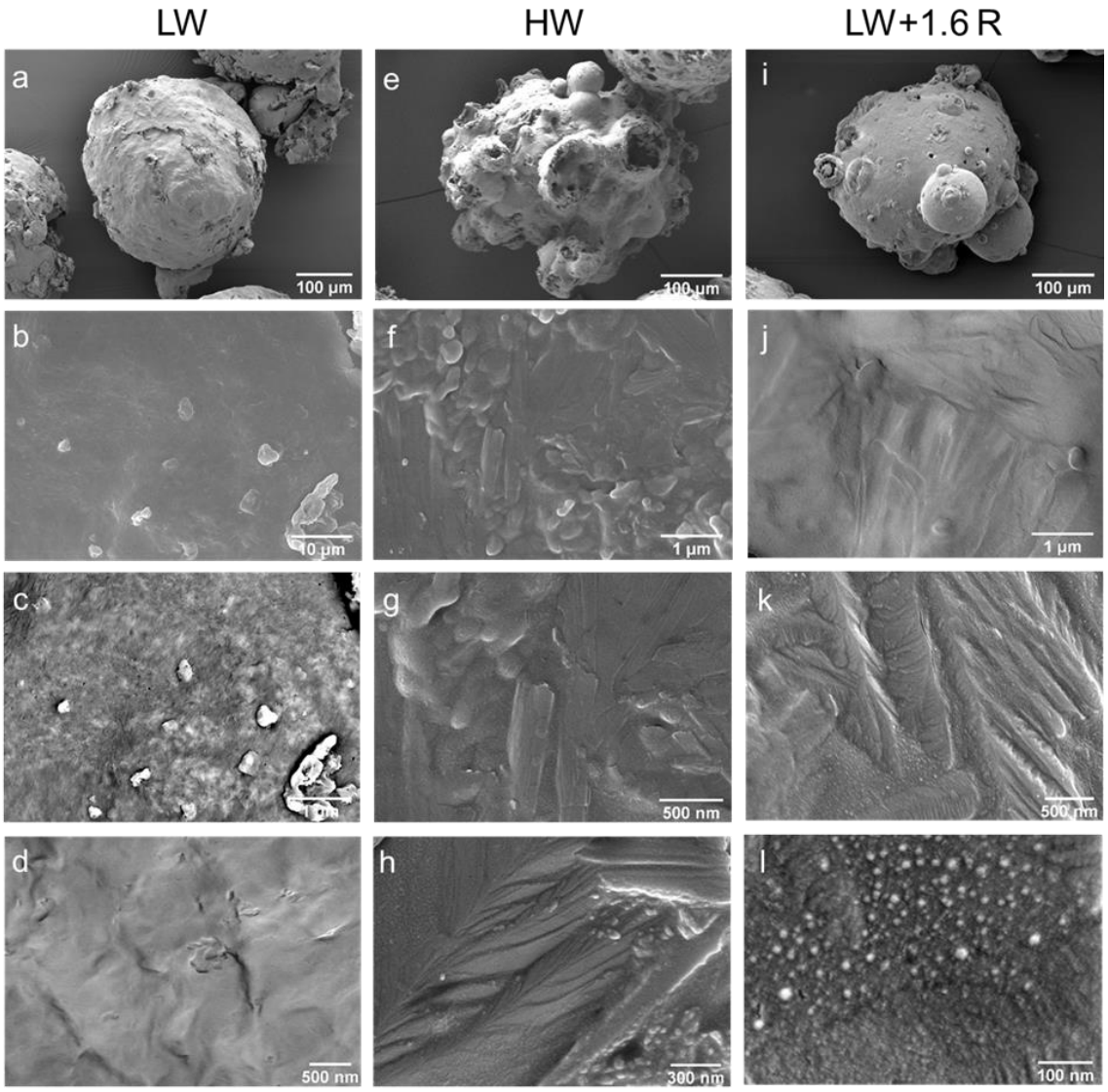

Figure 3.12 Micrograph of spray-dried detergent granules. (a) A spray-dried detergent granule produced from low-water content slurries and its higher magnification image (b). (c) Shows the same region in (c) obtained from a backscattered electron detector, giving larger contrast differences between the crystals and their background, and its higher magnification image showing the background (d). (e) A spray-dried detergent granule produced from high-water content slurries and its higher magnification image (f, g, and h). (i) A spray-dried detergent granule produced from low-water content slurries containing 1.6 SiO_2Na_2O R and its higher magnification images from a relatively smooth region (j), and its more crystalline region (k) and nano-sized crystals of sodium sulphate can be observed in (l).

3.2.4 Bulk analysis of self-assembled nano-structures

3.2.4.1 Polymorphs of inorganic salts (Sodium sulphate)

The development of spray-dried detergent powders with improved functional properties highly relies on a better understanding of the structure of dispersed phases, *e.g.*, self-assembled surfactant nano-structures and inorganic crystals. In SEM micrographs, a variety of crystalline morphology was observed, particularly on the surface of the granules. The presence of such crystal habits may arise from the existence of different polymorphs of sodium sulphate which can be examined by wide-angle x-ray scattering technique (WAXS). It is well established that sodium sulphate can exist in different polymorphic forms which are referred to as phase I-V. Two anhydrous polymorphs of Na_2SO_4 (V) and Na_2SO_4 (III) have been shown to crystallize out of a supersaturated solution of sodium sulphate upon evaporation among which Phase V (thenardite) is considered to be the most stable anhydrous phase at room temperature (25 ºC). Phase Na_2SO_4 (III), which is also known as metastable phase, can remain stable for considerable periods of time at typical room temperatures and humidities. However, this polymorph may undergo a phase transition to phase V at humidities above its deliquescence humidity, *i.e*. RH >83.5% at 25 ºC. Other polymorphic forms of sodium sulphates, *i.e*., I, II and IV, are considered as high-temperature polymorphs and there has been no precedent for the presence of the aforementioned polymorphs at near ambient temperature (Rodriguez-Navarro et al., 2000, Linnow et al., 2006) In this study all the detergent powders exhibited well-defined, sharp diffraction peaks which are characteristics of well-ordered crystal lattices of phase III and V forms of sodium sulphate (Figure **3.13**).

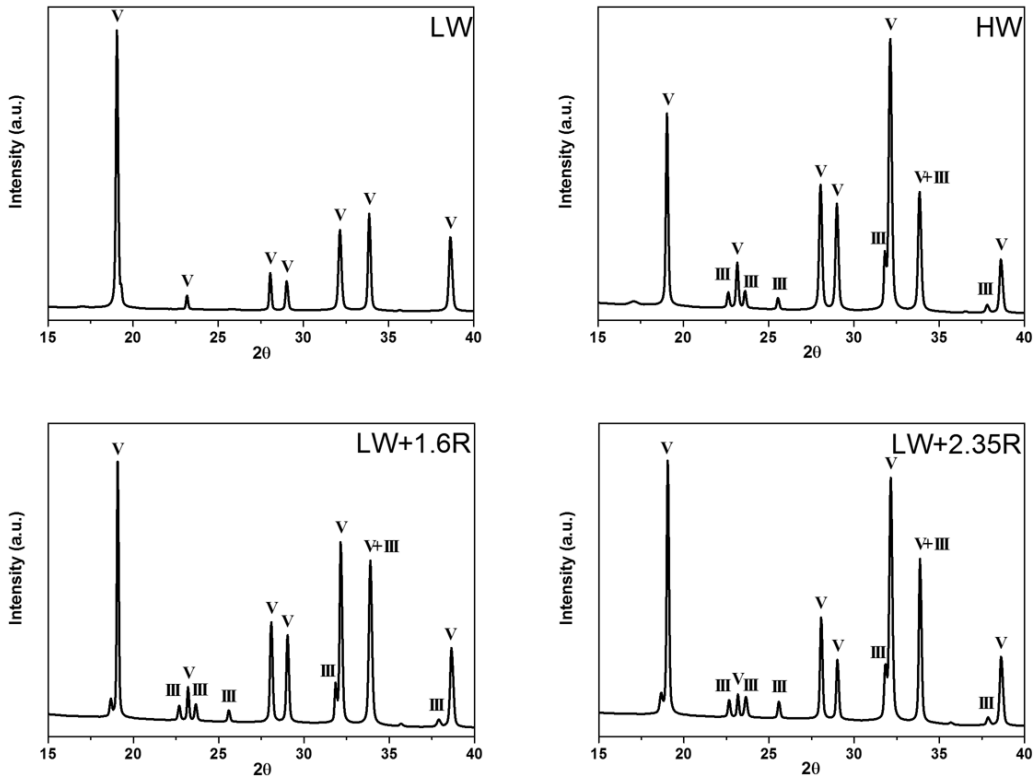

Figure 3.13 Wide-angle x-ray diffraction (WAXS) patterns of spray-dried powders showing the presence of phase III and phase V.

The XRD patterns, revealed the presence of thenardite (phase V) as the only existing anhydrous polymorph in detergent powders produced from the low water-content slurry (LW). Increasing the amount of water or adding sodium silicate gave rise to the formation of the metastable phase III in resulting powders. A clear splitting of a diffraction peak at 23.2° 2θ and the emergence of two new peaks at 25.6 and 37.9° 2Θ are characteristics in a change in lattice parameters from thenardite (phase V) to phase III. Arising from the XRD patterns, the diffraction peaks at 22.7, 23.7 and 25.6 ° 2θ belong to phase III (Rodriguez-Navarro et al., 2000). It has been suggested that thenardite crystal lattice builds up from parallel chains consisting of SO4 tetrahedra and deformed NaO6 octahedra at which isolated sulphates share two of their edges with distorted octahedra. The other corners of each octahedral NaO6 is shared with four sulphate ions giving rise to the formation of a 3D network. Thenardite is bipyramidal in shape which has been reported to have an orthorhombic unit cell. The structure of metastable polymorph (phase III), however, is thought to be built up from deformed tetrahedral and octahedral chains. In the latter crystal

structure there are two types of NaO6 in terms of Na-O distances, which connect to each other with a common face (Rasmussen et al., 1996, Vidya and Lakshminarasappa, 2013). Unlike thenardite (phase V), metastable sodium sulphate (III) forms needle like crystals, although it similarly crystalizes in an orthorhombic crystal system. The presence of non-equilibrium crystals (Phase III) in detergent powders produced from high-water-content slurries can be explained by the possibility of spontaneous nucleation under metastable conditions (Mehrotra, 1981). Phase (III) was similarly observed in XRD patterns of detergent powders containing sodium silicate. A likely explanation for this can be due to the adsorption of negatively charged silicate species on intermediate clusters of sodium sulphate, thereby regulating the nucleation and growth of sodium sulphate crystals. The interaction between negatively charged additives and sodium sulphate nuclei has been previously reported by Ruiz-Agudo et al. (2006). The authors investigated the crystallization of thenardite (phase V) and mirabilite (Na2SO4.10H2O) and suggested that phosphonate derivatives can function as nucleation and growth inhibitors. It was found that, depending on the PH value, while the crystallization of one phase is favoured the growth of another phase is inhibited. Silicate species are known to have a strong tendency to adsorb onto a variety of surfaces of metal oxides and clays. It has been shown that dissolved silica species can affect both the nucleation and crystal growth of inorganic minerals (Anderson and Benjamin, 1985, Gal et al., 2010). In the early stage of crystallization, silicate species can modify the rate and extent of cluster aggregation, i.e., nucleation, by shielding the positively charged precursors. In terms of crystal morphology, in the late stages, these anions can adsorb on specific faces, thereby regulating the growth rate of these faces, consequently this changes the crystal habit (Kellermeier et al., 2013, Ruiz-Agudo et al., 2006). Therefore, a possible reason for the presence of metastable polymorph (Phase III) in silicate-containing detergent powders can be due to the adsorption of negatively charged silicate ions on the positively charged precursors (existing as small amorphous particles) of sodium sulphate, which consequently not only inhibits regular packing, but also disturbs the charge equilibrium within the crystal lattice (Gal et al., 2010).

A variety of crystalline structures on the surface and within the matrix of the granules was earlier shown by the SEM micrographs. Figure **3.14** illustrates the morphology of crystallites within the matrix of a granule produced from high-water content slurries containing NaLAS and sodium sulphate. The morphology of these submicron-sized crystals corresponds well to that of thenardite as compared with the reported habits of anhydrous sodium sulphate (Phase V) (Atzeni et al., 1995, Vidya and Lakshminarasappa, 2013). Interestingly, it was found that both the crystal size and the crystal habit within the matrix were comparatively different from those on the surfaces of detergent granules. Indeed, the increased water content of detergent slurries or addition of sodium silicates gave rise to the formation of dendritic crystals on the granule surface. The morphologies of the observed tiny branched crystals (Figure.3.12 g and j), which consist of elongated needles assembled as dendrites, are roughly consistent with the those of the metastable phase (phase III), as previously reported by others (Rodriguez-Navarro et al., 2000). Additionally, the prismatic crystals on the particle surfaces were relatively smaller. Considering the both changes in the crystal size and the crystal habit on the particle surfaces compared with those within the matrices, it can deduced that existence of such non-equilibrium thenardite morphologies might be either due to a spontaneous nucleation under metastable conditions or crystallization inhibitory effects of sodium silicate as discussed earlier. In contrast, the micrograph of spray-dried detergent powders produced from low-water content slurries, and in the absence of sodium silicate, illustrates that the outer layer of the shell is considerably smooth and less crystalline.

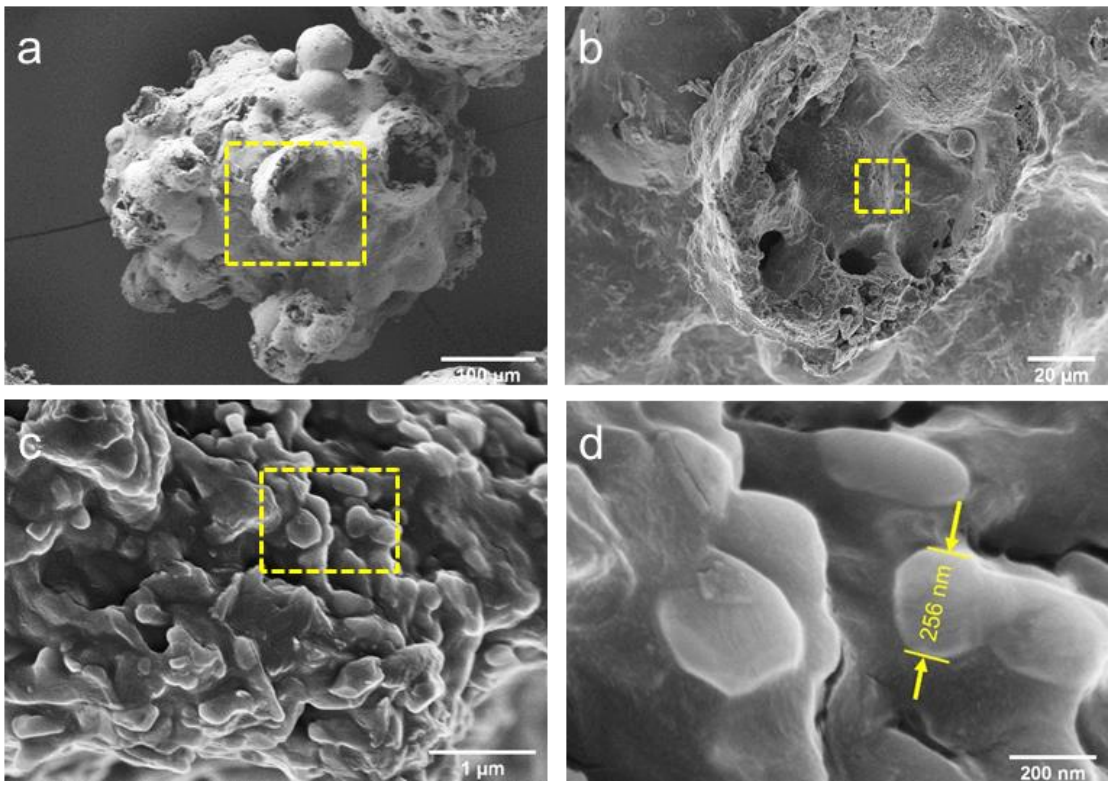

Figure 3.14 Micrograph of a spray-dried detergent granule produced from high-water content slurries (a), and a region of interest (b), and higher magnification images illustrating the morphology of thenardite crystals (c) and (d).

3.2.4.2 Phase behaviour of surfactant (NaLAS) molecules

Amphiphilic molecules are known to have a tendency to arrange themselves, in the presence of water, into various ordered nanostructures (1, 2 and 3 dimensional self-assemblies) depending on the concentration and molecular shape. While the formation of micellar structures is favoured at concentrations equal to or greater than critical micellar concentration (CMC), higher concentrations may give rise to the formation of disk-like or rod-like micelles and particularly liquid crystalline phases (Israelachvili, 2011, Kulkarni et al., 2011). The phase behaviour of self-assembled structures of NaLAS molecule is of significant interest due to its potentially significant effect on the physical properties, flowability, dissolution rate and physical stability of laundry powders. In the current study, small-angle X-ray scattering (SAXS) was used to determine the molecular organisation of NaLAS surfactants in spray-dried detergent powders. Diffraction patterns of four formulations are shown in Figure **3.15**. In all cases XRD patterns revealed the presence of multiple lamellar coexisting phases as evidenced by the occurrence of several sets of

equidistance Bragg diffraction peaks. The lamellar phase is one of the most common structures of liquid crystalline phases, and its first-order reflection in XRD patterns can describe the periodicity (*d*-spacing) of the structure.

In the low-water content formulation (LW) (Figure **3.15**a), four different sets of Bragg diffraction peaks can be observed in the ratio of 1:2 and/or 1:2:3 with respect to the first order of peaks. In these samples, the largest *d*-spacing (43.0 Å) can be found at q =0.146 $Å^{-1}$ which corresponds to the first-order reflection in lamellar phase, labelled *a*. The overall *d*-spacing values of lamellar phases can be observed in Figure **3.15**b. The multiple lamellar phases were also seen in detergent powders produced from high-water content slurry (HW), though interestingly the intensity of first-order peaks a_1 and b_1 at q =0.14 and 0.16 $Å^{-1}$, were noticeably reduced. These reductions in scattering intensities signifies a decrease in population of the lamellar phases (Bolze et al., 2000) having relatively larger lattice *d*-spacing. The XRD patterns of detergent powders containing sodium silicate LW + 1.6 and LW + 2.35, show a remarkable similarity with each order, indicating the silicate ratio has no effect on the self-assembled surfactant structure. The largest *d*-spacing (33.6 Å), corresponding to the first-order reflection in lamellar phase *c*, can be found at q =0.187 A^{-1}. This reduction in number of co-existing phases leads to a more uniform system with stronger Bragg peaks.

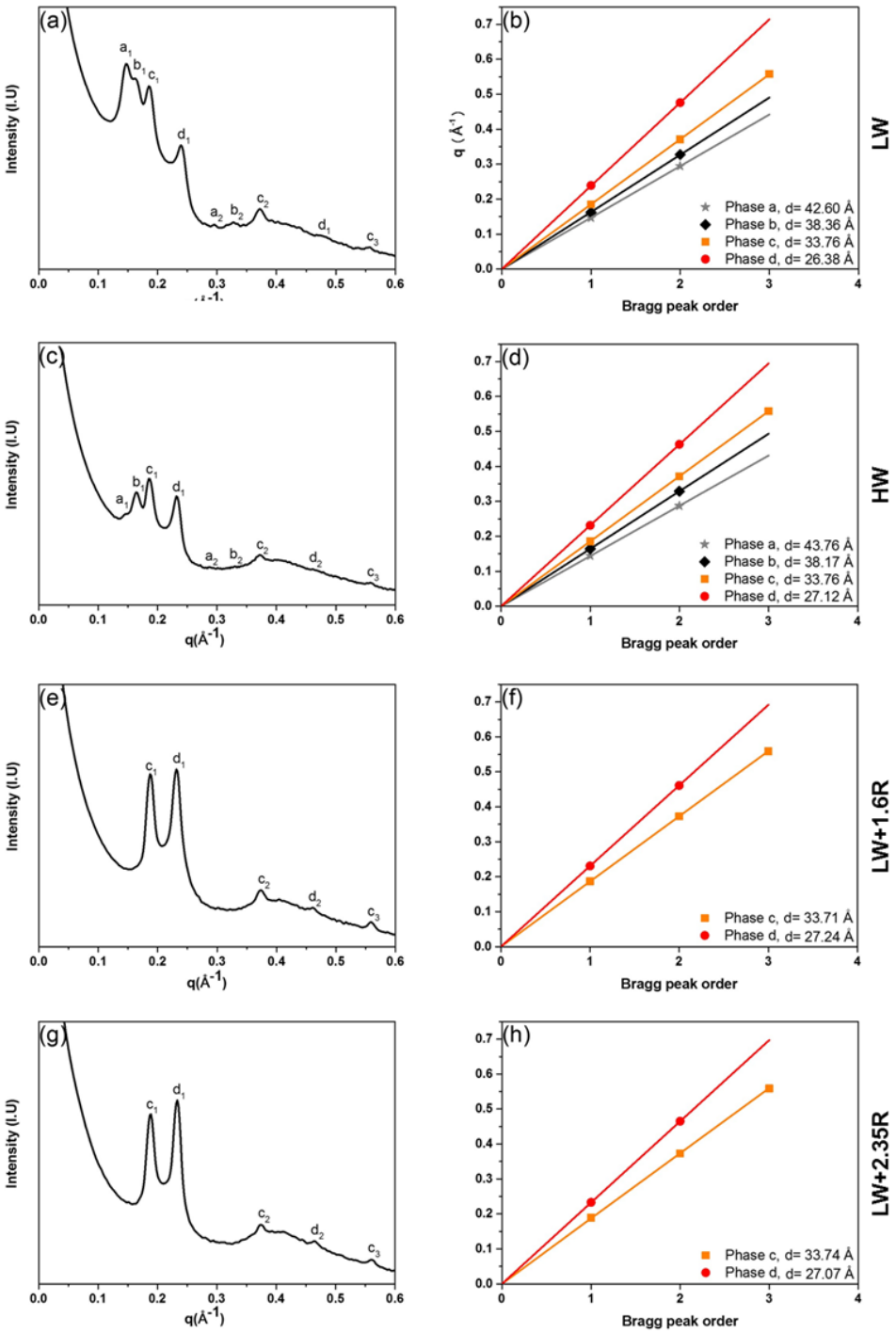

Figure 3.15 Small-angle x-ray diffraction (SAXS) patterns of spray-dried powders produced from low water content slurries (left) and their corresponding lamellar *d*-spacing values determined from the slopes of Bragg peak position versus peak orders (right).

The occurrence of coexisting lamellar phases of NaLAS in liquid detergent systems has been previously reported by Richards et al. (2009) and Stewart et al. (2009), which, according to the authors, was attributed to the natural heterogeneity of the chemical structure of NaLAS. It was

suggested that NaLAS isomers possessing a benzene ring substituted in the middle of hydrocarbon chain, *i.e.*, *v*-shaped isomers, trigger the formation of lamellar phases, while NaLAS isomers with a benzene ring at the extremities of the hydrocarbon chain, but not terminal $–CH_3$, promote the formation of micellar phases. Richards et al. (2007) explained the occurrence of multiple lamellar phases by the local segregation of different NaLAS positional isomers, possessing different alkyl chain length, within the bilayers ,which subsequently swell to different extents upon exposing to elevated temperatures. Liaw et al. (2003) showed that the addition of sodium silicate with the SiO_2:Na_2O molar ratios of 2.0 to NaLAS slurries, gives rise to the formation of more sphere and tightly packed multi-lamellar vesicles. These structural changes in NaLAS paste were concomitant with a reduction in lamellar *d*-spacing which is in good agreement with the SAXS results presented here. The SAXS patterns signify the presence of a relatively more uniform lamellar phase containing two co-existing phases with well-defined periodicities. As mentioned earlier, the presence of multiple lamellar phases is an indication of lateral separation of the different LAS isomers within the bilayers. This phenomenon can be associated with severe dehydrations during a drying process as well as storage in low relative humidity conditions (Bryant and Wolfe, 1989). Therefore, detailed information is essential to understand the state of surfactant in spray-dried detergent powders. A fundamental understanding of these structural changes in lamellar phase can be achieved by exposing the samples to different relative humidity conditions followed by reconstructing electron density profiles (EDP) of the one-dimensional repeat of bilayer stacking through Fourier analysis (see Chapter 4).

3.2.5 Conclusion

In this study, the structure of spray-dried detergent powders was defined as a solid multi-component colloidal system where sub-micron crystals of inorganic salts along with lamellar liquid crystals of NaLAS are dispersed within a porous matrix saturated with inorganic salts. It was shown that the initial water content of the slurries play a crucial role in determining the matrix composition and microstructure of the resulting detergent powders. This was evidenced in the

quantities of remaining undissolved sodium sulphate as measured by the x-ray tomography technique. The greater the initial water content in detergent slurries, the greater the ratio of dissolved sodium sulphate to NaLAS "active matter" within the matrix. This was also reflected in surface microstructures where a more crystalline surface was observed as the result of the increased water content. The addition of binders, *i.e*., sodium silicates, and the amount of initial water content of the slurries considerably governed the morphological properties. The increased water content resulted in the formation irregular particles with sharp edges. These powders also showed the largest mean particle size (377 μm). On the contrary, near spherical particles were produced from low-water content slurries, though some degree of surface agglomeration, the adhesion of fine particles on the surface of larger parent granules, was observed upon the addition of sodium silicates. Spray-dried powders produced from low-water content slurries are either hollow or semi-solid. In the latter case, remaining undissolved sodium sulphate occupies most of the internal space of the granules as a large crystallite. The hollow structures were particularly observed in coarse particles in which undissolved sodium sulphate crystallites are distributed around a large central vacuole. The addition of sodium silicate gave rise to the formation of a large number of voids, macro-pores, within the granule matrix. The internal structure, however, became noticeably different once the initial water content of the slurries increased to 63.0 wt%. This resulted in the formation of foam-like structures, at the macro-scale, where central vacuole is not a commonly encountered characteristic. At the micro-scale, the influence of the increased water content was evident from the micrographs of microtome-polished detergent powders showing irregular connected pores within the matrix. The dispersed nano-structures, *i.e*, sodium sulphate polymorphs and lamellar liquid crystalline phases, were shown to be influenced by the initial chemical composition of the slurries. The WAXS results suggested that the increased water content and the addition of sodium silicates results in the formation of metastable polymorphs of sodium sulphate (phase III). From the SAXS results it was found that the addition of sodium silicate leads to a more uniform lamellar phase with a narrower *d*-spacing distribution. The

influence of the addition of sodium silicate on the phase behaviour of liquid crystalline phases of NaLAS will be discussed in more detail in chapter 4.

Chapter 4 Liquid Crystalline Phases of Linear Alkylbenzen sulphonate

In previous chapter spray-dried detergent granules were described as a solid multi-component colloidal system in which crystals of inorganic salts along with multi-lamellar stacks of surfactant molecules are dispersed. Also, it was found that the addition of sodium silicate leads to a more uniform system with stronger Bragg peaks. This chapter focuses on the influence of the initial water content of the detergent slurry and the addition of alkaline sodium silicate, with the SiO_2:Na_2O molar ratios of 1.6 and 2.35, on the molecular structure of stacked lamellae using small-angle x-ray scattering. More detailed information on the lamellar phases are obtained by reconstructing electron density profiles (EDP) of the one-dimensional repeat of bilayer stacking through Fourier analysis. The parameters of lamellar *d*-spacing, bilayer thickness (d_{HH}) and water layer thickness (d_W) are determined. Additionally, extended information about hydrocarbon chain conformational order of NaLAS molecules is obtained by employing FTIR. This gives good insight into the hydrocarbon subcellular packing as well as interdigitated hydrocarbon domains within the lamellar phases.

4.1 Materials and Methods

4.1.1 Materials

Detergent granules were produced with a pilot-scale spray dryer in Procter & Gamble Newcastle Innovation Centre as it was described earlier in Chapter 3. The resulting detergent powders were then stored in desiccators with a specific relative humidity, *i.e.,* 11, 33, 54, and 72%, created using a saturated solution of lithium chloride, magnesium chloride, magnesium nitrate hexahydrate, and sodium chloride respectively, at 21 ±1˚C for four weeks.

4.1.2 Micro-computed tomography (Micro-CT) scanning

The morphology and internal structure of spray-dried detergent powders were qualitatively examined using a Phoenix Nanotom CT scanner (GE Measurement and Control, Wunstorf, Germany). This provides good insight into the distribution of high-density and low-density phases within the powder. The high-density regions are due to initially undissolved inorganic salts, *i.e*., sodium sulphate crystallites, and low-density regions are pores and vacuoles.

A sieved size cut (300-350 μm) of the sample powders were mounted on a rotating stage between an X-ray source and X-ray detector. Samples were then scanned in the full range of 0–360°. A series of X-ray micrographs were obtained and three-dimensional volumes were reconstituted using the VGStudio software package. To improve the 3D data visualisation, a number of different image processing tools including filtration and segmentation, were applied to the X-ray micrograph data using the Avizo software package. A non-local means filtration was applied to the grey scale projections to reduce image noise. The segmentation of highly dense regions, corresponding to initially undissolved sodium sulphate particles, from the matrix was conducted using an interactive thresholding tool in Avizo.

4.1.3 Small X-ray scattering (SAXS)

SAXS measurements were carried out using a Xeuss 2.0 SAXS camera system (Xenocs, Sassenage, France). A Cu-K_α X-ray source (λ=0.154 nm) and a camera set-up with scatterless collimating slits was used. The scattering angle was calibrated using silver beenate with the known *d*-spacing of 5.84 nm (Huang et al., 1993); the scattering vector modulus is defined in this work as $q = 4\pi/\lambda \sin(\theta)$, with 2θ being the scattering angle.

The SAXS data were further analysed by reconstructing electron density profiles (EDP) of the one-dimensional repeat of bilayer stacking by Fourier analysis. Note, in-plane densities along the x,y-coordinates of the bilayer are assumed to be constant, while the electron density contrast, $\Delta\rho$, along the z-coordinate and can be expressed as:

$$\Delta\rho(z) = \sum_{h=1}^{h\,max} \pm F_h \ cos\left(\frac{2\pi z h}{d}\right), \qquad (3)$$

where *h* is the order of the Bragg peaks, *z* is the distance in real-space, *d* gives the repeat spacing, and F_h are the form factors. Note, F_h were determined by the square-root of the peak intensities, I_h, having applied beforehand a Lorentz correction of h^2. From the EDP maxima positions, we estimated the average distance between NaLAS headgroups, *i.e.*, the bilayer thickness, d_{HH} (see Figure **4.1**; right). The hydration water layer, d_W, is then given as $d_W = d - d_{HH.}$

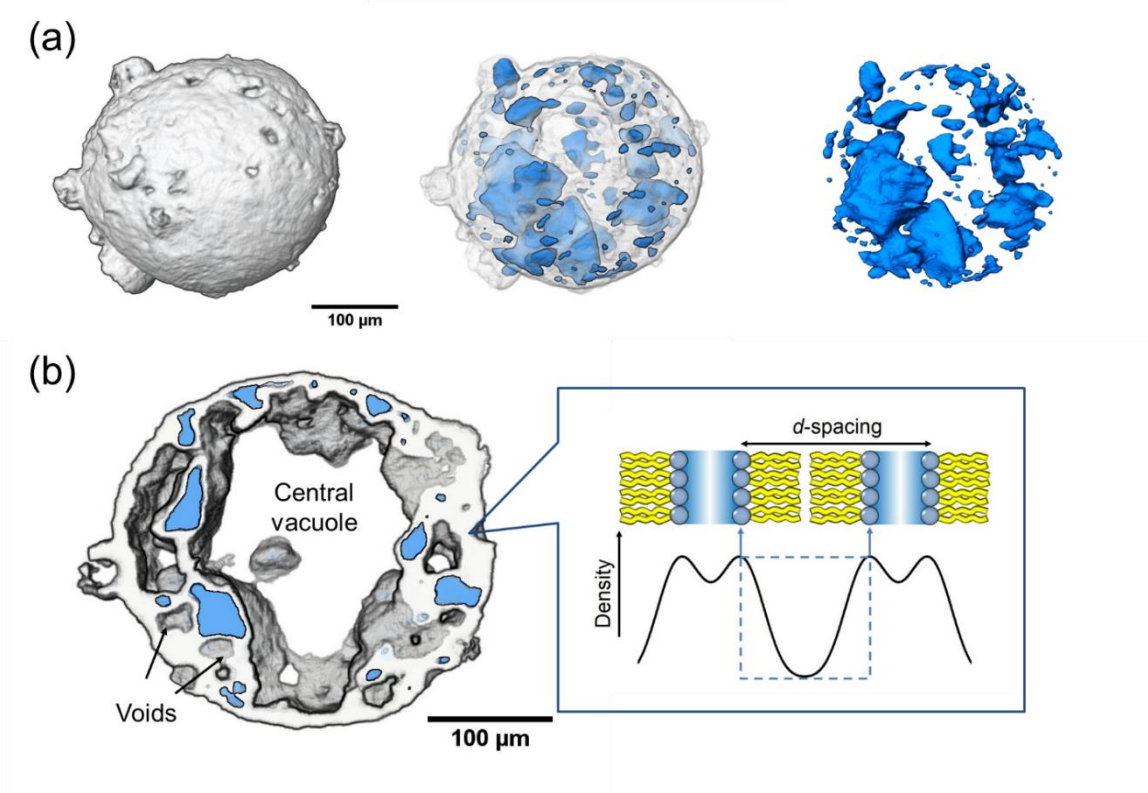

Figure 4.1 (a) A 3D X-ray micrograph (Voxel size: 1.74 µm) of a typical detergent granule (equivalent dimeter: 287.8 µm) produced from low-water content slurries, with different transparencies, showing morphological properties and distribution of large crystals and/or remaining undissolved sodium sulphate (blue particles); and (b) shows its 3D central cross section (68 microns thick) illustrating the distribution of voids and sodium sulphate crystallites (left), and a typical electron density profile of lamellar liquid-crystalline phases is illustrated in a cartoon (right).

4.1.4 ATR-FTIR measurements

The infrared spectra were recorded with a Thermo Fisher Scientific Nicolet iS10 FT-IR spectrometer using the attenuated total reflection (ATR) method. The detergent powders were mounted on the top of a high-refractive index ATR crystal and then slightly pressed onto it by a pre-mounted sample clamp. The infrared signal was obtained by measuring the infrared light, which is entirely internally reflected in the medium of ATR crystal. Background corrected spectra were measured over a range of 550-4000 cm^{-1} with 4 cm^{-1} resolution.

4.2 Results and Discussion

4.2.1 Small-angle X-ray scattering measurements (SAXS)

In previous chapter, the phase behaviour of self-assembled nano-structures of LAS molecules in spray-dried detergent powders was examined. The SAXS patterns revealed the presence of multiple lamellar coexisting phases as evidenced by the occurrence of several sets of equidistant Bragg diffraction peaks. Furthermore, it was found that the addition of sodium silicate to detergent slurries resulted in a reduced number of coexisting lamellar polymorphs as indicated by the SAXS data. These series of experiments, focus on the effect of different relative humidities during the storage on the periodicity (*d*-spacing) of lamellar structures. Furthermore, detailed information on the humidity-induced structural changes, *i.e.*, the hydration water layer thicknesses and the hydrocarbon chain lengths, have become accessible throughout determination of the electron density profiles of the bilayer stacking (as it was explained in section 4.1.3). The SAXS patterns of detergent powders obtained from low-water content slurries, containing LAS and sodium sulphate are shown in Figure **4.2**a. At 33% RH, four different sets of lamellar stacks were detected, showing the presence of multiple lamellar phases in samples with different *d*-spacings.

The occurrence of multiple lamellar phases of NaLAS have been previously studied by others. Stewart *et al.*, (2009) showed that the heating of concentrated aqueous systems of NaLAS, where the system is well within a micellar-lamellar region, results in the formation of coexisting lamellar phases. These authors demonstrated that the increased temperature leads to the swelling (a lamellar *d*-spacing of up to 44 Å), and to the increasing multiplicity of the Bragg reflections. It was also suggested that the number of resulting heat-induced reflections diminishes upon cooling to lower temperatures, and that the swollen lamellar phases return to their original *d*-spacing. Most recently, Poulos *et al.*, (2016) studied the structure and flow behaviour of concentrated NaLAS solutions and found evidence for the occurrence of coexisting lamellar phases with various lattice dimensions. According to the authors, this was partially attributed to the intrinsic polydispersity of NaLAS surfactants. It has been reported that the isomeric complexity of NaLAS,

may favour the local segregation of LAS isomers, which possess different alkyl chain length depending on the position of benzene ring. This local segregation within fluid bilayers gives rise to the formation of domains of different compositions, which subsequently swell to different extents upon hydration or exposing to elevated temperatures. Similar coexisting lamellar phases of various periodicities are also reported by Richardson et al., (2007). The latter authors and Stewart et al., (2009) demonstrated that NaLAS aqueous solutions, within the micellar-lamellar region, show a single Bragg reflection with a lamellar d-spacing value of around 34 Å at ambient temperature. This lamellar d-spacing corresponds fairly well to the peak c_1 in our SAXS data measured at 21 ±1˚C.

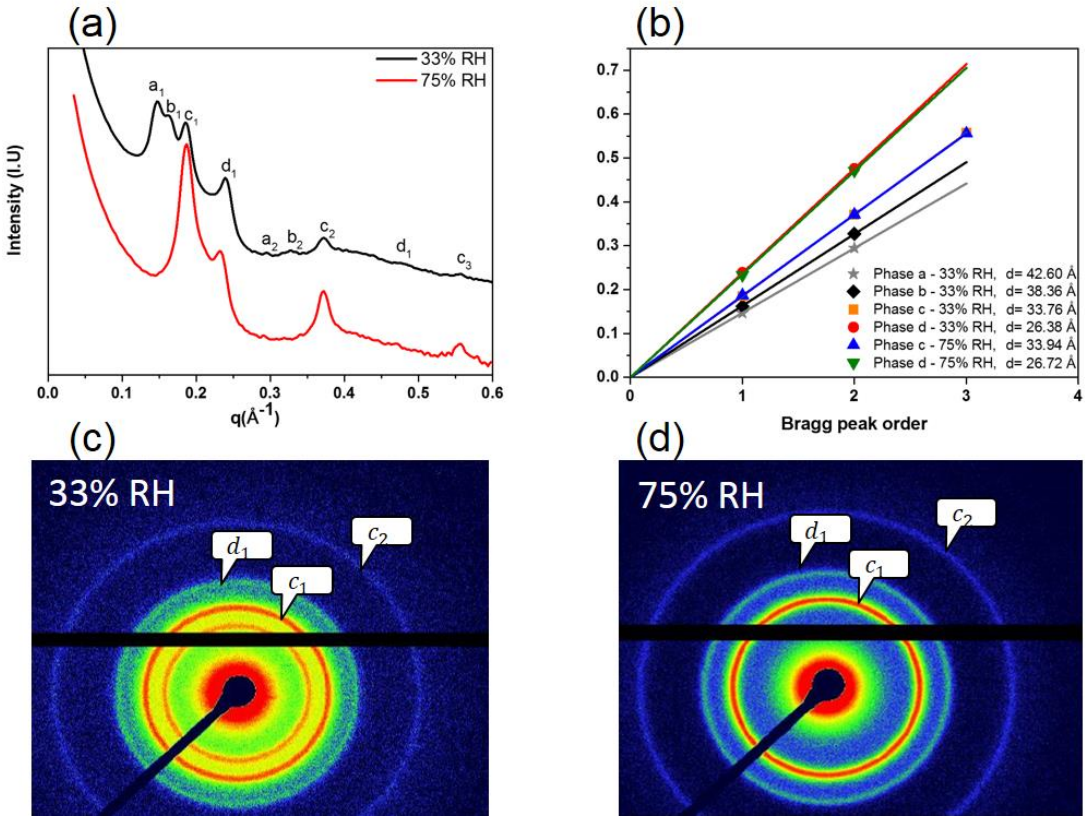

Figure 4.2 (a) Small-angle X-ray scattering (SAXS) patterns of spray-dried powders produced from low-water content slurry. (b) Shows the lamellar *d*-spacings of phases a, b, c and d as determined from the slopes of Bragg peak position versus peak orders. (c) and (d) illustrate 2D SAXS images of spray-dried detergent powders stored at 33% and 75% RH respectively.

As the lamellar phases of NaLAS are known to have a tendency to swell and coexist as multi-lamellar structures, the influence of relative humidity shall provide further information about the

occurrence of multiple Bragg peaks. When silicate-free samples were exposed to a higher relative humidity (75% RH) a noticeable change in their SAXS pattern was observed. The peaks at 0.14 and 0.16 $Å^{-1}$, corresponding to relatively long-periodicities of 42.7 and 39.2 Å, were surprisingly absent, leading to two coexisting phases only. This is also evident in the observation of fewer diffraction rings in corresponding 2D SAXS image (Figure **4.2**d). These changes also coincide with significant increases in lamellar *d*-spacing as well as the intensity of the Bragg diffraction peaks at larger scattering vectors, *i.e.*, 0.37 and 0.47, and 0.55 $Å^{-1}$.

In previous studies (Ockelford et al., 1993, Richards et al., 2007), the reason for the increased multiplicity at elevated temperatures was explained by the diminution of counter ion/head group association, leading to a decrease in attraction forces between the bilayers. On the contrary the above situation was suggested to alter once temperature decreases which results in the increased attractive forces between bilayers and consequently a decrease in number of lamellar phases. In the current study the increased humidity (75% RH) indeed gave rise to the formation of a narrow *d*-spacing distribution, where the largest *d*-spacing (33.6 Å) can be found at 0.187 $Å^{-1}$ which corresponds to the most intense peak c_1 in SAXS patterns (Figure **4.2**a). There are two possible scenarios, which can potentially explain these humidity-induced changes. A possible explanation for the disappearance of Bragg reflection peaks and a reduction in the sets of lamellae at RH 75%, may be due to the hydration of lamellar stacks which results in a perturbation in tightly packed arrays and hence a reduction in long-range orders in partially dehydrates lamellar phases. However, it can be seen that the Bragg peaks corresponding to phase *c* and *d* become more resolved at 75% RH. While the first possibility cannot be ruled out entirely, the second possibility can be due to an increase in fluidity of the lamellar phases. It has been known that membrane fluctuations are more energetically favourable as the level of hydration increases. In close-packed bilayers, *e.g.*, dehydrated lamellar phases, the undulation fluctuations are remarkably suppressed by the mutual hindrance of fluctuating bilayers (Nagle and Tristram-Nagle, 2000, Sornette and Ostrowsky, 1984). With increasing the thickness of the water layer, however; the mutual steric hindrance can be increasingly relieved (Katsaras, 1998). This leads to the enhanced amplitudes

of undulation fluctuations and the corresponding entropy of the system, and consequently a reduction in the bending rigidity of stacked bilayers (Ma et al., 2015, Podgornik and Parsegian, 1992). Therefore, the formation of local lamellar regions having different *d*-spacing, across the lamellar phase is energetically less favourable. Additionally, the increased fluidity can be accompanied by a transition from *trans* to *gauche* conformation in hydrocarbon chains. The conformation of hydrocarbon chains is defined by an arrangement that can be altered through an internal rotation, τ, around the C-C axis of methylene group ($-CH_2$) of alkyl chains. A relatively smaller rotation angle for gauche conformers ($\tau = \pm 60°$) as compared with trans conformers ($\tau = \pm 180°$), cause them to adopt a nonplanar structure (Sato, 2018). In general, the greater the number of the gauche conformers, the shorter is the mean length of the hydrocarbon chains (Lewis and McElhaney, 2013). Therefore, under humid conditions, the existence of domains with large lamellar *d*-spacing consisting of *trans* conformers are energetically unfavourable, leading to the merging of Bragg reflections and hence an intermediate lamellar lattice. Liaw, et al. (2003) examined shear-induced microstructural changes in LAS pasts and found evidence for the formation of multi-lamellar vesicles during shearing flow. Therefore, it should be noticed that during the production of detergent slurries, the multi-lamellar phases are likely to already exist within the slurries due to the severe operating conditions, *e.g.*, high-shear mixing, supersaturated sodium sulphate concentration and a considerably high process temperature (85 $^{\circ}$C). As the life time of the spray droplets is very short during the drying process, the dehydrated and, more probably, rigid multi-lamellar phases might have been fixed within a solid crystalline matrix. Additionally, the extent of dehydration and spatial distribution of water molecules across the spray-dried detergent granules can be of significant factors influencing the coexistence of lamellar phases. The localized compositional changes as the results of uneven distribution of water molecules and electrolytes might give rise to the formation of local patches with different lamellar *d*-spacing. Therefore, the exposure of spray-dried powders to a considerably high relative humidity value may have increased the molecular mobility, *e.g.*, undulation fluctuations, and consequently the tendency of the multi-lamellar phases to transform to their energetically more

stable forms (as discussed earlier). The influence of relative humidity on the multi-lamellar phases, however, can be more pronounced in the presence of hygroscopic components in spray-dried detergent powders. Figure **4.3** a exhibits SAXS data from detergent granules produced from low-water content slurries containing sodium silicate with the SiO_2:Na_2O molar ratio of 1.6. At 33% RH the diffraction patterns were quite similar to those of silicate-free detergent powders subjected to 75% RH.

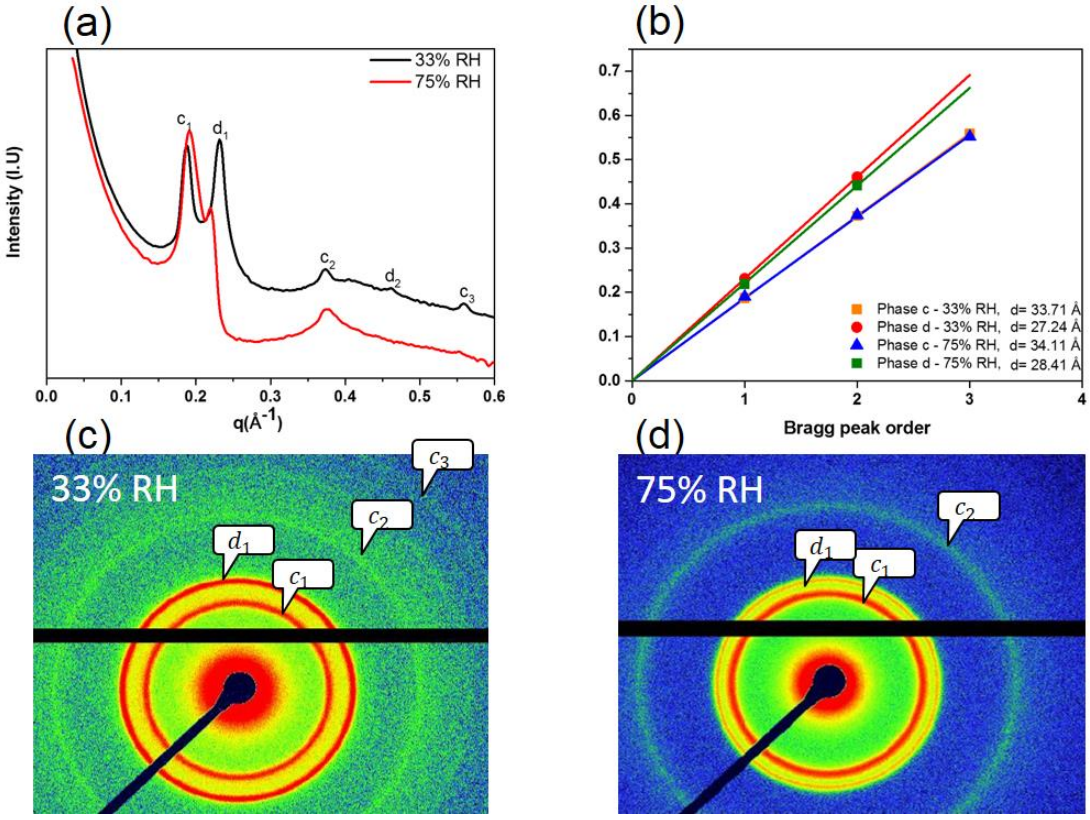

Figure 4.3 (a) Small-angle X-ray scattering (SAXS) patterns of spray-dried powders containing sodium silicate (1.6 SiO_2:Na_2O R). (b) Shows the lamellar *d*-spacings of phases c and d as determined from the slopes of Bragg peak position versus peak orders. (c) and (d) illustrate 2D SAXS images of spray-dried detergent powders stored at 33% and 75% RH respectively.

For these powders, the SAXS patterns show two distinct sets of diffraction peaks, which are in the *q* ratios of 1:2 and/or 1:2:3 with respect to the first order of diffraction peaks. This signifies the presence of a relatively uniform lamellar phase containing two co-existing phases with well-defined periodicities. The reason for the reduction in multiplicity of reflection peaks even at such relatively low RH value (33%) can be explained by the hygroscopic nature of sodium silicate

which consequently results in the adsorption of a larger quantities of water molecules, thereby destabilising the multi-lamellar phases *a* and *b* in spray-dried powders. In terms of hygroscopic characteristics, a great deal of research has previously been carried out on the adsorption and evolution of water layers on hydrophilic silicate species (Asay and Kim, 2005, Uchino et al., 1991, Warring et al., 2016). This point will be discussed later in ATR-IR results.

In contrast to free-silicate detergent powders, the overall lamellar spacing was found to increase when the powder was exposed to a higher humidity level, *i.e*., 75% RH. However, a more detailed picture of the humidity-induced structural changes can be obtained by probing the lamellar *d*-spacing and intensity of individual Bragg reflections. Considering 2D SAXS images, the first-order reflection of phase *d* can be detected as a diffused ring at 75% RH. This reduction in scattering intensity was also concomitant with an increase in its *d*-spacing value to 28.7Å. On the contrary, it was noticed that lamellar *d*-spacing of peak c_1 decreased to 33Å. These changes in lamellar *d*-spacings imply the approaching of the co-existing lamellar phases. This can also be observed in corresponding 2D SAXS images, showing the first-order rings (c_1 and d_1) coming close together. Therefore, it can be inferred that coexisting lamellae tend to merge together with increasing the relative humidity, until they reach an equilibrium structure.

In this study, no significant change in SAXS patterns of spray-dried detergent powders was observed when the initial water content of the detergent slurries was increased to ~ 62 wt%. Similarly, the overall *d*-spacing of the lamellar phases increased when the resulting powders were exposed at 75% RH. This concomitantly occurred with the disappearance of phases *a* and *b*. On the other hand, much like detergent powders containing sodium silicate with the SiO_2:Na_2O molar ratio of 1.6, the same humidity-induced structural changes were observed when the SiO_2:Na_2O molar ratio of sodium silicate was increased to 2.35. Due to the aforementioned similar behaviour, the SAXS results of detergent powders produced from high-water content slurries and those containing sodium silicate with the molar ratio of 2.35, are presented in Table **4.1**.

Table 4.1 The lamellar *d*-spacings determined from the slopes of Bragg peak positions versus peak orders.

		% RH	d(Å)
HW	Phase *a*	33	42.60
	Phase *b*	33	38.36
	Phase *c*	33	33.73
	Phase *c*	75	33.90
	Phase *d*	33	27.24
	Phase *d*	75	27.72
LW+2.35R	Phase *c*	33	33.54
	Phase *c*	75	34.02
	Phase *d*	33	27.01
	Phase *d*	75	28.16

HW = high-water content slurry; LW+2.35R = low-water content slurry containing 2.35 SiO_2:Na_2O R.

Specifically, the quantitative values obtained from diffraction peak positions, include the information about the bilayer thickness and the interlamellar water layer, together. However, it would be more interesting to attain detailed information about those two parameters separately. This can be better elucidated through the electron density calculations by Fourier reconstruction approach as described in the Materials and Methods section. To examine these humidity-induced structural changes, the lamellar phase *c* and *d* were selected for the electron density calculations, since their reflection peaks were common in all samples, had a sufficiently good resolution for curve fitting and were relatively stable even at 75% RH. For silicate-free samples, the electron density profiles obtained from Fourier analysis of Bragg reflection peaks are presented in Figure **4.4**. In these profiles the sulphonate head groups of NaLAS can be identified through the maximum of electron density map due to their close packing on the head group/water interface. The electron-rich head groups are separated by a low-density hydrocarbon region at which the electron density gradually decreases towards the bilayer centre and reaches its minimum value at

Z=0, where the terminal methyl groups of hydrocarbon chains meet each other. Also, a more electron-dense region, but yet markedly less than that of head groups, can be observed between the adjacent maxima which is associated with the electron density of water layer. Data on the values of bilayer thickness (d_{HH}), water layer thickness (d_W) are summarised in cartoons of lamellar phases in the figure. It can be seen that in phase *c* the average size of bilayer (d_{HH}) decreases slightly from 23.6 Å at 33% RH to 23.5 Å upon exposing at 75% RH Figure **4.4**b. This was concomitant with an increase in size of water layer thickness (d_W) at 75% RH. These results indicate a change from more ordered to a disordered conformation in the hydrocarbon chains of lamellar phase as the relative humidity increases. The conformational order of hydrocarbon chains, *e.g.*, the presence of *gauche* and *trans* conformations, will be discussed later in FTIR-ATR section. In general, the higher conformation disordering, *i.e.*, the presence of *gauche* conformers, has been suggested to results in a shorter hydrocarbon chain length (Nagle and Tristram-Nagle, 2000). The chain shortening has been reported in other studies on phospholipid bilayers, which was attributed to an increase in number of *gauche* conformers (Drasler et al., 2015). Much like the phase *c*, the same tendency in bilayer and water layer thicknesses were observed in the phase *d*. These structural changes resulted in a noticeable increase in lamellar *d*-spacings where the average sizes decreased to 33.94 and 26.72 Å for phases *c* and *d*, respectively (Figure **4.2**b).

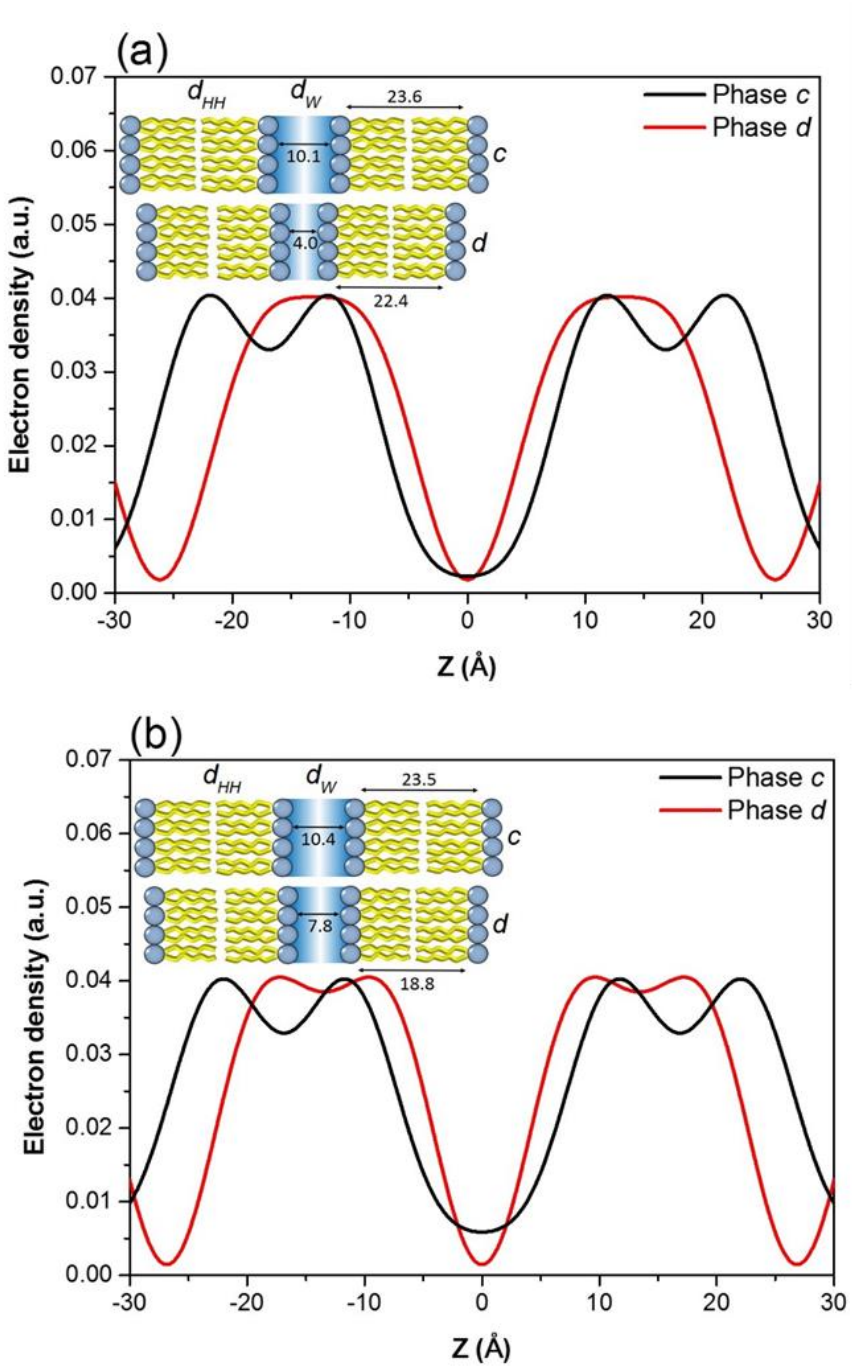

Figure 4.4 The electron density profiles of co-existing lamellar phases for silicate-free detergent powders stored at 33% RH (a) and their equivalents at 75% RH (b). The electron density profiles calculated from the phase combination of (-1, -1, +1). The electron rich head groups can be detected by the maximum of electron density profiles. The minimum electron density can be found at Z=0 where the hydrocarbon chains meet each other. The parameters of bilayer thickness (dHH) and water layer thickness (dW) are summarised in cartoons of lamellar phase.

In detergent powders containing sodium silicate, a greater degree of swelling in water layers and a greater reduction in bilayer thicknesses was observed at 33% RH. For these samples the

thickness of water layers in phase *c* at 33% RH was considerably larger than those of silicate-free powders even at 75% RH. This was expected since these powders was shown, according to our DVS measurements in Chapter 5, to have a relatively larger moisture content even at 33% RH than those in the absence of sodium silicate at the highest relative humidity, *i.e.*, 75% RH. Interestingly, it was also noticed that this increase in water layer thickness was concomitant with a noticeable increase in electron density within the hydrocarbon chain regions (Z=0) (Figure **4.5**a). It has been suggested that the increased amount of water of hydration leads to a reduction in lateral attractive interactions between head groups and hence their packing density. The increased separation of head groups may cause the hydrocarbon chains to minimize the energy by adopting an interdigitated arrangement in hydrocarbon chain where the tail ends of the surfactant molecules overlap (Kranenburg et al., 2004, Lewis et al., 2001). This conformation results in a close-packed arrangement of the chain ends in the centre of the hydrocarbon region which can be consequently reflected in electron density profiles. Therefore, it can be concluded that it is the existence of an interdigitated conformation in phase *c* that was responsible for the increased electron density at Z=0.

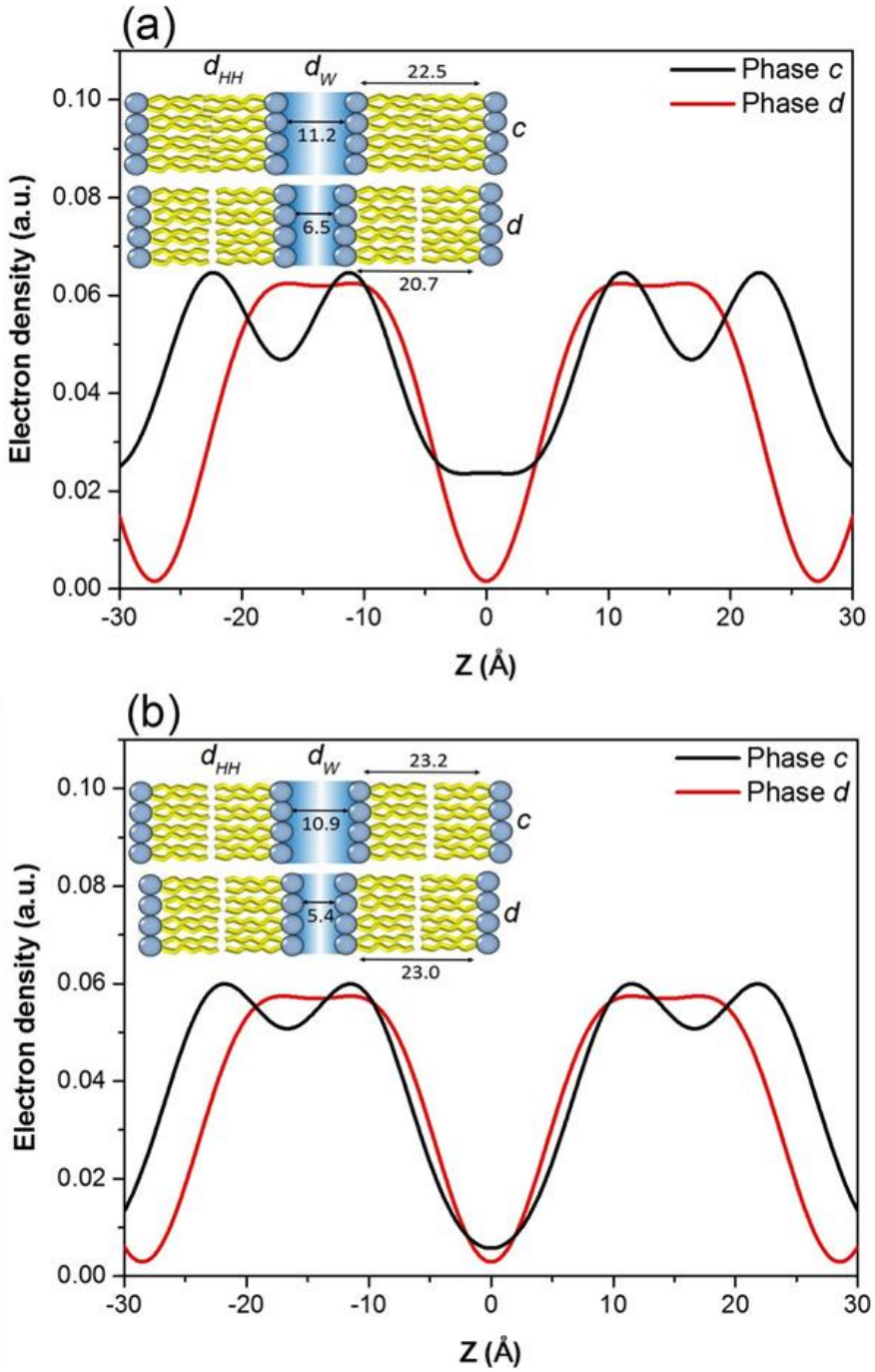

Figure 4.5 The electron density profiles of co-existing lamellar phases for spray-dried detergent powders containing sodium silicate, 1.6 R SiO_2:Na_2O, at 33% RH (a) and their equivalents at 75% RH (b). The electron density profiles calculated from the phase combination of (-1, -1, +1). The electron rich head groups can be detected by the maximum of electron density profiles. The minimum electron density can be found at Z=0 where the hydrocarbon chains meet each other. The parameters of bilayer thickness (d_{HH}) and water layer thickness (d_W) are summarised in cartoons of lamellar phase.

The behaviour of the lamellar phases was, however, more complex at 75% RH (Figure **4.5**b).

Considering phase *c*, it can be noticed that the overall lamellar periodicity was slightly increased

from 33.71 to 34.11 Å at 75% RH. This increase in *d*-spacing was also accompanied by a an increase in d_{HH} value to 23.20 Å and a decrease in the mean size of water layer to 10.90 Å. Furthermore, these conformational changes concomitantly occurred with a noticeable decrease of the electron density within the surfactant tail region at Z=0, signifying the straightening of the hydrocarbon chains. The deswelling of water layers on one hand, and a transition to a more stretched chain conformation on the other hand point to a change in balance of interactions between multi-lamellar phases. Since the water layer thickness in phase c is relatively large (~ 11 Å), the hydration repulsive force might have been less significant compared with other interbilayer interactions. Therefore, there might have been alterations in van-der-Waals forces and/or bending fluctuations, *i.e*., undulation forces which most probably account for the increased attractive forces and consequently contraction of the bilayers. It has been well demonstrated that the interactions between multi-lamellar phases can be largely modified by specific ion effects of salts of the Hofmeister series. For example, it has been shown that monovalent salts with water-structure-breaking effect, *e.g*., KCl and KBr, cause phospholipid bilayers to swell by interacting with their head groups and screening the van-der-Waals interactions (Pabst et al., 2007, Petrache et al., 2006). Alsop et al. (2016) investigated the influence of divalent metal ions, *e.g*., magnesium and calcium, on the swelling of hydration water layer and suggested that cations bind closer to the phospholipid head groups and are therefore more effective at reducing the dipole moment and hence screening van-der-Waals attractive forces. The above-mentioned salts of Hofmester series are referred to as chaotropes. In contrast to these ions, sugars and polyols, *e.g*., trehalose and glycerol, are classified as water-structure makers or kosmotropes which have a tendency to order water molecules around themselves leading to a substantial disruption of the tetrahedral order of water molecules (Shimizu and Matubayasi, 2014). Two main mechanisms have been proposed for these molecules which account for their effects on lipid bilayers. Lee et al. (1989) investigated the effect of trehalose on the bilayer structures and showed evidence for the inhibition of axial diffusion of phospholipid molecules in the presence of trehalose. This, according to the authors, was attributed to the sugar-head group hydrogen bonding. The formation of hydrogen bonds

includes the replacement of tightly bound water molecules by OH functional groups from the interface, which consequently leads to a reduction in surface dipole potential. Also, many studies have suggested that the direct interaction of OH compounds may involve intercalation of bound molecules into the polar head groups which therefore laterally expands the bilayer (Disalvo et al., 2008). Similarly, the provision of hydrogen bonding by other sugars, *e.g*., sucrose and glucose, has been demonstrated by Andersen et al. (2011) and Roy et al. (2016). The early authors, however; argued an additional effect of these compounds which largely arises from their kosmotropic nature by which the osmotic pressure is regulated. It has been hypothesized in multitudes of studies that sugar molecules are excluded from the interfacial region of bilayer membrane. According to the exclusion hypothesis, this gives rise to increasing build-up of osmolytes at the membrane interface, consequently establishing an osmotic gradient and thus extruding water from the bilayers. As a consequence, the head groups may undergo a conformational arrangement by which their effective area is reduced (Roy et al., 2016, Westh, 2008). Andersen et al. (2011) showed that the partial or preferential exclusion effects dominate at high sugar concentrations, while the head group-hydrogen bonding is of significant importance at low concentrations. The authors suggested that these two proposed mechanisms may overlap, and that the overlapping effect can be influenced by the concentration of OH compounds. As discussed earlier, silica species possess hygroscopic characteristics, and are capable of ordering water molecules around themselves (Asay and Kim, 2005, Leroch and Wendland, 2012), which implies their water-structure-making properties. Venugopal et al. (2011) studied the effect of varying concentrations of silica nanoparticles on the phase behaviour of lipid-based lyotropic liquid crystals and showed that lamellar *d*-spacing initially increased, reached a maximum value, with increasing the concentration of silica nanoparticles and then begins to decrease once the concentration exceeds a critical level. This reduction in lamellar *d*-spacing was explained by ordering of the water molecules around silica nanoparticles which consequently extrudes water from the bilayers. In the current study, a noticeable reduction in water layer thickness in the presence of sodium silicate, even though it should have increased due to a greater equilibrium

moisture content at 75% RH, implies a change in mechanism by which the kosmotrope, *i.e.*, sodium silicate, affect the bilayer interactions. As the relative humidity increases, the amorphous sodium silicate may undergo a transition from the glassy to rubbery state as a consequence of water plasticisation. This allows a greater number of hydrophilic silanol groups (Si-OH), which are buried inside the glassy sodium silicate, to be exposed to the surroundings which consequently enhances their hygroscopic characteristics. Furthermore, the exposure to a sufficiently high relative humidity may increase the relative populations of siloxide (SiO^-) and silanol (Si-OH) groups as a result of the hydroxylation of siloxane (Si-O-Si) bridges in sodium silicate, which subsequently cooperate in hydrogen bonding (Warring et al., 2016). Therefore, while the silicate-head group hydrogen bonding might have been the dominant effect of these kosmotropes at low relative humidity values (33% RH), leading to a greater degree of swelling, the hygroscopic characteristic of sodium silicate become of significant importance at higher relative humidity values.

4.2.2 FTIR measurements

As discussed earlier, the humidity-induced structural changes of multi-lamellar phases were more pronounced in the presence of sodium silicate. However, the effect of sodium silicate on the multi-lamellar phases can be two folds. It was shown that such binders have hygroscopic characteristics, thereby favouring the formation of more uniform lamellar phases by enhancing the equilibrium moisture content of the samples. On the other hand, these binders were found to have a significant effect on the bilayer interactions, leading to a reduction in water layer thickness. These structural changes might be due to an interaction between silicate species and surfactant head groups through direct hydrogen bonding or preferential exclusion (indirect interaction), which is probably enhanced with the increased water adsorption. In these series of experiment ATR-FTIR was used to gain a greater insight into the effects of sodium silicate itself on the structural changes of co-existing lamellar phases. These effects can be primarily studied by probing the vibrational

modes of hydrophilic head groups of NaLAS molecules. Infrared spectrum of detergent powders, in the absence of sodium silicate, can be seen in Figure **4.6**a.

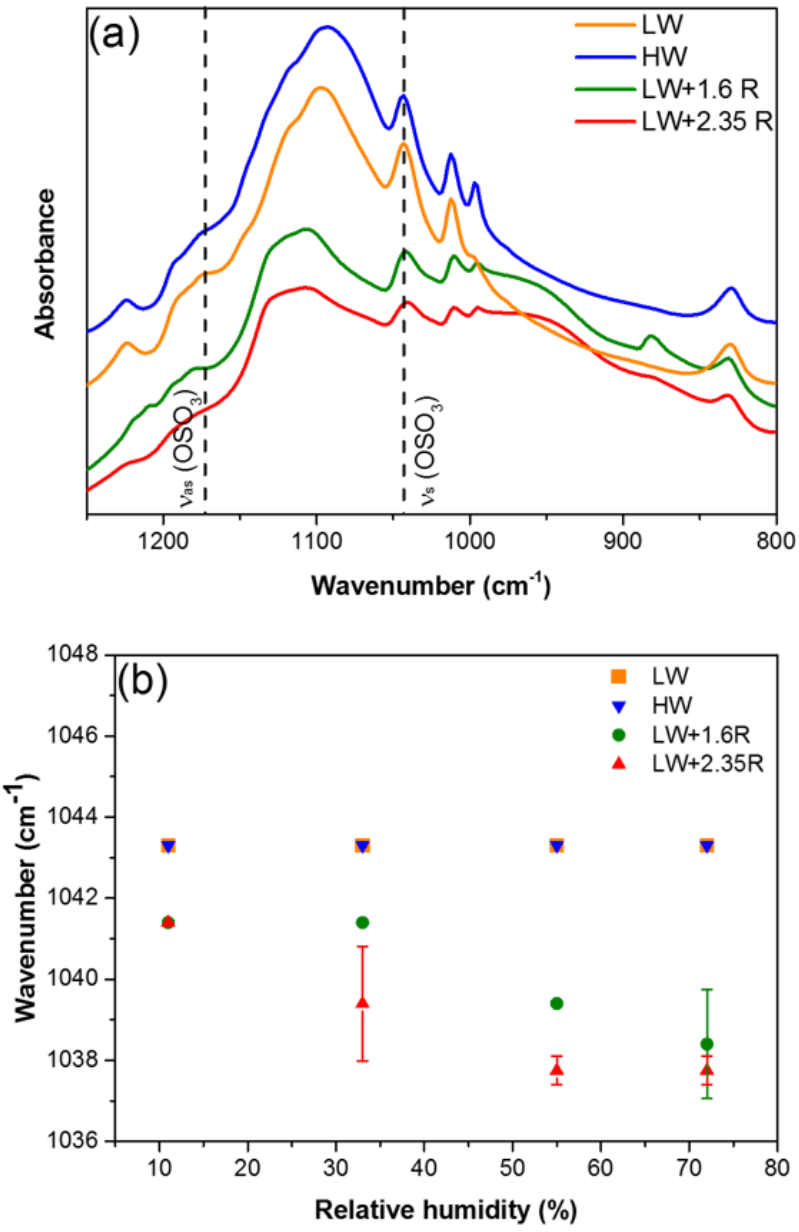

Figure 4.6 (a) Selected region (800-1200 cm^{-1}) of ATR-FTIR spectra for sprayed-dried detergent powders with different formulations. The dashed lines show the symmetric and asymmetric stretching vibrations of S-O bonds in NaLAS. (b) Humidity-induced variations in the wavenumber of the S-O symmetric stretching vibrations in spray-dried detergent powders.

The most intense peak at 1100 cm^{-1} is attributed to stretching vibrations of S-O bonds of SO_4^{-2} anion with a tetragonal symmetry T_d, in the lattice of the anhydrous sodium sulphate crystal (phase

V). Phase III, metastable sodium sulphate, can be identified by the appearance of a weak band around 997 cm^{-1}, suggesting the distortion of sulphate anion within the crystal lattice (Durie and Milne, 1978, Vidya and Lakshminarasappa, 2013). However, in the LAS structure, the symmetry of the SO_4^{-2} ion is reduced from T_d to monodentate sulphate coordination, *i.e.*, C_{3v} symmetry, due to the electrophilic aromatic substitution. This results in the appearance of two bands around 1043 and 1172 cm^{-1}, which are assigned to symmetric and asymmetric stretching vibrations respectively (Wang et al., 2012, Xu and Braterman, 2003). As the symmetric stretching band of S-O bonds is well resolved and sharp for all RH values, this mode was chosen to examine changes of hydrophilic head groups as a function of increasing relative humidity. Humidity dependence of this vibrational mode is shown in Figure **4.6**b for all spray-dried powders.

In the presence of sodium silicate, the peak of the symmetric stretching shifts down in frequency from 1041 cm^{-1} to around 1037 cm^{-1} at the highest relative humidity, suggesting a distortion of the molecular symmetry. This down-shift in frequency can be explained by the formation of hydrogen bonds between the hydrophilic sulphonate groups and water molecules, as one may expect. It has been suggested by several authors that hydrogen bond formation may diminish the strength of S-O bonds, leading to a down-shift in symmetric stretching band (Ohno et al., 2000, Wang et al., 2005). However, in the absence of sodium silicate, it can be seen that the symmetric stretching mode remains unchanged and no detectable peak shifts can be observed even at the largest RH value. This observation was in good agreement with the findings of Boissière et al. (2002) who suggested that the symmetric stretching vibration of S-O bonds is not affected by water layer thickness. The isolated silanol groups (Si-OH) have been shown to have a tendency to interact with polarizable objects such as benzene rings via hydrogen bonding (Onida et al., 2005). Evanson and Urban (1991) studied the interaction between sodium alkylbenzensulphonate and acidic copolymers and found evidence for hydrogen-bonding interactions between sulphonate groups of the surfactant and carboxylic groups of copolymer, which according to the authors, was attributed to the nucleophilic attack of sulphur atoms in sulphonate groups by the acidic hydrogen atom. Therefore, a possible explanation of the noticeable frequency shift can be due to a hydrogen

bonding between silicate species and sulphonate head groups. Figure **4.6**b shows a considerably larger downshift in frequency at 54 and 75% RH values indicating a greater degree of hydrogen bonding with sulphonate head groups. These results suggest that with increasing relative humidity, more and more silanol groups might have been exposed to the humid environment, most probably due to the hydroxylation of siloxane groups (Warring et al., 2016), leading to the enhanced hydrogen bonding. As mentioned earlier in the results of electron density profiles, the hydrogen bonding of kosmotropic compounds can be accompanied by some degree of intercalation into the membrane head groups which therefore leads to an increase in head group separation and consequently the interdigitation of hydrocarbon chains. This view is in line with the behaviour of lamellar phases, and more particularly phase *c*, in the presence of sodium silicate at 33% RH, showing the largest water layer thickness and a noticeable interdigitated bilayer. However, at 75% RH, the deswelling of water layers and a transition to a more stretched chain conformation can be explained by the water-structure-making effect of sodium silicates.

The structural evolution of the adsorbed water molecules with the variation of relative humidity can be studied by investigating the O-H stretching vibrational mode (Figure **4.7**). In the absence of sodium silicate, it can be observed that the most intense band at 3450 cm^{-1}, which is attributed to the multi-layer water, become considerably dominant over the O-H stretching region at 75% RH. This was also accompanied by a slight increase in population of free water molecules, *i.e.*, bulk water, at ~ 3617 cm^{-1} , while the high-energy peak of the bound water, *i.e.*, ice-like water, remained unchanged around 3200 cm^{-1}. Spray-dried detergent powders containing sodium silicate, however, showed remarkable changes in the spectral shape as follows: The shoulder at 3200 cm^{-1} grows in intensity even at a considerably low relative humidity, *i.e.*, 33% RH, becoming a well-defined strong band at 75% RH, suggesting the growth of an ice-like structure in water molecules. This was concomitant with a significant increase in the population of multi-layer water molecules. A decrease in the frequency of this component to ~ 3400 cm^{-1} correlates with a greater degree of hydrogen bonding. The appearance of a sharp peak at 3620 cm^{-1} in free water vibration region, can be assigned to vicinal silanol groups in sodium silicate (Warring et al., 2016). These

structural evolutions at the elevated relative humidity suggest that the water-structure-making effect of sodium silicate becomes dominant due, most probably, to the exposure of a larger number of silanol groups as a consequence of the increased hydration, which consequently alters the molecular configuration of water from a less ordered to a highly ordered ice-like structure. This can potentially explain the considerable reduction in water layer thickness of lamellar phases, phase *c*, at 75% RH.

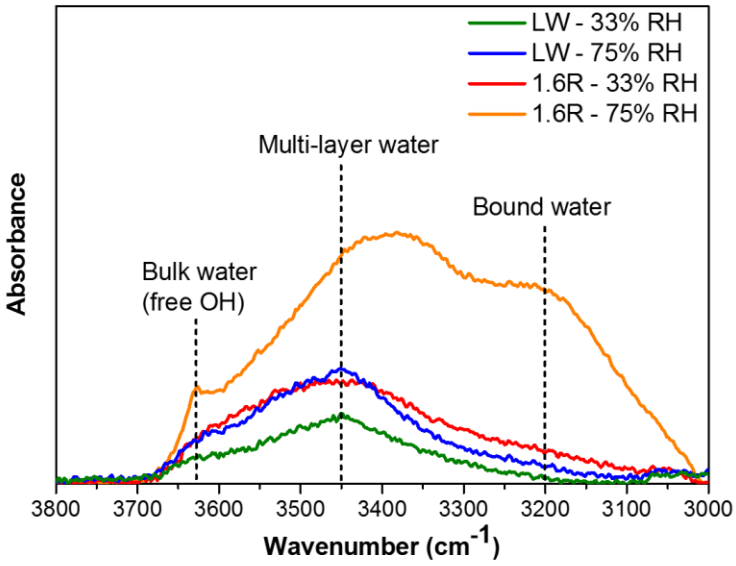

Figure 4.7 ATR-FTIR spectra (3000-3800 cm^{-1}) for sprayed-dried detergent powders, showing the structural evolution of water molecules at different relative humidity. The dashed lines show the O-H stretching vibration positions of bound water, multi-layer water and bulk water and/or free OH.

It was earlier demonstrated that the bilayer domains were highly influenced by the variation of relative humidity values. For example, from the analysis of electron density profiles, hydrocarbon chain domains were found to become shorter as the relative humidity increased. This chain shortening was attributed to the presence of gauche conformers arising from the loosening of the lateral packing of hydrocarbon chains. Furthermore, in spray-dried detergent powders containing sodium silicate this reduction in bilayer thickness was suggested to be accompanied by interdigitation of hydrocarbon chains. The influence of relative humidity on the lateral packing and conformational order of hydrocarbon chains can be studied by probing the CH_2 scissoring mode in the 1420-1475 cm^{-1} region. When hydrocarbon chains take a monoclinic, triclinic or

hexagonal subcellular packing, a singlet can only be observed in this region. However, it is well known that splitting of this mode into two components is a distinguishable signature of orthorhombic hydrocarbon chain packing. Also, the frequency and magnitude of this splitting has been suggested to be associated with the degree of lateral chain packing and side-by-side chain interactions (Boncheva et al., 2008). For crystalline n-alkanes in which all alkyl chains adopt an all-*trans* conformation, this mode is split into two distinct peaks at ~1463 and ~1473 cm^{-1} (Parikh et al., 1999).

The vibrational frequencies in the CH_2 scissoring region for the silicate-free powders can be observed in Figure **4.8**a. For detergent powders exposed to 11% RH a doublet appeared at 1458 and 1466 cm^{-1}. The observed doublet implies that the hydrocarbon chains of lamellar liquid-crystalline phases adopt an orthorhombic packing mode where there are two chains per unit cell. However, as the relative humidity increased, the lower frequency component of the correlation field splitting was less resolved, though the frequencies remained unchanged. These spectral features suggest that the hydrocarbon subcellular packing in lamellar phases has been distorted because of the weakening of lateral interactions between hydrocarbon chains, and the increases in number of gauche conformers (Lewis and McElhaney, 2007). It was earlier demonstrated that the exposure of silicate-free detergent powders to 75% RH led to the increasing water layer thickness (d_W) and to decreasing the bilayer domain (d_{HH}) of the lamellar phase. Therefore, these humidity-induced changes in CH_2 scissoring region can provide a good evidence supporting the reason for the reduction in bilayer thicknesses (d_{HH}) of lamellar phases upon exposure to the highest relative humidity, which was earlier explained by the increased conformational disorder as a consequence of the swelling and a reduction in lateral attractive interactions between head groups.

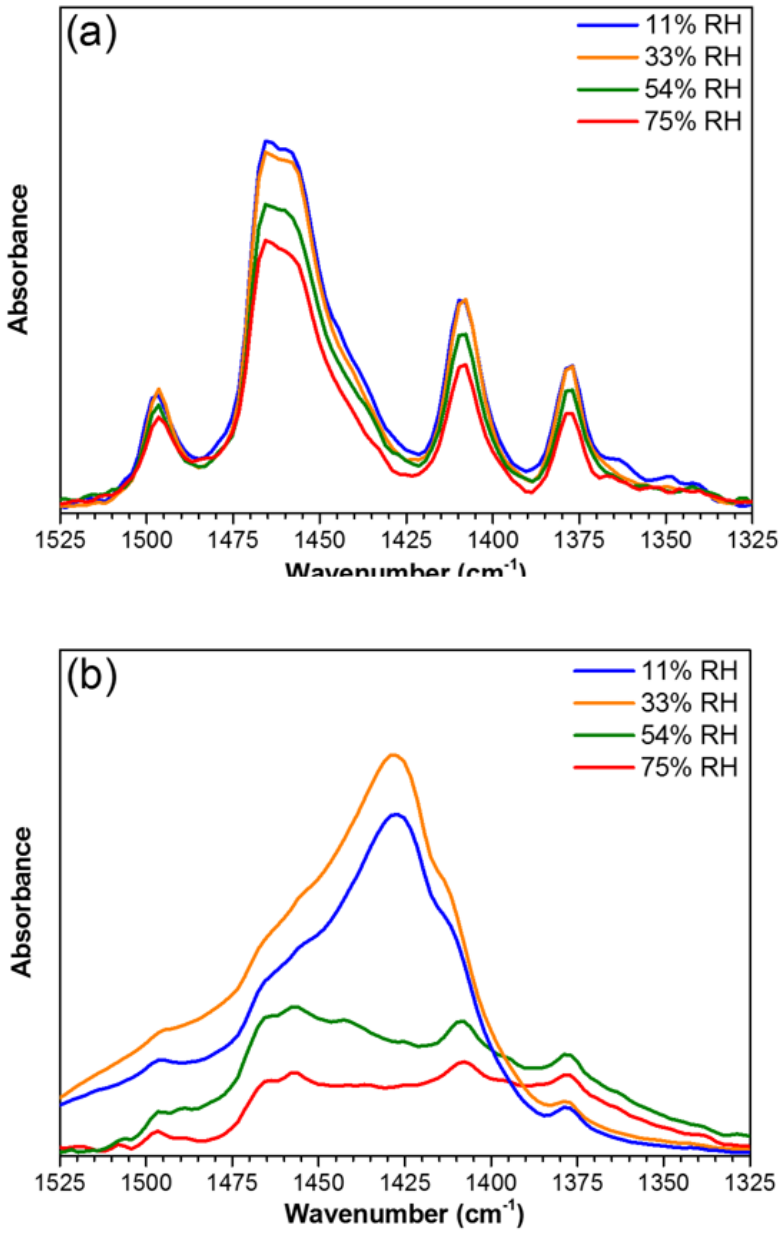

Figure 4.8 (a) Selected region (1525-1325 cm^{-1}) of ATR-FTIR spectra of the CH_2 scissoring vibration for silicate-free detergent powders at different relative humidity. (b) CH_2 scissoring vibration for spray-dried detergent powders containing sodium silicate at different relative humidity.

Interestingly, the vibrational behaviour of hydrocarbon chains in the presence of sodium silicate was quite complex. Figure **4.8**b illustrates the infrared spectra of spray-dried detergent powders containing sodium silicate. It was noticed that at 11% RH, the components of the split scissors band appeared as weak shoulders on a sharp peak centred at 1429 cm^{-1}. At a higher RH value

(33% RH), the doublet are more attenuated and are barely discernible. These observations suggest that the hydrocarbon chains are no longer in their perfect orthorhombic arrangement. However, it can be seen that with the increase of relative humidity, the predomination of the peak at 1429 cm^{-1} remarkably diminished, while the scissoring doublet at 1458 and 1466 cm^{-1} became sufficiently well resolved. These spectral features became of significant interest as viewed in conjunction with the results of electron density profiles suggesting the occurrence of interdigitation at 33% RH and the straightening of hydrocarbon chains at 75% RH.

The presence of an unusual low-frequency band around 1420 cm^{-1}, within the CH_2 scissoring region of infrared spectra, was previously reported by Lewis and McElhaney (1993) in mixed interdigitated gel phases of phospholipid bilayers, which was attributed to the conformational difference between the esterified acyl chains. Therefore, in the current study, it can be inferred that the observed spectroscopic changes in the presence of sodium silicate can be associated with interdigitated hydrocarbon domains in lamellar phases, though the resulting subcellular packing mode cannot be readily interpreted due to the existence of a very limited range of known modes for lateral arrangement in spectroscopic data (Lewis and McElhaney, 2013).

While spectroscopic features of CH_2 scissoring vibrations are very sensitive indicators of the lateral packing of hydrocarbon chains, the frequency position of C-H stretching vibrations monitors the conformational order of hydrocarbon chains. The C-H aliphatic stretching frequency occurs in the range of 2840-3000 cm^{-1} where the spectra are dominated by symmetric and asymmetric stretching vibrations of methyl groups ($-CH_3$) and methylene groups ($-CH_2$) of the alkyl chains. The ratio of intensities and positions of these bands are extensively used to characterize disorder of hydrocarbon chains. Considering the infrared spectra of spray-dried detergent powders in Figure **4.9**a, two sharp peaks can be observed around 2854 and 2917 cm^{-1} which are produced by symmetric and asymmetric stretching vibrations of methylene groups of NaLAS, while two relatively weak peaks around 2956 and 2871 cm^{-1} are attributed to stretching vibrations of terminal methyl groups of the surfactant (Watry and Richmond, 2000). In general, for highly crystalline n-alkanes in which all alkyl chains adopt an all-trans conformation, the

symmetric and asymmetric stretching vibrations occur in the range of 2846-2850 and 2916-2920 cm^{-1} respectively. It is known that with increasing the conformational disorder, as it can be seen in liquid phases of n-alkanes, these vibrational modes shift to higher wavenumbers, *e.g.*, 2856-2858 and 2924-2928 cm^{-1} for symmetric and asymmetric stretching vibrations. In the current study, infrared spectra of all detergent powders exhibited a vibrational band at 2854 cm^{-1} corresponding to the methylene symmetric vibration, which is between those of crystalline and liquid n-alkanes. Moreover, for all detergent powders the position of this vibrational band was found to remain unchanged upon exposure to changes in relative humidity.

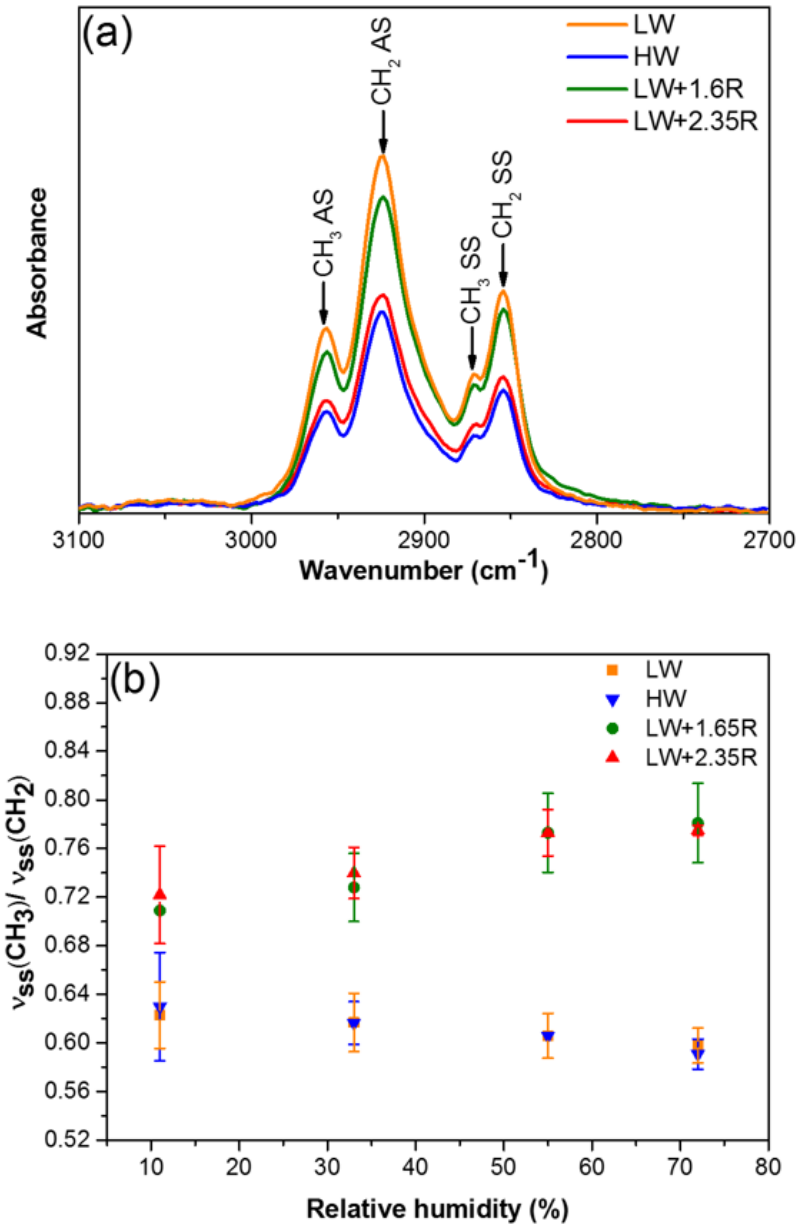

Figure 4.9 (a) Selected region (3100-2700 cm^{-1}) of ATR-FTIR spectra of the C-H stretching vibrations for a typical sample stored at 11% RH. (b) Humidity-induced variations of the intensity ratio of the methyl ($-CH_3$) stretching mode peaks to the methylene ($-CH_2$) stretching mode peaks for spray-dried detergent powders.

The intensity ratio of symmetric stretching vibrations of methyl group to that of methylene group is known to be sensitive to the conformational order of hydrocarbon chains. For crystalline n-alkanes this value is around 2.0, while it decrease to ~0.7 for their liquid counterparts. The variation of this ratio at different relative humidity values are displayed in Figure **4.9**b. For

silicate-free detergent powders exposed to 11% RH, the mean intensity ratios, $I_{2880}/I_{2850,}$ were ~0.62. However, it can be observed that the intensity ratio decreases with increasing the relative humidity value. This was expected since the swelling of lamellar phases results in a reduction in lateral attractive forces between surfactant head groups, thereby increasing the conformational disorder of hydrocarbon tails as discussed earlier. Surprisingly, spray-dried detergent powders containing sodium silicate showed a relatively larger intensity ratio at 11% and 33% RH as compared with those in the absence of sodium silicate. The reason that the exposure of these samples to 33% RH resulted in a considerably larger intensity ratio ~ 0.74, even though it should have increased the conformational disorder due to the greater degree of swelling as was reflected in electron density profiles, can be explained by the existence of interdigitated hydrocarbon domains where side-by-side chain interactions can be relatively larger at the extremities of the hydrocarbon tails (Venkataraman and Vasudevan, 2001). Additionally, the increased ordering can also be partially attributed to the localization of head groups to silica species through hydrogen bonding which therefore may decrease the conformational mobility of hydrocarbon chains due to a steric effect (Conboy et al., 1997, Lee et al., 1989). At higher relative humidity, however; it was noticed that the intensity ratio was increased, signifying the increases in hydrocarbon chain lengths as reflected in Figure **4.5**b. It is observed that in the presence of sodium silicate the mean d_{HH} value of lamellar phases significantly increases at 75% RH, while at the same relative humidity d_{HH} value decreases in silicate-free detergent powders. This was expected since as water-structure-making effect of sodium silicate becomes dominant at higher relative humidity value (RH > 33%), the hydration water is excluded from the lamellar phase, leading to a reduction in separation of head groups which consequently results an increase in hydrocarbon chain conformational order.

4.3 Conclusion

Several sets of lamellae were detected in spray-dried detergent powders. This was explained by the presence of domains of different compositions, which subsequently swell and/or dehydrate to

different extents upon hydration or dehydration. The relative humidity was found to be a critical factor affecting the coexisting lamellar polymorphs. The exposure of these samples to a high relative humidity level resulted in a reduced number of coexisting phases. This was accompanied by a transition from an orthorhombic packing mode of hydrocarbon chains to their less ordered arrangement in lamellar phases. As the relative humidity increases, the swelling of lamellar phases results in the shortening of hydrocarbon chains which, therefore, decreases the population of those polymorphs having more trans conformers and larger *d*-spacing values. Consequently, this gives rise to the formation of a narrower *d*-spacing range and hence the merging of Bragg diffraction peaks into fewer sets of peaks. For spray-dried detergent powders containing sodium silicate, the fewer sets of lamellae as compared with those free-silicate samples, even at a low RH value (33% RH) was partially attributed to the hygroscopic nature of sodium silicate, leading to a greater moisture content in spray-dried detergent powders. Additionally, the provision of hydrogen bonding by silicate species was suggested to be a contributing effect for the enhanced separation of head groups. The lamellar phase of these samples were found to possess the largest water layer thickness (d_W) at 33% RH. The greater degree of swelling as a consequence of the increased separation of head groups, also caused hydrocarbon chain interdigitation in bilayer domain.

For these samples, a noticeable reduction of d_W value upon exposure to a considerably higher relative humidity value (75% RH) was attributed to the kosmotropic nature of sodium silicate by which the osmotic pressure is regulated. It was hypothesized that a transition from the glassy to rubbery state at such humid conditions may have resulted in the exposure of a greater number of buried silanol groups whereby a larger osmotic gradient is established and thus extruding water from the bilayers. In other words, while at low relative humidity the hydrogen bonding properties of sodium silicate might have been of significant importance, their kosmotropic effect become predominant at higher RH values.

Chapter 5 The Evolution of surface microstructure and moisture sorption characteristics of spray-dried detergent powders

In previous chapter the relative humidity value of the surroundings was found to be a critical factor affecting the coexisting lamellar polymorphs. Additionally, from the technological point of view, detergent powders are known to have a tendency to cake and agglomerate during the storage at humid conditions. Several mechanisms have been proposed to the powder caking phenomenon, which mainly include the van der Waals forces, electrostatic forces, liquid bridge forces, surface roughness and plastic deformation (Zafar et al., 2017). However, at high levels of relative humidity the stickiness and caking of powders were shown to be associated with the formation of liquid bridges formed between the powders (Peleg, 1977). Therefore, water uptake may adversely affect the functional properties of these powders during storage or transport to the customer if the environmental RH is above a critical point. Water sorption isotherms are widely used to describe the interactions between materials and water vapour molecules, and to predict product stability during the storage. The sorption behaviour of food and pharmaceutical powders prepared by spray drying, has been extensively reported in many studies. However, studies on detergent products are limited. Therefore, the objectives of this chapter were to determine the moisture sorption isotherms of the spray-dried detergent powders, and to evaluate the suitability of three common mathematical models for prediction of the experimental data. This chapter deals with the influence of the granule morphology and the addition of a hygroscopic binder, i.e., sodium silicate, on the water sorption properties of spray-dried powders. The moisture sorption isotherms of the powders were gravimetrically determined using a dynamic vapour sorption (DVS) technique. The experimental sorption data was fitted to three mathematical model: Brunauer–Emmett–Teller (BET), Guggenheim–Anderson–de Boer (GAB) and Oswin. Furthermore, the effect of water sorption as a function of the relative humidity on microstructural evolution of the detergent powders was examined using x-ray diffraction studies, microscopic observations and ATR-IR spectroscopy.

5.1 Materials and methods

5.1.1 Materials

Detergent granules were produced with a pilot-scale spray dryer in Procter & Gamble Newcastle Innovation Centre as it was described earlier in Chapter 3. The resulting detergent powders were subsequently sieved and a sieve fraction of 300-350 μm, which was approximately representative of the mean particle size, was chosen for the experiments. Prior to the microscopic observations, ATR-IR and XRD measurements the sieve fractions, 5.0 g, were stored in desiccators with a specific relative humidity, *i.e.*, 11, 33, 54, and 75%, created using saturated solutions of lithium chloride, magnesium chloride, magnesium nitrate hexahydrate, and sodium chloride respectively, at 21 ±1°C for four weeks.

5.1.2 X-ray diffraction (XRD) measurements

In these series of experiments, the existence of polymorphs of anhydrous sodium sulphate was investigated by X-ray diffraction, XRD, (D8 Advance, Bruker AXS, Karlsruhe, Germany) using a Cu Kα X-ray source. The samples were packed tightly in a sample holder with a 2mm indent. The scanning region of the diffraction angle was between 10 -70° (2θ).

5.1.3 Microscopic observations

The surface microstructure of the detergent powders was examined using SU8230 Hitachi scanning electron microscopy (SEM). Prior to SEM observation, sputter coating was conducted to form an ultra-thin coating of gold which inhibits charging during SEM examination.

5.1.4 Micro-computed tomography (Micro-CT) scanning

The internal structure of spray-dried detergent powders were qualitatively examined using a Phoenix Nanotom CT scanner (GE Measurement and Control, US). This provides good insight into the distribution of high density and low density phases within the powder. The high density regions are due to initially undissolved inorganic salts, *i.e.*, sodium sulphate crystallites, and low

density regions are pores and vacuoles. Individual detergent granules (300-350 µm) were placed on a double-sided tape and mounted on a rotating stage between an X-ray source and X-ray detector. Samples were then scanned in the full range of 0–360°. A series of x-ray micrographs were obtained and three-dimensional volumes were reconstituted using the VGStudio software package. The spatial resolution, *i.e*., voxel size, of the reconstructed 3D images was 1.76 µm. To improve the 3D data visualisation, a number of different image processing tools including filtration and segmentation, were applied to the X-ray micrograph data using the Avizo software package. A non-local means filtration was applied to the grey scale projections to reduce image noise. The segmentation of highly dense regions, corresponding to initially undissolved sodium sulphate particles, from the matrix was conducted using an interactive thresholding tool in Avizo.

5.1.5 ATR-IR measurements

The molecular configuration of water molecules adsorbed by spray-dried powders as a function of relative humidity, was evaluated with a Thermo Fisher Scientific Nicolet iS10 FT-IR spectrometer using the attenuated total reflection (ATR) method. The detergent powders were mounted on the top of a high-refractive index ATR crystal and then slightly pressed by a pre-mounted sample clamp. The infrared information was obtained by measuring the infrared light which is entirely internally reflected in the medium of ATR crystal. Background corrected spectra were measured over a range of 550-4000 cm^{-1} with 4 cm^{-1} resolution.

5.1.6 Dynamic vapour sorption

The dynamic sorption behaviour and isotherms of spray-dried detergent powders were gravimetrically determined using a dynamic vapour sorption (DVS) technique (DVS Advantage, Surface Measurement Systems, Middlesex, UK). The instrument can be considered as a temperature-controlled incubator consisting of ultra-sensitive microbalances which enable measuring the highest resolution changes in sample mass. The samples were loaded in a sample pan (100 µl) and an empty pan was used as a reference. The instrument is fully automated, allowing pre-programming of sorption and desorption isotherms. The DVS profiles were obtained

by raising humidity from 0% to 70% RH and back to 0% RH in increments of 10% RH steps. At each RH step the sample was allowed to reach a gravimetric equilibrium, when the change in mass (dm/dt) is lower than 0.002 mg/min, and then the sample progressed to the next RH step.

The sorption isotherms were modelled using the Brunauer–Emmett–Teller (BET), Guggenheim–Anderson–de Boer (GAB) and Oswin equations. The BET equation is an effective method for estimating the amount of water molecules bound to specific hydrophilic groups in dehydrated multi-component systems. This model has been successfully applied to sorption of water by foods and pharmaceuticals, even though its application is restricted to a limited range of water activities (~ 0.05-0.45)(Basu et al., 2006). This restriction is due to deviation of the linearity of BET graphs at larger relative humidity values. The BET equation can be written as follows:

$$M_e = \frac{M_b C a_w}{(1- a_w)[1+ (C-1)a_w]} \qquad (4)$$

$$\frac{a_w}{(1-a_w)M_e} = \frac{1}{M_b C} + \frac{C-1}{M_b C} a_w \qquad (5)$$

Where M_e is the equilibrium moisture content (dry basis), M_b is the BET monolayer moisture content (dry basis), representing the amount of water molecules which are tightly bound to the hydrophilic and polar groups, a_w is water activity, and C is a constant related to the affinity of the solid components with the adsorbate, *i.e.*, water molecules, and hence to the heat of sorption of monolayer region. The GAB equation, with a sound theoretical foundation, is a developed version of BET model (Lewicki, 2009). This model is one of the most widely used equations to describe the experimental adsorption isotherms of water in a wide range of water activities from 0 to 0.9. The GAB equation can be expressed as follows:

$$M_e = \frac{M_g C K a_w}{[(1-Ka_w)(1-Ka_w+CKa_w)]} \qquad (6)$$

Where, once again, M_e is the equilibrium moisture content, M_g is the GAB monolayer moisture content, a_w the water activity, C the constant related to the heat of sorption of water molecules adsorbed as a monolayer, and K the correcting constant which takes into account the energies of

interaction between the first and following water layers. The model parameters can be obtained by rescaling the above equation in a second-order polynomial form, of the GAB equation (Kelly et al., 2016, Timmermann et al., 2001) (Eq. 7):

$$\frac{a_w}{M_e} = \alpha a_w^2 + \beta a_w + \gamma \qquad (7)$$

Parameters of the above quadratic expression, *i.e.*, α, β and γ, can be determined by non-linear regression analysis of the experimental values of a_w/M_e as a function of a_w. From the values of α, β, γ obtained in their way the original GAB parameters can be determined through the following equations:

$$M_g = \frac{1}{\sqrt{\beta^2 - 4\alpha\gamma}} \qquad (8)$$

$$K = \frac{\beta - \left(\frac{1}{M_g}\right)}{-2\gamma} \qquad (9)$$

$$C = \frac{1}{M_g K \gamma} \qquad (10)$$

The Oswin model is a two-parameter empirical model which is a series expansion for the sorption isotherms having sigmoidal-shaped profile. The equation has been successfully used for many food products containing polymeric compounds, *e.g.*, starch, protein, and can be written as follows (Labuza and Altunakar, 2007):

$$M_e = A\left(\frac{a_w}{1 - a_w}\right)^B \qquad (11)$$

Where A and B are model parameters, M_e is the equilibrium moisture content and a_w is the water activity. The parameters were determined by plotting a log (M_e) versus log (a_w/1-a_w).

The accuracy of prediction of each sorption model was evaluated by calculating the mean percentage deviation modulus (*E*). *E* value correlates the predicted and experimental data, and is defined as

$$E = \frac{100}{N} \sum_{i=1}^{n} \left| \frac{m_{ei} - m_{pi}}{m_{ei}} \right| \qquad (12)$$

In the above equation m_e is the experimental moisture content, m_p the predicted moisture content and N is the number of experimental data used in the analysis. According to the literature, a sorption model is considered acceptable for practical purposes if the *E* values are lower than 10% (Kaymak-Ertekin and Gedik, 2004, Peng et al., 2007). The coefficient of determination (R^2) was used to evaluate the goodness of fit of each sorption model (Bonner and Kenney, 2013). The coefficient of determination can be defined as

$$R^2 = 1 - \frac{\sum (m_{ei} - m_{pi})^2}{\sum (m_{ei} - \bar{m}_{ei})^2} \qquad (13)$$

5.2 Results and discussion

5.2.1 Microscopic observation

It was previously shown that low-water content slurries, containing NaLAS and sodium sulphate, resulted in the formation of spherical granules with smooth characteristics. In these series of experiments the influence of relative humidity on the structural evolution of the surface of spray-dried detergent powders during storage was examined. Figure **5.1**a and b, illustrates two distinct morphologies on the particle surface as a function of relative humidity in surrounding air. The freshly-produced granules appeared to be mainly covered with a non-crystalline and smooth skin, although there may also be some shallow wrinkles on the surfaces. Figure **5.1**a illustrates the surface microstructure of a typical granule after 4 weeks of storage at 33% RH. Microscopic observations showed no significant structural changes on the particle surface, upon the exposure to a higher relative humidity value (54% RH). However, exposure to a relatively higher partial water vapour pressure (75% RH), resulted in a considerable change in surface morphology (Figure **5.1**b). Considering the micrograph, it appears that the non-crystalline matrix might have receded inward where embedded small-sized crystals of sodium sulphate become apparent, even though the crystals are still localized under the surface. However, SEM of spray-dried detergent

powders produced from high-water content slurries showed that they possess a crystalline surface. These powders were stable and did not develop any noticeable humidity-induced structural change at 33% (Figure **5.1**c) and 54% RH. Upon exposing of spray-dried powders to 75% RH, the surface of powders became rougher and a considerable amount of sodium sulphate crystals was observed on the surfaces (Figure **5.1**d). The reason for the differences between surface evolutions of both above-mentioned detergent powders can be explained by the fact that they differ in matrix composition. In previous chapter, we showed that initial water content of the slurries had a great influence on the matrix composition. According to the quantities of undissolved sodium sulphate obtained from x-ray microtomography technique, a higher water content (63 wt%) led to a significantly smaller quantity of undissolved sodium sulphate (~23 wt%) in detergent powders as compared with the amount of undissolved sodium sulphate (~65 wt%) in detergent powders produced from low-water content slurries. Based on these results the matrix of detergent powders produced from low-water content slurries, was estimated to be rich in NaLAS surfactant (56 wt%), while the NaLAS content of the matrices significantly decreased to 20 wt% in the case of the high water content slurry, leading to a more crystalline appearance in resulting detergent powders.

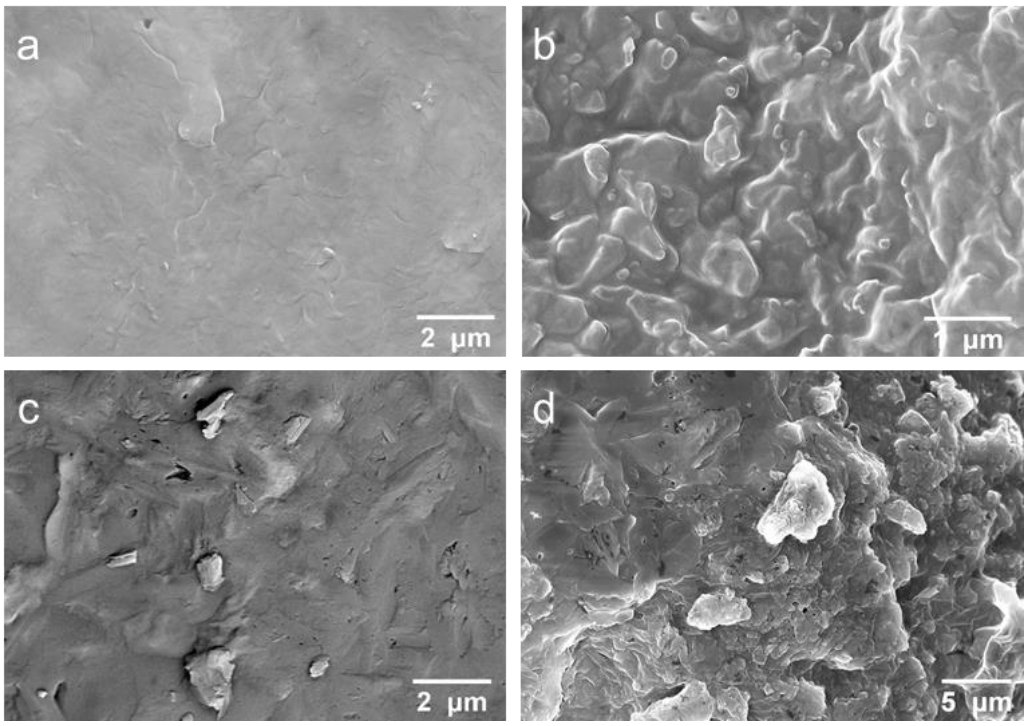

Figure 5.1 High-magnification SEM micrographs of spray-dried detergent powders. (a) A typical surface morphology of a detergent granule produced from low-water content slurries, stored at 33% RH, and its equivalent at 75% RH (b). (c) shows a typical crystalline surface of a detergent granule produced from high-water content slurries, stored at 33% RH, and (d) illustrates the microstructural evolution of these powders as a consequence of the increased relative humidity (75% RH).

For freshly-produced detergent powders containing sodium silicates, two distinct morphological features can be observed on the granule surface. In these powders some regions (Figure **5.2**a) are relatively smooth and similar to those observed in spray-dried powders produced from low-water content, nil-silicate slurries, other regions (Figure **5.2**b) have a crystalline appearance, and a considerable amount of nano-sized prismatic crystals can be observed on the surface. Upon exposing of these powders to 33% RH, the morphological characteristics of both regions remained unchanged during the storage. However, unlike the nil-silicate formulations, spray-dried powders containing sodium silicate were susceptible to humidity-induced structural changes at 54% RH. As seen in Figure **5.2**c, at 54% RH, some deep as well as shallow wrinkles/folds can be observed on the surface. Additionally, it was found that the crystalline regions have undergone a noticeable morphological change at this value of relative humidity (Figure **5.2**d). The initial nano-sized prismatic crystals were transformed to larger crystals signifying a moisture-induced crystal

growth of sodium sulphate (Linnow et al., 2006). Comparing the surface evolution of these powders with those in the absence of sodium silicate, it can be concluded that it is the presence of sodium silicate that increases the susceptibility of detergent powders to the surface structural changes at 54% RH. A possible explanation for this observation may be due to the enhanced water sorption of detergent powders arising from the hygroscopic nature of sodium silicates. In this study, the influence of sodium silicates on the structural profile of the adsorbed water molecules in spray-dried detergent powders has been studied with a FTIR spectroscopy, and will be discussed in section 5.2.4.

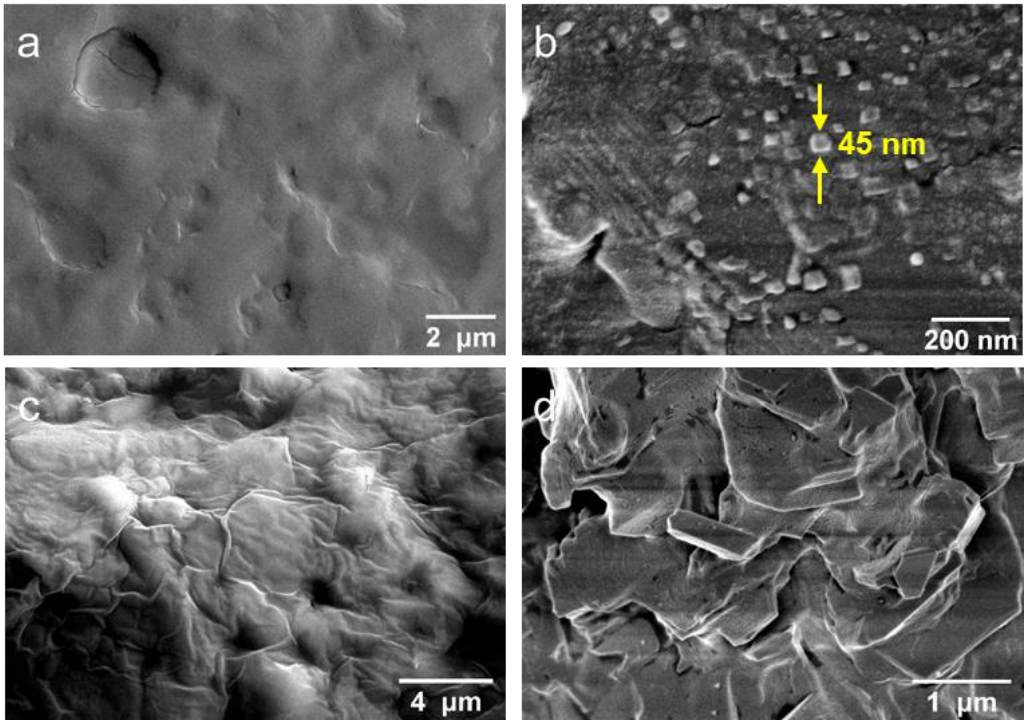

Figure 5.2 High-magnification SEM micrographs of a spray-dried detergent granule containing sodium silicate showing two distinct morphological features, i.e., smooth regions (a) and crystalline regions (b), at 33% RH. The smooth regions showed some deep, as well as shallow wrinkles/folds during the storage at 54% RH (c). In (d) the transformation of nano-sized crystals of sodium sulphate to relatively larger crystals, at 54% RH, is quite noticeable.

Figure **5.3**a displays the morphological features of spray-dried powders containing sodium silicate, exposed to a higher relative humidity value (75% RH). It can be seen that relatively large crystalline structures, in comparison to the overall granule diameter, exist on the surfaces. Returning to the morphological properties of these powders in Chapter 3, no evidence was found

for the presence of such crystalline structures on the granule surface. Figure **5.3**c shows that the granule surface is progressively covered by small prismatic crystals. Also, interestingly SEM micrographs revealed the presence of a distinctly different crystal habit on the surfaces that was quite different from those observed in other stored powders. Figure **5.3**f depicts the morphology of these crystals. The morphology of these elongated crystals correspond more closely to that of mirabilite, *i.e.*, sodium sulphate decahydrate, compared with the crystal habits reported in other works (Atzeni et al., 1995, Rodriguez-Navarro et al., 2000) showing efflorescence of thin, straight whiskers. Wide-angle x-ray diffraction (WAXS) was therefore carried out to reveal the nature of these nano-structures.

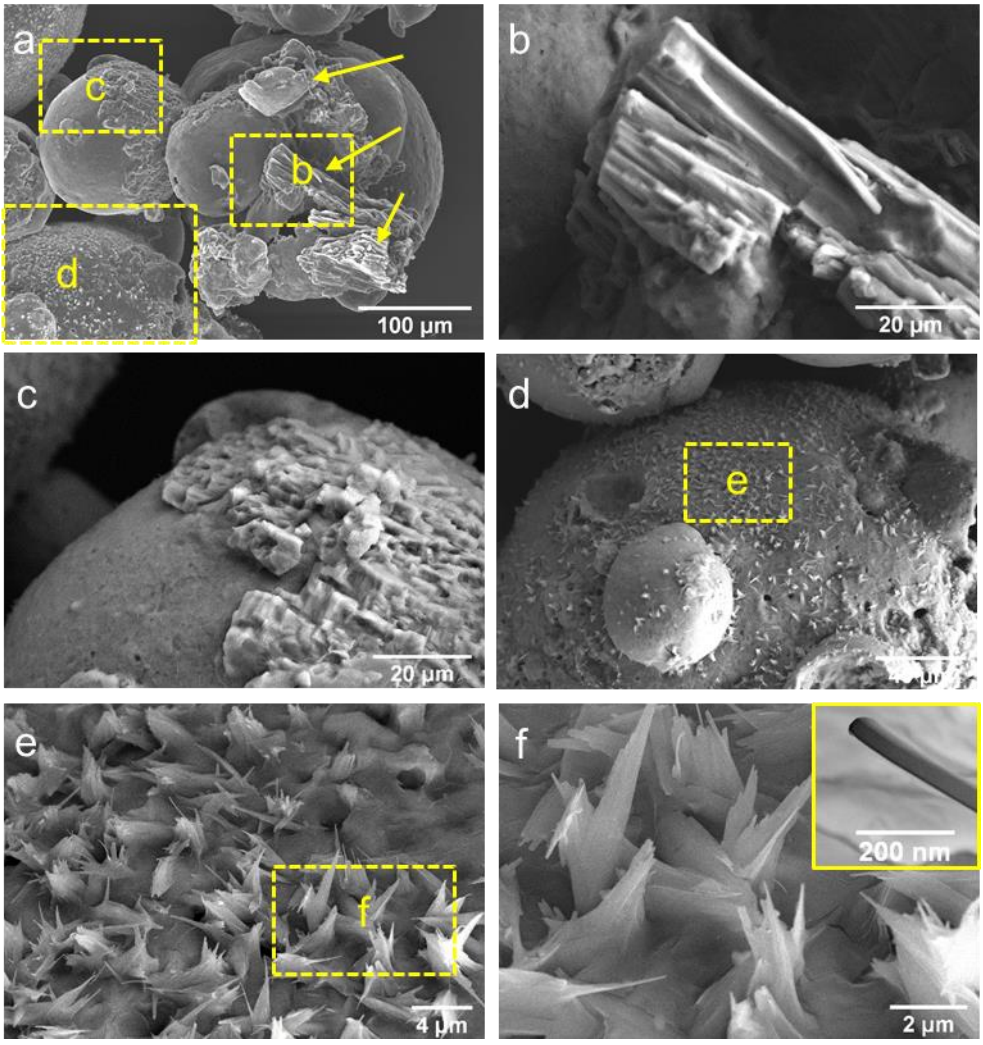

Figure 5.3 SEM micrographs of a typical detergent granule containing sodium silicate with the SiO_2:Na_2O molar ratios of 2.35, stored at 75% RH. The arrows highlight the presence of relatively large crystalline structures on the granule surface (a). Figure (b) shows the presence of a typical large crystalline structure. Figure (c) shows the growth of sodium sulphate crystals covering the granule surface. The emergence of a new crystal habit (d), also shown in higher magnification images (e) and (f), is clearly visible. This illustrates the presence of bundles of elongated crystals and morphological characteristic of a single crystal (see insect).

5.2.2 Wide-angle x-ray diffraction measurements (WAXD)

In this section the influence of relative humidity on the stability of Na_2SO_4 polymorphs is evaluated. The XRD patterns of freshly-produced detergent powders were found to be dominated by the presence of sodium sulphate, and all detergent powders showed well-defined, sharp diffraction peaks which are characteristics of well-ordered crystal lattices of sodium sulphate (Figure **5.4**). Two stable polymorphs of sodium sulphate, *i.e.*,Na_2SO_4 (V) and Na_2SO_4 (III), were

identified in spray-dried detergent powders. In general, these anhydrous polymorphs have been shown to crystallize out of a supersaturated solution of sodium sulphate upon evaporation among which Phase V (thenardite) is considered to be the most stable anhydrous phase in room temperature (25 ˚C). Phase Na_2SO_4 (III), which is known to be a metastable phase, can remain stable for considerable periods of time, at room temperature and dry conditions. However, this polymorph may undergo a phase transition at enhanced relative humidity and turns into phase V (Rodriguez-Navarro et al., 2000, Linnow et al., 2006).

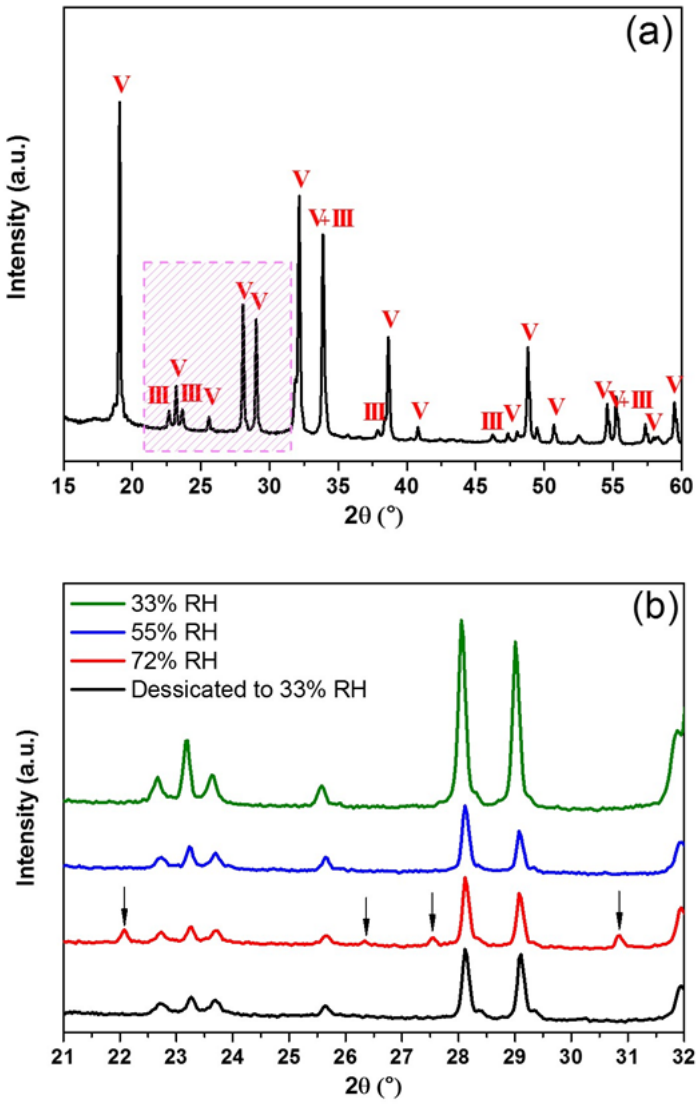

Figure 5.4. (a) A typical wide-angle x-ray diffraction (waxs) pattern of spray-dried powders containing sodium silicate 1.6 SiO2:Na2O R, showing the presence of two anhydrous polymorphs, i.e., III and V at 33% RH. (b) A selected region, highlighted zone in a, of the patterns

exposed to various RH values from 33% to 75% RH followed by a desiccation to 33% RH. The arrows indicate the emergence of new peaks at a high relative humidity (75% RH).

Considering the XRD patterns, thenardite (phase V) can be identified as the only existing anhydrous polymorph in detergent powders produced from low water-content slurries in the absence of sodium silicate. Increasing the amount of water or adding sodium silicate to detergent slurries, gave rise to the formation of metastable phase in resulting powders. A clear splitting of a diffraction peak at 23.2° 2θ and the emergence of a new peak at 25.6 ° 2θ signify a change in lattice parameters of thenardite (phase V). From the XRD patterns, the diffraction peaks at 22.7, 23.7 and 25.6° 2θ belong to Na_2SO_4 (III) (Rodriguez-Navarro et al., 2000). The reasons for the existence of metastable polymorphs in these powders due to the addition of sodium silicates or the increased water content of the initial slurries have been discussed in chapter 3.

After 4 weeks of storage, the XRD patterns of silicate free powders exhibited no change even at the highest relative humidity (75% RH), which suggests that the anhydrous polymorphs were quite stable. More precisely, well-defined Bragg peaks remained intact and no amorphous phase was identified at the highest RH value. In studies on the crystallization of sodium sulphate in $Na_2SO_4 – H_2O$ systems, it has been demonstrated that the deliquescence of metastable phase (III) and thenardite (V) start at 80 and 83% RH respectively (Linnow et al., 2006). Therefore, the stability of anhydrous polymorphs was expected since the relative humidity in the current study was far below the deliquescence humidity of either of the two anhydrous polymorphs. In the case of detergent powders containing sodium silicate, the diffraction peaks similarly remained unchanged up to 54% RH. However, as samples were exposed to 75% RH at 21 ±1°C, examination of XRD patterns revealed the presence of a number of new peaks at 22.1, 24.2, 26.4, and 30.9 ° 2θ, signifying a phase transition at such humid conditions. Interestingly, as the samples were desiccated back to a lower relative humidity (33% RH) the aforementioned peaks disappeared and detergent powders exhibited the same diffraction patterns as they showed initially under dry conditions. The disappearance of these new peaks after desiccation at 33% RH can be a good evidence of the formation of a hydrated crystal form of sodium sulphate. Comparing

the diffraction patterns, as well as SEM images, with previous scientific studies on the crystallization of sodium sulphate, it can be concluded that it was decahydrate $Na_2SO_4.10\ H_2O$ (mirabilite) that was formed during the storage at 75% RH. The formation of mirabilite at a relative humidity far below the deliquescence of sodium sulphate can be explained by a solid-state reaction pathway. Rodriguez-Navarro et al (2000) showed that the conversion of anhydrous polymorphs of sodium sulphate to mirabilite at enhanced relative humidity can take place through a solid-solid transition reaction at which the hydration of anhydrous polymorphs proceeds smoothly without actual solvation of the solid phase. Moreover, in this series of experiments, the reason for the susceptibility of anhydrous polymorphs to solid-solid transition reaction and hence mirabilite formation in the presence of sodium silicate can be attributed to the hygroscopic nature of sodium silicate. This point will be discussed in section 5.2.3.

5.2.3 Dynamic vapour sorption (DVS) measurements

5.2.3.1 Characteristics of moisture sorption

The total running time obtained from sorption and desorption cycles, can describe the ability of a product to adsorb water vapour from the surrounding air. The typical step-wise moisture sorption-desorption profiles of spray-dried detergent powders are shown in Figure **5.5**. It can be seen from Figure **5.5**a, that for detergent powders produced from low-water content slurries and in the absence of sodium silicate, the equilibration times are very short (~ 20 min) up to 50% RH. Also, a near-linear increase in equilibrium moisture content (EMC) is evident in its corresponding sorption isotherm. However, at higher relative humidity the isotherm shows a deviation from the linear behaviour and the EMC value significantly increases and reaches its maximum value (1.72 %) at 70% RH. The sorption isotherms of these powders were typical type II sigmoidal curves according to Brunauer classification (Brunauer et al., 1940), indicating adsorption on macroporous adsorbents with strong adsorbent-adsorbate interactions (Aranovich and Donohue, 1998).

The noticeable increase in EMC values above 50% RH, signifies a change in mechanism of water sorption. Several mechanism have been proposed for the interactions between water vapour and adsorbent molecules which mainly include surface adsorption, bulk adsorption, hydration, gelation, and deliquescence (Ouyang et al., 2015). It has been suggested that at low relative humidity values water vapour sorption is an entropy-controlled process which is associated with the number of available sorption sites as well as randomness of the motion of water molecules. As the relative humidity increases, the more polar available sites are occupied which in turn increases the order of the system, giving rise eventually to the formation of subsequent layers of adsorbate (Bonilla et al., 2010). Therefore, the relatively lower moisture uptake up to 50% RH can be explained by the mechanism of surface adsorption which is a function of the powder surface microstructure. However, at medium and high relative humidity values bulk water sorption occurs. This can be accompanied by interactions between the sorbate and sorbent, leading to some structural changes. *e.g*., deliquescence, swelling and glass transition, which therefore allow water molecules to penetrate into the internal structures (Maher et al., 2014). Smith (1947) studied the water sorption properties of many polymers and suggested that the swelling behaviour of polymeric substances results in the development of free volumes within the gel structure which progressively increases the effective sorbing surfaces of the polymer. Our previous studies on liquid crystalline phases of NaLAS in spray-dried detergent powders revealed that hydrocarbon chains of the lamellar phases adopt an orthorhombic subcellular packing at low relative humidity conditions (11-33% RH), however; at a higher RH value (54% RH), the hydrocarbon chains are no longer in their perfect orthorhombic arrangement as a consequence of the swelling of lamellar liquid-crystalline phases. Therefore, the progressively increased EMC values can be partially attributed to the structural changes of these lamellar phases, allowing the diffusion of larger quantities of water molecules into the matrix structure.

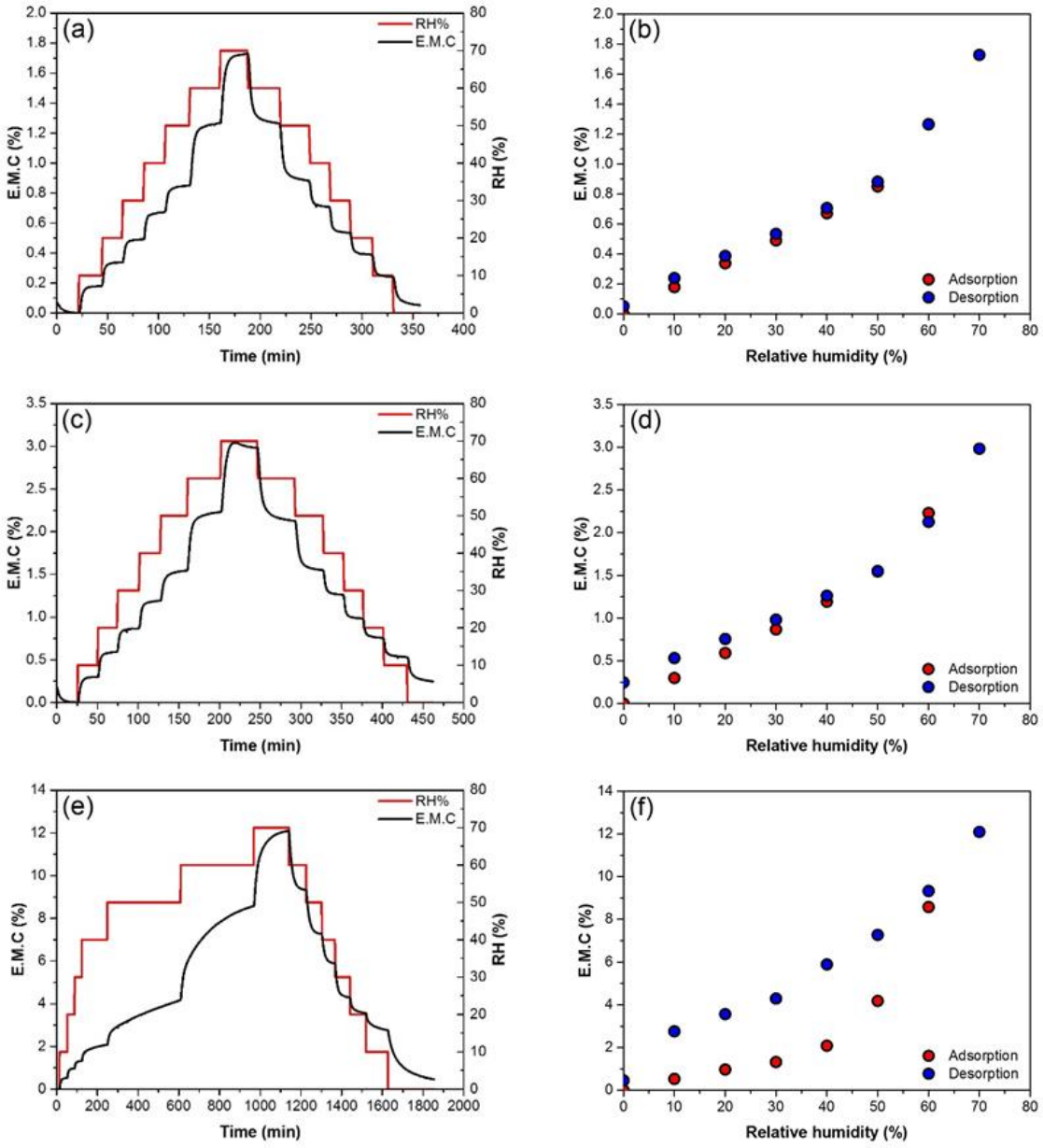

Figure 5.5. Equilibrium moisture sorption-desorption profiles for spray-dried detergent powders produced from low-water content (a) and high-water content slurries (c), and detergent slurries containing sodium silicate (e). Panels b, d and f show the corresponding sorption isotherms for the aforementioned samples, respectively.

Spray-dried detergent powders produced from high-water content slurries displayed similar step-wise moisture sorption-desorption profile (Figure **5.5**c), though the total running time was relatively longer (462 min) and the EMC value was considerably larger at any given relative

humidity. The total time required to complete the adsorption cycle and its subsequent desorption cycle, is associated with moisture sorption capacity of the material. The reason for the relatively larger moisture uptake can be attributed to the morphology and surface characteristics of the samples. It was previously demonstrated that a greater initial water content in detergent slurries gives rise to formation of a more irregular structure and a rougher surface. SEM observations of the microtome-polished cross-sections of these powders also revealed the presence of irregular open pores with some degree of connectivity within the granule matrix. A typical appearance of these powders was also earlier shown in a micrograph (Figure **5.1**c). X-ray microtomography technique can provides good insight into the internal structures of these powders. Typical examples of the internal morphology as a consequence of the initial water content are illustrated in Figure **5.6**. It is clear from Figure **5.6**d that the increased water content has led to the formation of a "foam-like" structure. Consequently this increases the effective surface area exposed to the water vapour and hence the permeability of the powder. A small sorption hysteresis below 30% RH can be attributed to a failure to establish a true equilibrium during the desorption process. Indeed, a relatively higher moisture uptake capacity as compared with those produced from low-water content slurries, results in a greater degree of structural changes, *e.g*., the swelling of lamellar phases. This consequently slows down the escape of water molecules from the powder matrix during the desorption process.

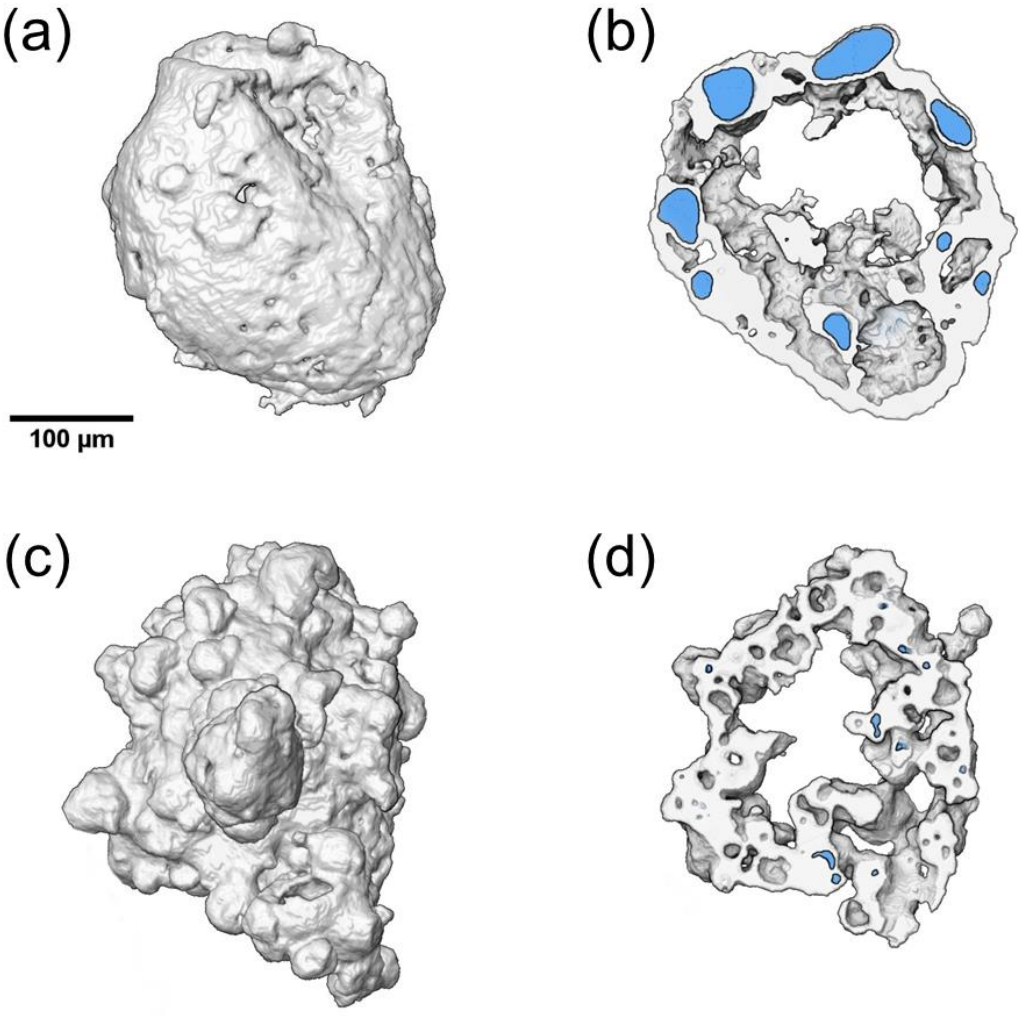

Figure 5.6. 3D X-ray tomograph (Voxel size: 1.76 µm) of spray-dried detergent powders. (a) Shows a typical detergent granule produced from low-water content slurries; and (b) shows its 3D central cross section (52.8 microns thick) illustrating the distribution of voids and sodium sulphate crystallites (blue regions). (c) Shows a typical detergent granule produced from high-water content slurries; and it's corresponding cross section (56.8 microns thick) (d).

Interestingly, the addition of sodium silicate to the slurries caused considerable differences in the moisture sorption-desorption profile, total running time, EMC values and sorption hysteresis. From Figure **5.5**e, three distinct regions can be identified in the sorption-desorption profile, namely 0-30% RH, 30-50% RH and RH > 50%. At low relative humidity region, *i.e.*, 0-30% RH, the equilibration times are relatively short (~ 37 min), though still considerably longer than those of silicate-free powders. At intermediate level of relative humidity, *i.e.*, 40-50% RH, a prolonged equilibration time (350 min) can be detected. Above 50%, the EMC value progressively increases until it reaches the maximum value (12.10 %) at 70% RH. In this region, spray-dried detergent

powders displayed a considerably larger EMC value at any given RH as compared with those in the absence of sodium silicate, indicating a strong ability of these powders to interact with water vapour molecules. Additionally, in contrast to free-silicate detergent powders, as seen in Figure **5.5**f, all desorption points between 0 and 60% RH are located above the sorption points, *i.e.*, desorption branch does not coincide with the adsorption branch, thus indicating a hysteresis loop.

Dried sodium silicates have numerous hydroxyl groups, but not all of the functional groups are accessible to water vapour molecules. Therefore, a likely explanation for the increased capacity of moisture uptake can be attributed to structural changes in sodium silicate which probably occur above 40% RH. This leads to the increased exposure of the hydrogen binding sites, and consequently hydration and swelling of the hardened glassy silicate. These plausible alterations are also reflected in the step-wise moisture sorption-desorption profile (Figure **5.5**e), where the structure responds to its new physico-chemical state by requiring a noticeably prolonged equilibration time between 40 and 50% RH (Hill et al., 2010). The relative humidity value of 40%, can be considered as a critical threshold above which the physical properties of sodium silicate changes from a rigid glassy state into a rubbery state. Upon this phase transition, the subsequent desorption occurs from a highly hydrated and swollen matrix having a different physical state from that initially present during the sorption stage of the process. This phenomenon is therefore manifested as hysteresis (Hill et al., 2009), clearly noticeable in Figure **5.5**f.

The increased moisture uptake as a consequence of the phase transition; however, may concomitantly induce surficial hydroxylation reactions in sodium silicates which consequently enhance the sorption capacity of the powders. As water vapour molecules diffuse into the interstitial spaces of the matrix, hydrogen bonding with surficial hydroxyl group forces water molecules to form an ordered water monolayer. At a sufficiently high relative humidity, surficial hydroxylation may occur due to the opening of siloxane rings (Warring et al., 2016). This consequently alters the surface chemistry of the adsorbent, thereby increasing its hydrogen bonding capacity. ATR-FTIR studies of these samples stored at various RH values, can provide

some clues as to the origin of aforementioned changes in kinetics of water sorption at high relative humidity conditions. This point will be discussed in section 5.2.4.

5.2.3.2 Data modelling

Table **5.1** shows the estimated model parameters and statistical results. Amongst the models describing the sorption isotherms throughout the entire range of relative humidity (0-70 % RH), the GAB model provided the closest fit to the experimental moisture data for spray-dried detergent powders in the absence of sodium silicate. The GAB model demonstrated the lowest mean percentage deviation modulus (E %) and the highest coefficient of determination (R^2) for both the adsorption and desorption isotherms.

The estimated value of the monolayer water (M_g), obtained by applying the isotherm models, is of significant interest as it shows the amount of water which is tightly bound to specific hydrophilic sites, and helps to determine the appropriate storage conditions of the powders (Shrestha et al., 2007). The GAB monolayer values for detergent powders produced from low-water content slurries, were remarkably smaller than those of powders produced from high water content slurries. A considerably larger value of M_g (% d.b) for the latter case can be attributed to a greater surface area as discussed earlier.

It has been shown that for $C \geq 2$ and $0 < K < 1$ the GAB model describes properly sigmoidal-shaped isotherms type II under the Brunauer classification (Ben Abdelhamid et al., 2016, Blahovec, 2004). In the current study, for the samples produced from low-water content slurries, the mean values of K are slightly higher (K=1.06) than the limit. While GAB constant C is a measure of the difference of free enthalpy of the sorbate molecule in the first sorption layer and the layer above the monolayer, the constant K is related to the difference of free enthalpy of the sorbate molecule in the pure liquid and those in the multilayers. At too low K values water molecules are highly structured in multilayer domains. As K value approaches unity, water molecules are least bound to the monolayer region and have almost bulk liquid characteristics (Timmermann et al., 2001). K values higher than 1 are not feasible since the heat of adsorption

of water molecules in the second and upper layers should be less than the heat of liquefaction (Arthur et al., 2016). Evidence for the overcoming of the limits has been reported in many other studies (Kaymak-Ertekin and Gedik, 2004, Moraga et al., 2004, Vega-Gálvez et al., 2008). Pérez-Alonso et al. (2006) suggested that in some cases the GAB parameters may lack any physical meaning and the overcoming of the limits can be just due to the mathematical relationships between the parameters which exist in any curve fitting scenario. Even though in the current study the mean values of K were slightly higher than 1, some K parameters were found within the adequate range and reasonably below the unity, e.g., ~ 0.97. This may imply an extremely low difference between liquid molecules and multilayer molecules and suggest that the multilayers have the characteristics very similar to bulk liquid (Quirijns et al., 2005). A possible reason for this can be attributed to partial hydrophobicity of the granules surfaces arising from the presence of surfactant molecules. It has been suggested that the formation of multilayer domains on the hydrophobic surfaces are not energetically favourable. In the first sorption stage, adsorption onto hydrophobic sites, *e.g.*, methyl groups, occurs due to dispersion forces which are energetically weak. In subsequent layers, water molecules have no interactions with the hydrophobic surface and are highly entropic (Zettlemoyer, 1968). This consequently decreases the ordering of water molecules and causes water molecules to behave like bulk liquid. On the contrary, strongly hydrophilic surfaces have a tendency to favour multilayer growth (Sears, 2001).

Table 5.1 . Estimated model parameters and fit criteria for adsorption and desorption experimental data at 25 ˚C.

Model	Constants	Adsorption			Desorption		
		LW	HW	LW+2.35 R	LW	HW	LW+2.35 R
GAB	K	1.062 ± 0.031	0.993 ± 0.002	1.353 ± 0.024	1.077 ± 0.047	1.058 ± 0.008	1.094 ± 0.105
	C	3.940 ± 0.284	3.401 ± 0.450	3.518 ± 0.530	6.595 ± 0.076	9.238 ± 2.98	13.512 ± 2.158
	Mg	0.504 ± 0.033	0.889 ± 0.177	1.124 ± 0.289	0.5224 ± 0.042	0.787 ± 0.012	3.117 ± 0.803
	E (%)	1.755 ± 0.182	2.008 ± 0.68	15.857 ± 0.753	1.777 ± 0.074	1.580 ± 0.160	4.579 ± 0.523
	R^2	0.9973	0.9981	0.5770	0.9973	0.9982	0.9930
Oswin	B	0.732 ± 0.0219	0.729 ± 0.053	1.099 ± 0.037	0.461 ± 0.004	0.612 ± 0.066	0.568 ± 0.099
	A	0.924 ± 0.0184	1.552 ± 0.047	3.962 ± 0.531	0.939 ± 0.046	1.645 ± 0.027	6.913 ± 0.694
	E (%)	3.022 ± 0.938	3.334 ± 1.196	16.461 ± 0.388	3.567 ± 0.067	5.300 ± 0.817	8.538 ± 3.707
	r2	0.9932	0.9927	0.9534	0.9912	0.9792	0.9697
BET	C	3.671 ± 0.489	3.637 ± 0.746	4.425 ± 0.616	6.163 ± 0.134	9.619 ± 1.526	23.746 ± 7.953
	Mb	0.550 ± 0.021	0.913 ± 0.131	1.245 ± 0.156	0.532 ± 0.0114	0.902 ± 0.088	2.875±0.519
	E (%)	0.727 ± 0.434	1.284 ± 0.429	1.046 ± 0.708	1.618 ± 0.157	2.073 ± 0.678	0.291 ± 0.253
	R^2	0.9994	0.9985	0.9983	0.9986	0.9939	0.9996

Also, for the samples in the absence of sodium silicate, the Oswin model shows a good fit of the experimental data with $R^2 > 0.95$ and $E < 6\%$, though it was still less successful in describing the isotherms as compared with the GAB equation. However, for spray-dried detergent powders containing sodium silicate, both OSWIN and GAB equations were found to be unsuitable to describe the adsorption isotherms; *E* values were considerably above 10%. As can be seen in Figure **5.7**e, these models deviated from the real sorption isotherm at relative humidity larger than 50% RH. This deviation can be attributed to the changes of molecular structure in sodium silicate, which is not accounted for in the GAB theory.

On the contrary, these models showed good fits for the desorption data. This discrepancy can be explained by the fact that the sample has already experienced a substantial transition from the glassy to rubbery state during the adsorption process, which might not have been reversible simply by desiccating the sample (Carter and Schmidt, 2012). In the absence of any major changes in

molecular structure during the desorption part of process, one may expect a significantly better fit of the models to the experimental data.

The BET model displayed a good description of the isotherms of the powders in the range of RH < 40%. The largest M_b value can be found in detergent powders containing sodium silicate. This considerably larger moisture content in the initial monolayer region signifies a greater number of hydrophilic binding sites which strongly hold water molecules by hydrogen bonds (Cadden, 1988). As mentioned earlier, this hydrophilic characteristic can be attributed to the presence of silanol groups (Si-OH) of sodium silicate. This higher affinity of water molecules to the granule surfaces is also evident from the relatively larger C parameter suggesting larger interaction energies. Interestingly, for all samples both C parameter and M_b value significantly increased for desorption isotherms as expected. This was due to the humidity-induced structural changes that had already occurred during the adsorption part of the experiment, as was discussed above.

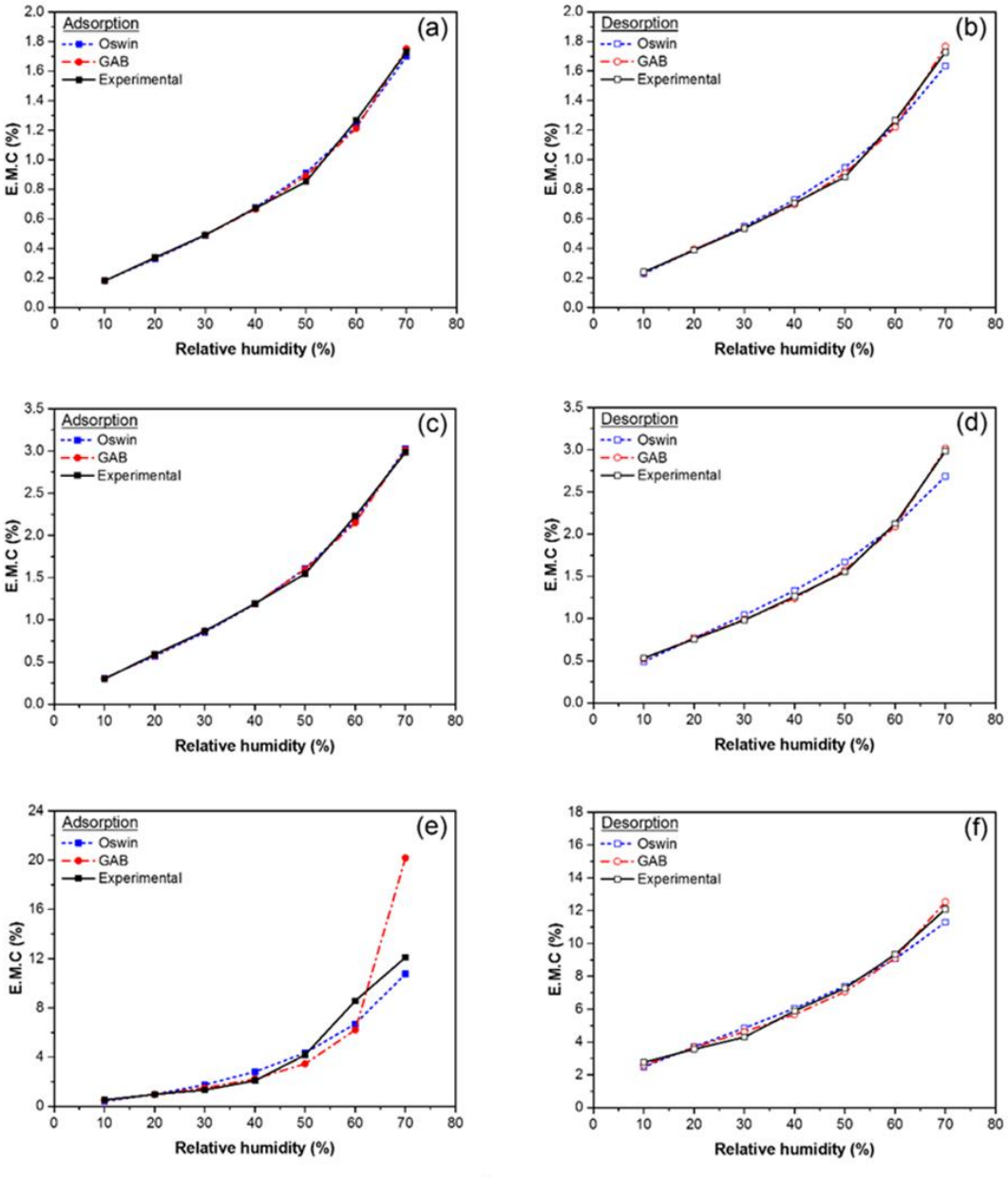

Figure 5.7. Experimental and predicted adsorption isotherms for spray-dried detergent powders produced from low-water content (a) and high-water content slurries (c), and detergent slurries containing sodium silicate (e). Panels b, d and f show the corresponding desorption isotherms for the aforementioned samples respectively.

5.2.4 ATR-FTIR measurements

The microscopic observations demonstrated that the presence of sodium silicate increases the susceptibility of the powder surfaces to the humidity-induced morphological changes. Returning to the dynamic vapour sorption data in Figure **5.5**f, it was shown that EMC value abruptly

increased at RH > 40%, which was explained by the moisture sorption-induced glass transition, leading to the exposure of a greater number of active binding sites within the matrix. The changes in hygroscopic characteristics of spray-dried detergent powders as the results of the moisture-induced phase transition can be better elucidated by probing the O-H stretching vibrations in the 3000-3800 cm^{-1} region. In this region the absorption intensity can be associated with the extent of adsorbed water molecules. The O-H stretching absorption is known to be composed of three components assigned to sites differing in intermolecular bonding. It is generally accepted the a vibrational peak, with the highest energy, at ~3200 cm^{-1} is attributed to " bound water" or "ice-water" structure at which the oxygen atoms of water molecules have four bounds including the covalent and hydrogen bonds. This leads to the formation of tetrahedral arrangements as can be seen in crystalline ice structures. The lowest energy peak around 3640 cm^{-1} is assigned to "free water", when the oxygen atoms are only bound to two hydrogen atoms. The medium-energy peak around 3450 cm^{-1} is assigned to "multi-layer water", when the oxygen atoms on average are bound to three hydrogen atoms. These water molecules are partially structured, and hence are referred to as intermediate water (Barnette et al., 2008).

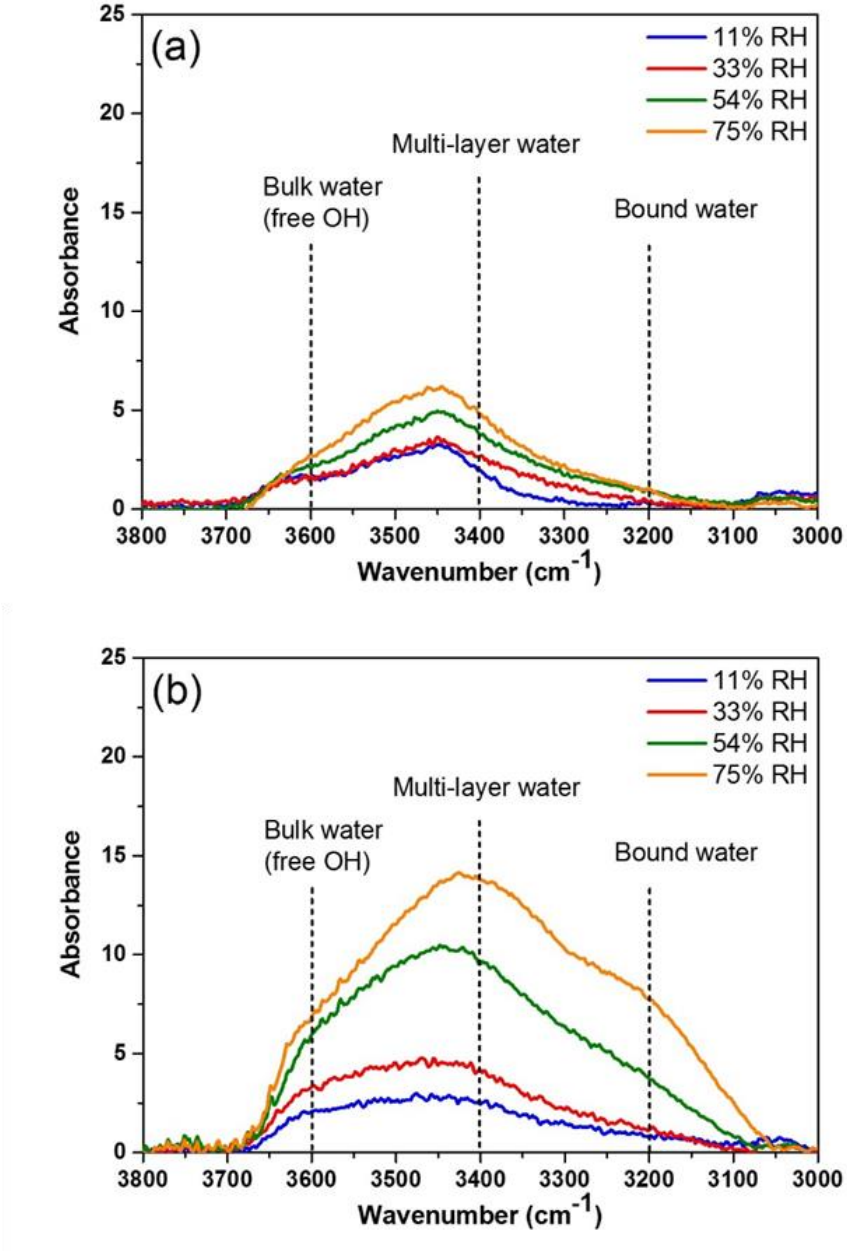

Figure 5.8. ATR-FTIR spectra (3000-3800 cm-1) for sprayed-dried detergent powders produced from LW formulation (a) and those containing sodium silicate (LW 2.35) (b), showing the structural evolution of water molecules at different relative humidity. The dashed lines show the O-H stretching vibration positions of bound water, multi-layer water and bulk water.

The infrared spectra of detergent powders, in the absence of sodium silicate, stored at different relative humidity values are shown in Figure **5.8**b. A broad absorbance can be seen at 11% RH value, which its intensity increases as the relative humidity increases. This broad 3000-3700 cm^{-1} absorbance is apparently composed of two broad bands at ~ 3450 and ~ 3620 cm^{-1}. A

considerably small peak also appears around 3200 cm^{-1}. It can be observed that the most intense band at 3450 cm^{-1} , which is attributed to the multi-layer water, is noticeably changes with increasing the relative humidity. At 75% RH, the population of multi-layer water become considerably dominant over the O-H stretching region, while the high-energy peak of the bound water remained unchanged around 3200 cm^{-1}. The increase in population of multi-layer water molecules can be associated with the swelling of liquid crystalline phases of NaLAS as was discussed in our previous work. Spray-dried detergent powders containing sodium silicate, however, showed remarkable changes in the spectral shape Figure **5.8**b. It can be seen that the intensity of the band at 3200 cm^{-1} is relatively higher than those in the absence of sodium silicate even at the lowest relative humidity (11% RH). This observation is consistent with the values of monolayer water obtained by BET model, suggesting the existence of a greater population of water molecules which are strongly bound to the hydrophilic binding sites. This band grows in intensity even with a small increase in relative humidity, *i.e*., 33% RH, becoming a well-defined strong band at 72% RH. This was concomitant with a significant increase in the intensity of the bands at 3450 and 3620 cm^{-1}. Considering the profiles of the O-H stretching absorption, an abrupt change in the molecular configuration of the water at 54% RH signifies a structural change in sodium silicate as was earlier reflected in the adsorption isotherms. There are two possible scenarios which can potentially explain these humidity-induced structural changes. On one hand, the increased relative humidity might have increased the molecular mobility of the amorphous sodium silicate and therefore have exposed the additional active surface area and hence buried hydrophilic silanol groups. On the other hand the increased moisture content may also concomitantly result in the conversion of surface siloxane (Si-O-Si) to silanol (Si-OH) groups (Warring et al., 2016), thereby enhancing the moisture sorption capacity.

5.3 Conclusion

This is the first time that the moisture sorption characteristics of spray-dried detergent powders are related directly to the microstructure and slurry formulation. The moisture sorption and

desorption isotherms of the spray-dried detergent powders were determined using a gravimetric method. The morphological properties were found to play an important role in the extent of moisture sorption. Spray-dried detergent powders produced from high-water content slurries, having a more porous structure and rough surfaces, showed a larger moisture uptake which was attributed to their greater effective surface area. The addition of sodium silicate was found to significantly increase the equilibrium moisture content of the detergent powders. For silicate-free samples, the mathematical models, *i.e*., BET, GAB and Oswin described the experimental data well. However, in the presence of sodium silicate, the GAB and Oswin models failed to predict the equilibrium moisture contents. This was due to a sudden rise in moisture uptake above 40% RH, which was assigned to the structural changes in sodium silicate, where the GAB and Oswin cannot account for. This was explained by this fact that in the glassy state sodium silicate species are densely packed, thereby showing a lower moisture sorption capacity as a consequence of smaller interstitial spaces as well as the effective number of functional silanol groups. However, increased plasticisation of amorphous glassy sodium silicate results in the exposure of a greater number of hydrophilic groups, including buried silanol groups, which consequently enhance the moisture sorption capacity of sodium silicate and hence spray-dried powders. These humidity-induced structural changes were also reflected in ATR-FTIR results suggesting the evolution of water structure at RH> 54%. The increased moisture sorption capacity of detergent powders as a consequence of the addition of binders, led to noticeable changes in the surface microstructural properties. A remarkable crystal growth on the granule surfaces was observed at 54% RH. The x-ray diffraction analysis along with the microscopic observations confirmed the emergence of sodium sulphate decahydrate at 75% RH. This was accompanied by the continued growth of sodium sulphate crystals covering the entire granule surface. The findings of the current work gives good insight into the influence of slurry formulation on the water sorption properties of spray-dried detergent powders, which can be potentially used to determine the process and storage conditions influencing the powder caking of spray-dried detergent powders.

Chapter 6 The role of inorganics on the flowability of spray-dried detergent powders

The flow characteristics of granular products play an important role in their handling and processing operations, *e.g*., feeding, mixing and compaction. Although a great deal of work has been previously reported in the literature on the flowability of many powders, there has been no systematic work on the flowability of detergent powders and how it is influenced by the slurry chemical composition. It was previously shown in Chapter 3 that the initial water content of the slurries plays a significant role morphology and matrix composition of spray-dried detergent powders. Typically, the spray-dried powders produced from low-water content slurries has a higher surface concentration of surfactant. This can potentially influence the flow behaviour of these powders. The silicate is thought to act as a binder and form a glassy continuum linking sulphate crystals and surfactant domains, which consequently increases the apparent granule strength. In this Chapter the influence of the initial water content of the slurry and the SiO_2:Na_2O molar ratio of sodium silicate on the powder flowability is investigated using the Schulze ring shear tester and the Hausner ratio. In the current study, the 3D packing of the granules along with the voidage is visualized using x-ray tomography. The chemical composition of the detergent powders was also probed using Raman confocal microscopy and x-ray microtomography techniques.

6.1 Material and methods

6.1.1 Materials

Spray-dried detergent powders were produced with a pilot-scale spray dryer at Procter & Gamble as was previously explained in Chapter3. Since particle size distribution is known to have a dramatic effect on the powder flowability, prior to flowability measurements detergent powders were sifted using a sieve shaker and a fraction of 300-350 µm was selected for the analysis. This also diminishes the influence of particle-particle adhesion forces, e.g., van der Waals forces, which become more pronounced compared with gravity forces, with decreasing the particle size (less than ~ 100 µm), though the effect of particle size can be a material specific (Liu et al., 2008b, Visser, 1989).

6.1.2 Flow properties

The flow behaviour of the resulting spray-dried detergent powders was investigated using a ring shear cell tester (Schulze RST-XS, Wolfenbüttel, Germany). For the measurement, the powder was loosely loaded into the annular shear cell (Figure **6.1**). After loading, the specimen was pre-sheared under a pre-sheared normal stress, *e.g.*, 2.0, 4.0, 6.0 and 8.0 kPa, until a steady-state flow is achieved (shear stress remains constant).

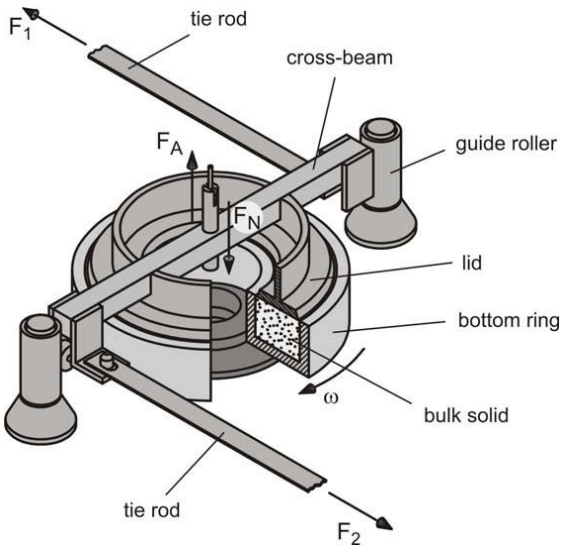

Figure 6.1 Shear cell of a Schulze ring shear tester (Schulze, 2007).

The second step of the test is shear to failure point, *i.e.*, unconfined yield strength. In this stage the critically consolidated specimens is sheared to failure under a normal stress, σ_{sh}, which is less than the initially applied normal stress, σ_{pre}, causing particles to move against each other. During shear testing the shear cell rotates, whereas the lid is prevented from rotation. Therefore, a shear deformation is created within the bulk powder and the required torque is measured and converted into a shear stress, τ_{sh}, and consequently a point of incipient flow is measured and yield locus constructed based on the individual shear points (σ_{sh} , τ_{sh}) by completing the procedure of consolidation and shearing under different levels of normal stress (Figure **6.2**).

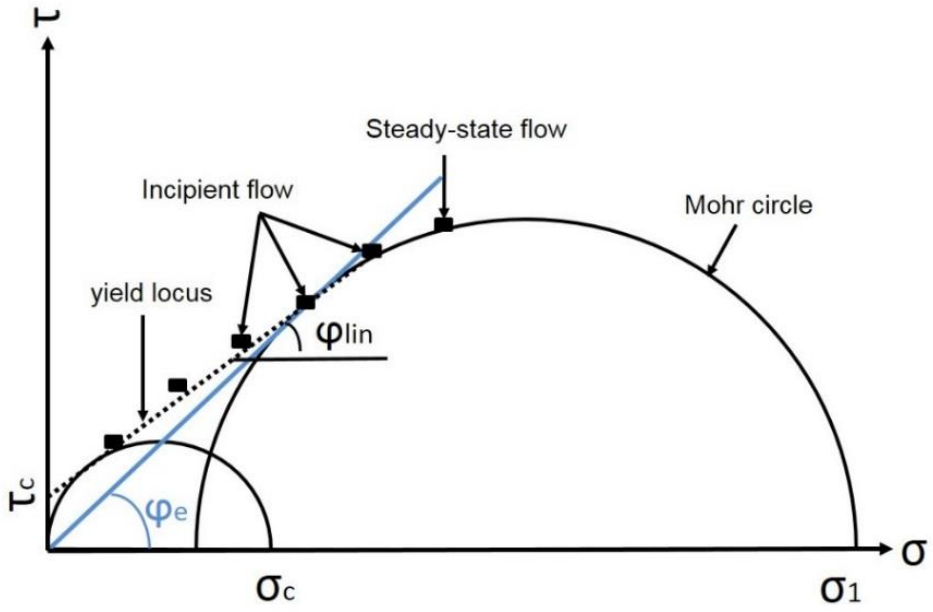

Figure 6.2 An example of yield locus for spray-dried detergent powders, obtained from a shear cell tester, presenting the Mohr circles, unconfined yield stress, σc, major consolidation stress, σ1, the friction angles, i.e. φlin and φe.

A yield locus is a plot of failure shear stress against normal stress, which can be used to determine the parameters describing the flow behaviour of the bulk solid. For example, the shear points, the points of incipient flow, on the yield locus describe the maximum shear stress required to cause the powder to fail (Opaliński et al., 2012, Schulze, 2007). The intercept of yield locus with the y-axis, τc, is referred to as cohesion coefficient which describes cohesion between particles in a solid bulk (Poszytek, 2005). The friction angles are related to the friction between particles. The

angle of internal friction at incipient flow, φlin, can be determined from the slope of the linearized yield locus which is tangent to both Mohr circles. The effective angle of internal friction, φe, can be determined from the slope of a straight line, i.e., effective yield locus, which is tangent to the larger Mohr circle, and pass through the origin of the σ,τ diagram. The effective angle of internal friction is a measure of friction between particles at steady state flow. A flow function plot can be generated by plotting the unconfined yield stress versus major consolidation stress. The inverse of the slope of the line gives a flow index, ffc, which is used to describe the flowability of a powder according to Jenikes's classification (Table **6.1**) (Jenike, 1967).

Table 6.1 Jenike's classification of powder flowability by flow index (ff_c).

Flowability	Very cohesive	Cohesive	Easy flow	Free flowing
Flow index (ff_c)	<2	<4	<10	>10

The flowability of spray-dried powders was also evaluated by Hausner ratio. The ratio of the tapped bulk density, ρ_{tapped}, to its initial bulk density, $\rho_{initial}$, is known as Hausner ratio which can be expressed as:

$$HR = \frac{\rho_{tapped}}{\rho_{initial}} \qquad (14)$$

The tapped bulk density was determined by pouring a known weight of the sample in a 50 ml graduated cylinder, followed by tapping the cylinder using a mechanical tapping device for 5 min, until no further change in the powder volume was observed. In general a free-flowing powder is less effected by tapping. Therefore, a lower Haunser ratio of a powder indicates a better flow characteristic (Liu et al., 2008a). Hayes (1987) has classified the flow behaviour of bulk solids according to their Hausner ratio (HR), as can be seen in Table **6.2**.

Table 6.2 Hayes's classification of powder flowability by Hausner ratio (*HR*).

Flowability	Very difficult flowing	Difficult flowing	Medium flowing	Free flowing
Hausner ratio (*HR*)	HR> 1.4	1.25<HR<1.4	1.1<HR<1.25	1<HR<1.1

6.1.3 Microscopic observations

The morphology of particles was examined using electron scanning microscopy (SEM). Prior to SEM observation, sputter coating was conducted to form an ultra-thin coating of gold which inhibits charging during SEM examination.

6.1.4 Micro-computed tomography (Micro-CT) scanning

In the present work, interstitial spaces between the granules, as a measure of packing density, were qualitatively examined using a Phoenix Nanotom CT scanner (GE Measurement and Control, US). Detergent powders were loaded in a plastic tube (internal diameter 2 mm, height 8.5 mm). After manually tapping on a flat surface, the plastic tube was mounted on a rotating stage between an X-ray source and X-ray detector. Samples were then scanned in the full range of 0–360°. A series of x-ray micrographs were obtained and three-dimensional volumes were reconstituted using a VGStudio software package. The original volume was cropped and a cube (1500×1500×1500 μm) was created for further image processing (Figure **6.3**). To improve the 3D data visualisation, a number of different image processing tools mainly including filtration and segmentation, were applied to the X-ray micrograph data using an Avizo software package. Prior to the segmentation process, a non-local means filtration was applied to the grey scale projections to reduce image noise. The segmentation was conducted using an interactive thresholding tool in Avizo.

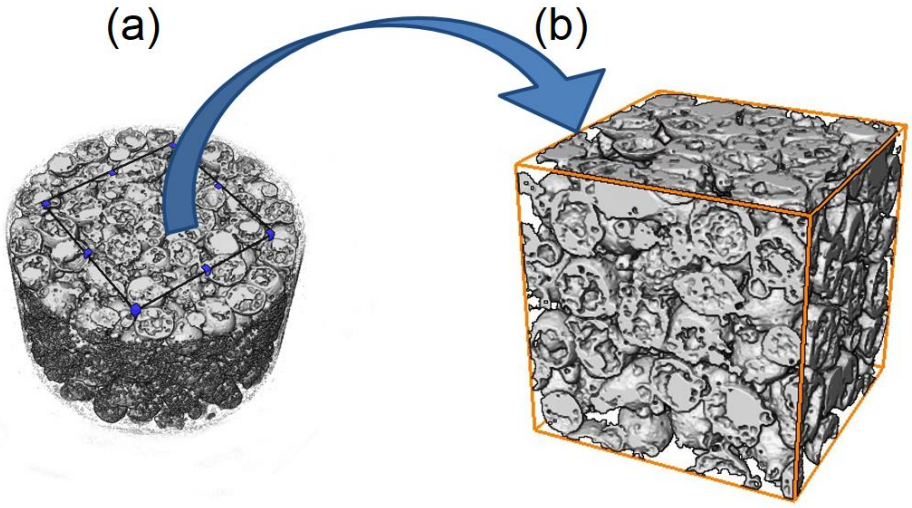

Figure 6.3 (a) 3D X-ray tomograph (voxel size: 2.56×2.56×2.56 µm) from a cross-section of a plastic tube loaded with detergent granules, showing the region of interest. (b) A cube (1500×1500×1500 µm) cropped from the original volume for the qualitative analysis of packing density.

6.1.5 Raman microspectroscopic analysis

All Raman spectra were obtained using a Raman microscope (Renishaw plc.) with 514 nm helium–neon laser excitation. A 50× objective lens was used, giving a laser spot diameter of 2 µm. The detergent powders were immobilised on a doubles-sided tape and spectra were obtained for one 30 sec exposure in the region 400-3200 cm−1 using the extended scanning mode of the instrument. Post-processing and data analysis were carried out with Renishaw WiRE 3.3 and Origin softwares. Laser-induced fluorescence which is frequently encountered in specimens containing organic compounds, results in baseline drifts distorting the spectrum towards the end. The sloping enhanced backgrounds were subtracted with a fifth-order polynomial. Each spectrum was then normalized to 1.0 with respect to its maximum intensity band (Marshall and Olcott Marshall, 2013).

6.1.6 Mechanical strength measurements

6.1.6.1 Single particle compression test

Compression tests were performed using an Instron Universal Testing Machine (Model 5566, Instron Crop., USA). For single particle compression test, 40 granules were compressed individually between two rigid platens in the axial direction at a slow rate of 0.5 mm/min. The detergent granules were subjected to a maximum compressive load of 0.05 N. The compression force was measured using a 10 N load cell transducer and, the axial load and the machine head displacement were continuously recorded by the system's computer. The force-displacement curves obtained from the compression tests were then evaluated to calculate the granule rupture strength, σ_r, Eq. (15) (Samimi et al., 2005).

$$\sigma_r = \frac{4F_r}{\pi D^2} \qquad (15)$$

Where Fr is the rupture force and D is the diameter of the granule. The rupture force can be determined from the peak failure force in force-displacement curves, where the first sharp decrease in loading force can be observed (Figure **6.4**).

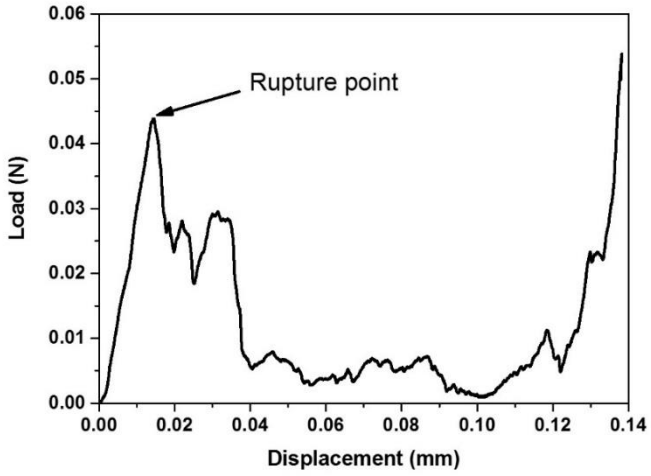

Figure 6.4 Typical force-displacement curve obtained from the single granule compression test.

6.1.6.2 Bulk compression test

The bulk compression tests were carried out using the same Instron machine. A known mass of the sample was poured into a cylindrical die with a height and diameter of 20 mm, and tapped until the volume did not decrease any further. The sample was then compressed with a close-fitting stainless steel piston until the maximum compaction force of 120 N was reached. The compression behaviour and the compaction mechanism of the detergent powders were subsequently investigated using the Kawakita model. This empirical equation was proposed by Kawakita and Lüdde (1971) for analysis of soft and fluffy powders, which expresses the relationship between volume and applied pressure during compression, Eq. (16).

$$\frac{P}{C} = \frac{1}{ab} + \frac{P}{a} \qquad (16)$$

Where C is the degree of volume reduction or engineering strain, and calculated as $C=(V_0-V)/V_0$, where V_0 is the initial powder bed volume and V is the powder volume at pressure P. The parameters a and b are the Kawakita constants. The parameter a is related to the initial bed porosity and mathematically describes the degree of compression at infinite pressure. The parameter b is related to the resistance force. The term 1/b describes the applied pressure required to compress the powder to one-half the maximum degree of compression or $a/2$. The parameter $1/b$ has been shown to be related to the yield strength and plasticity of the materials (Khomane et al., 2013). The Kawakita parameters can be determined by linear regression analysis of the experimental values of P/C as a function of P.

6.2 Results and discussion

6.2.1 Morphological properties

Figure **6.5** shows SEM micrographs of the granules produced from different detergent slurries. It can be seen that the granules produced from low-water content slurries are nearly spherical, though small fine particles can be occasionally observed on the particle surfaces in the presence

of sodium silicate. The granules produced from high-water content slurries; however, are less spherical and possess rough surfaces with a blister appearance. The reasons for these morphological properties were previously discussed in Chapter 3. The microscopic observations were highlighted here because morphological characteristics play an important role in flowability of granular products.

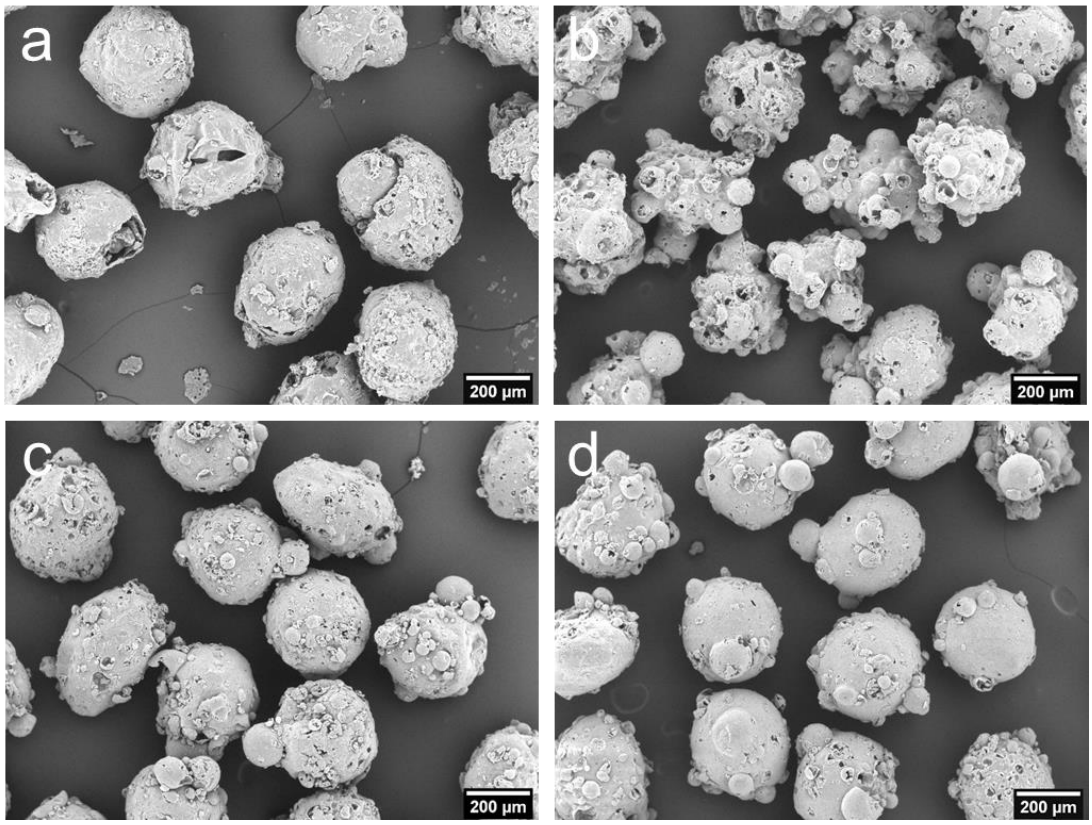

Figure 6.5 SEM micrographs of spray dried detergent powders (300-350 µm). Detergent powders produced from low-water content slurries (a), high-water content slurries (b), low-water content slurries containing 1.6 SiO2:Na2O R (c) and 2.35 SiO2:Na2O R (d).

6.2.2 Flowability measurements

The measured flow functions of spray-dried detergent powders are shown in Figure **6.6**. In general, a steep slope of the flow function represents a cohesive powder with poor flow characteristics. Flow becomes smoother as the flow function line moves in a clockwise direction towards the major consolidation stress axis. The flow index of each sample was determined from

the slope of flow function and summarised in Figure **6.6**. For detergent powders produced from low-water content slurries, the greater slope of flow function line implies that the granules have developed a greater strength upon consolidation, which is then required to be overcome by a greater force to initiate flow (Fitzpatrick et al., 2004). These samples showed the lowest flow function value, and were classified as a very cohesive powder ($ff_c < 2$). Interestingly, the increased water content of the slurries, considerably improved the flow-behaviour of the resulting powders, though they are still classified as cohesive materials ($ff_c < 4$). Returning to microscopic observations, it was shown that the latter samples were comparatively irregular and had a blistered appearance. In general, granules with a rougher surface have a larger number of contacts which results in a greater frictional inter-particle interaction, *e.g.*, mechanical interlocking, which renders the granules more cohesive than those that are smoother (Zhou and Qiu, 2010). The results suggest that even though granule morphology can play a significant role in determining flowability, other factors might have been more predominant. In general, poor powder flowability is a consequence of the combine effects of inter-particle interactions, *i.e.*, internal friction and cohesion, which are largely determined by chemistry and powder structure (Fitzpatrick, 2013, Zhou and Qiu, 2010). However, these factors are known to be more pronounced for fine particles (less than ~ 10 μm) than coarse particles. Therefore, the flowability was less likely to be governed by the cohesive forces such as molecular van der Waals force and liquid surface capillary force.

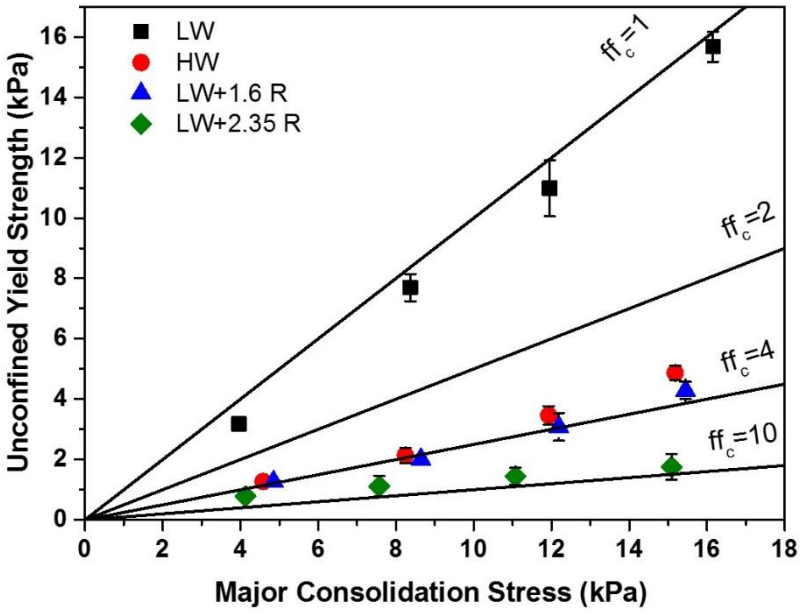

Figure 6.6 Instantaneous flow functions of spray-dried detergent powders.

A possible explanation of the improved flowability of the irregular detergent granules can be due to a change in matrix composition as a consequence of the increased water content of the slurries. This may consequently influence the powder structure and hence micro-properties, *e.g.*, particle contact stiffness, of the powders, thereby affecting their macro-behaviour, *e.g.*, flow-behaviour (Tomas, 2004a). The influence of initial water content of the slurries on the matrix composition and hence surface microstructure of the powders will be discussed later in section 6.2.3.

Also, an increase in flowability of detergent powders was observed upon the addition of sodium silicates. For low-water content detergent slurries, the addition of sodium silicate with the SiO_2:Na_2O molar ratio of 1.6 slightly improved the flow behaviour from very cohesive to cohesive characteristic. However, the detergent powders became free-flowing (ff_c < 10) once the SiO_2:Na_2O molar ratio of sodium silicate was increased to 2.35. The evaluation of consolidation behaviour of the powder beds during the pre-shearing stage can provides some clues to the role of components as well as the matrix composition on the flowability. Figure **6.7** shows the shear force-displacement curves during pre-shearing stages of shear cell test measurements. At the pre-

shearing stage, the powder bed may undergo an elastic deformation whereby the granules rearrange themselves and fill the voids within the powder bed. As the elastic deformation progresses by rearranging and sliding of the particles, as a consequence of the increasing normal stress, the bulk volume decreases due to the reduction of interstitial spaces. This gives rise to increasing the number of contacts between the particles, consequently developing shear forces within the powder bed. The build-up of shear force at this stage can also be accompanied by frictional plastic deformation of the sheared particles until a constant shear force is reached. For free-flowing powders, the powder bed reaches the steady-state flow at a lower shear force, while for cohesive powders a shear force maximum can be achieved at the pre-shearing stage (Hintz et al., 2008).

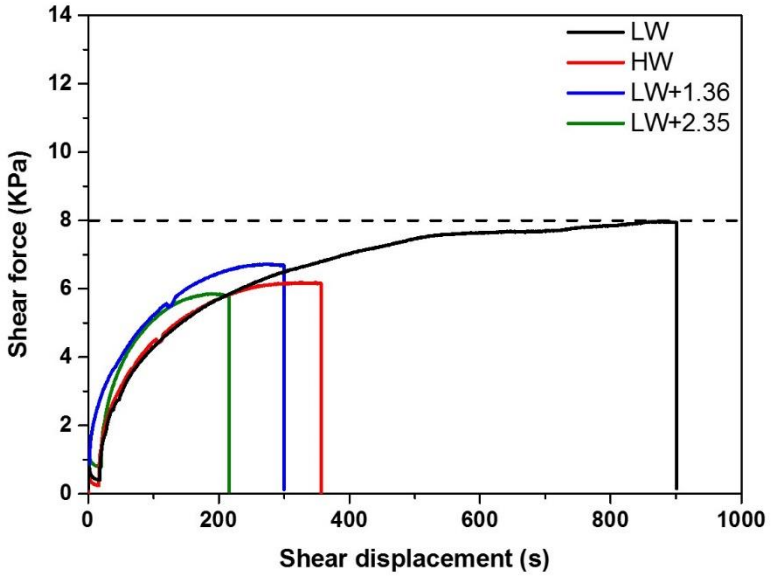

Figure 6.7 Results of force-displacement obtained from the pre-shearing stages, measured at 8.0 kPa, σpre.

From Figure **6.7** it can be seen that for spray-dried powders produced from low-water content slurries, a relatively long time is required to obtain a constant shear rate. In other words, a large deformation within the powder bed is required to reach a steady-state flow. This implies a structurally loose powder bed, possibly due to the presence of many voids, i.e., interstitial spaces, which collapses with increasing the applied normal force. As mentioned earlier, the puild-up of

the shear force upon the reduction of the interstitial spaces, can concomitantly occurs with the plastic deformation. For very cohesive detergent powders, a considerably prolonged shear-displacement after 500 s of pre-shearing can be due to a frictional plastic deformation. Tomas (2004a) investigated the fundamentals of flow behaviour of cohesive powders, both theoretically and empirically, and showed a complete set of physically based equations for different states of power flow, e.g., steady-state flow and incipient flow, during a shear test. The author suggested that the effect of surface micro-properties, e.g., surface contact stiffness or softness, on the flowability, can be indirectly described from the angles of internal friction at steady-state and incipient flows. The smaller the differences between these values, the stronger the particle contact points and, hence, the more free-flowing powder. The flow properties of spray-dried powders, at 8.0 KPa normal pressure, are shown in Table **6.3**.

Table 6.3 Flow indices and friction angles, i.e. φlin and φe of spray-dried detergent powders measured under a pre-sheared normal stress of 8.0 kPa

Description	ff_c	φ_e	φ_{lin}
LW	1.03	76.6	21.6
HW	3.09	44.9	36.4
LW+1.6 R	3.40	43.4	35.3
LW+2.35 R	8.60	37.6	34.7

Considering the angles of internal frictions, a relatively large difference can be seen between φe and φlin for the detergent powders produced from low-water content slurries. This likely points to softer surface contacts between the detergent granules. From the analysis of the results of shear-cell test measurements, it can be inferred that very cohesive detergent powders are likely to possess a structurally loose, and low-bulk density bed in which the detergent granules probably undergo a greater frictional plastic deformation with increasing the shear force. The influence of the matrix composition on the mechanical properties of the detergent granules will be discussed

in section 6.2.4. X-ray microtomography technique can provides good insight into the packing of the granules within bulk solids. The 3D reconstructions of the regions of interest from the original volumes, plastic tubes, are illustrated in Figure **6.8**. The presence of remarkably large interstitial spaces, *i.e.*, inter-particle voidag, is evident within the bulk powders produced from low-water content slurries. This observation is in good agreement with the pre-consolidation behaviour of these powders (Figure **6.7**), showing a relatively prolonged shear-displacement until ~ 500 s, which mainly arises from the plastic deformation of the powder bed.

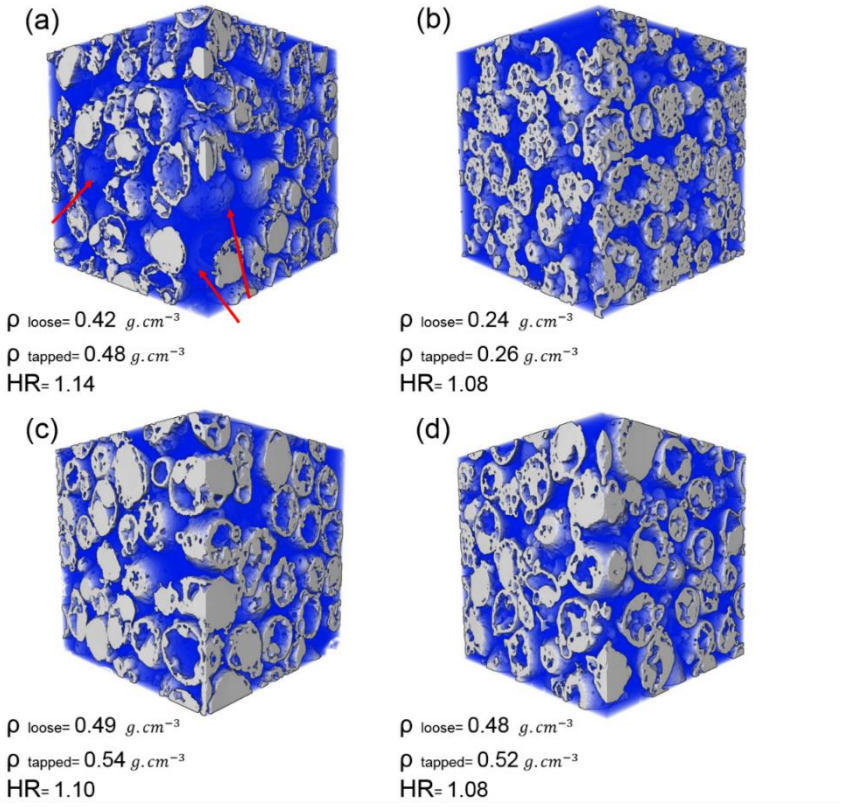

Figure 6.8 XRT visualization (voxel size: 2.50 μm) of the packing of spray-dried detergent powders produced from low-water content (a) and high-water content slurries (b), and detergent slurries containing sodium silicate with the SiO2:Na2O molar ratio of 1.6 (c) and 2.35 (d). The 3D cubes (1500×1500×1500 μm) were cropped from their original volume. The arrows present the existence of relatively large interstitial spaces (blue regions) within a tapped powder bed. The results of bulk density measurements, i.e., ρ loose and ρ tapped, obtained from the mechanical tapping device, and the corresponding Hausner ratios (HR) are summarized on the panels (a-d).

From the bulk density measurement results, obtained from the mechanical tapping device, once again it was noticed that spray-dried detergent powders produce from low-water content slurries had the poorest flow among the all samples. These powders showed the largest Hausner ratio (*HR*=1.14) and were considered to be medium flowing according to the classification of Hayes (**Table 6.2**.).

These results suggest that the aforementioned granules have a tendency to form a structurally loose powder bed with many interstitial spaces upon pouring in a container, which subsequently undergo a greater degree of particle rearrangement upon tapping (Li et al., 2004b, Nordström and Alderborn, 2011). In general, the greater the compressibility, the poorer the flowability. Although these powders are classified as medium flowing here, they were earlier shown to be very cohesive powders according to the Jenike's classification. A reason for this discrepancy can be simply explained by lower stresses applied to the powders under tapping conditions. For the characterization of bulk solids under free surface conditions, *e.g*., Hausner ratio method, particles predominantly show some degree of rearrangement upon pouring into a cylinder, though a slight plastic deformation on particle contact points can still occur due to the disturbance induced by tapping. Therefore, a possible reason for a poor flow characteristics of these powder under the action of higher stresses, might have been due to the plastic deformation at particle surface contacts during the shearing in shear cell tester. This consequently develops cohesion between powder particles as a consequence of the increased contact points. Nevertheless, even under low stress conditions, spray-dried powders produced from low-water content slurries in the absence of sodium silicate, showed a poorer flow characteristics as compared with other samples. Therefore, although the rigidity of particle contacts has a major effect in determining the flow characteristics, an additional factor must also play a significant role in the observed flow behaviour of these powders.

6.2.3 Surface and matrix composition

Surface composition of the granular products is known to have a significant effect on their flow behaviour. This not only influences the intra-particle forces, *e.g.*, van der Waals and capillary forces, between powder particles, but also determines the micro-properties, *e.g.*, stiffness and softness, in particle-surface contacts. Raman spectroscopy is known to be a convenient probe for qualitative and quantitative analysis of the functional groups of material surfaces since the Raman signal is proportional to the concentration of the molecules. When Raman spectrometer is combined with a confocal microscope, it is possible to preferentially collect detailed information regarding the chemical composition from the particle surface (Kudelski, 2008). Figure **6.9** shows the Raman spectra of spray-dried detergent powders in the 400-1250 cm^{-1} region. The Raman spectra are dominated by a very sharp and intense band at ~ 990 cm^{-1} which is attributed to symmetric stretching vibrational mode (υ_1) of the free SO_4^{-2}anion with a tetragonal symmetry T_d, in the lattice of sodium sulphate crystal. The peaks corresponding to the asymmetric stretching vibrational mode ($\upsilon 3$) of sodium sulphate can be observed in the high-wavenumber side with respect to υ_1 mode, while the bending vibrational modes (υ_2 and υ_4) can be detected in the low-wavenumber side (Hamilton and Menzies, 2010). For the detergent powders produced from high-water-content slurries, three sharp and distinct Raman bands at 1099, 1132 and 1150 cm^{-1} are assigned to the υ_3 mode of the sulphate in sodium sulphate crystal lattice. A doublet is clear in υ_2 region with peaks at 447 and 464 cm^{-1}, and finally, well-defined triple peaks assigned to υ_4 mode, occur between 618, 631 and 646 cm^{-1}. These well distinguished and very sharp peaks demonstrate the existence of anhydrous sodium sulphate crystals, *i.e.*, thenardite, on the particle surface (Ben Mabrouk et al., 2013). The Raman peaks observed at 1047 and1191 cm^{-1} can be assigned to the symmetric and asymmetric stretching vibrations of S-O bonds in sulphonate group of NaLAS, which is in good agreement with the FTIR patterns reported in the literature (Wang et al., 2012, Xu and Braterman, 2003). For the above-mentioned powders, two peak components at 1047 and 1191 cm-1 are very weak and appear as a shoulder.

For detergent granules produced from low-water content slurries, however; the Raman peaks at 1101, 1132 and 1150 cm^{-1}, which are assigned to the asymmetric S-O stretch of sodium sulphate crystals, are less resolved and of lower intensity than those of powders produced from high-water-content slurries. On the other hand, the peaks at 1047 and 1191 cm^{-1}, assigned to asymmetric stretching vibration of S-O bonds in LAS, are noticeably stronger. This remarkable differences in spectral features implies a relatively higher concentration of the surfactant on the particle surface of the detergent powders produced from low-water-content slurries.

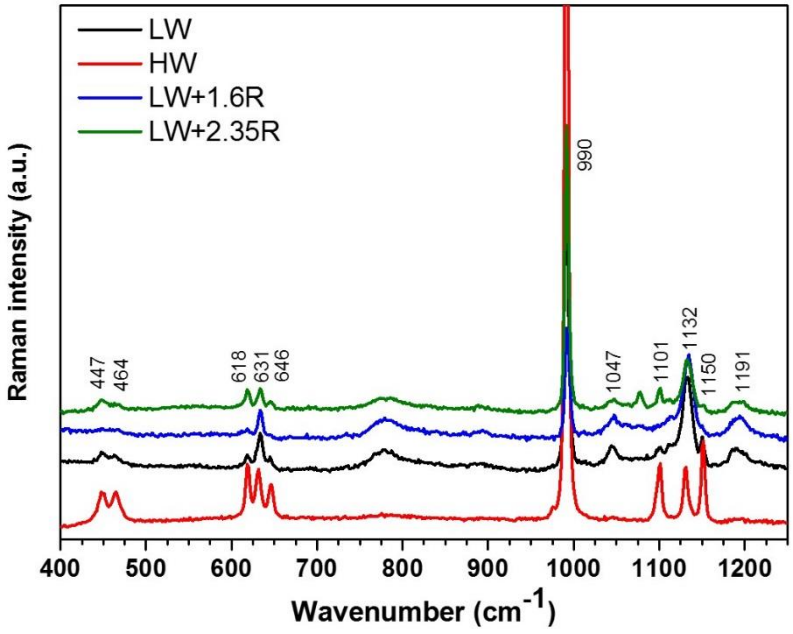

Figure 6.9 Raman spectra (400-1400$\boldsymbol{cm^{-1}}$) of spray-dried powders as a function of detergent formulation. Notes: (LW) low-water content slurry; (HW) high-water content slurry; (LW+1.6 R) low-water content slurry containing 1.6 SiO_2:Na_2O R.

The C-H aliphatic stretching frequency occurs in the range of 2800-3000 cm^{-1} where the spectra are dominated by symmetric and asymmetric stretching vibrations of methyl groups (-CH_3) and methylene groups (-CH_2) of the alkyl chains. The peaks between 3000 and 3100 cm^{-1} are assigned to aromatic C-H stretching modes of benzene rings (Li et al., 2005, Watry and Richmond, 2000). Since LAS surfactant molecules possess a benzene ring attached to a long hydrophobic alkyl chain in their structures, the intensities of the aforementioned stretching modes in Raman spectrum can

be, more specifically, used to evaluate the concentration of NaLAS on the granule surface. Typical Raman spectrum obtained from the detergent granules can be seen in Figure **6.10**. For detergent powders produced from low-water content slurries, in the absence of sodium silicate, a relatively higher intensity of peaks between 2917 and 2850 cm^{-1}, signify larger quantities of LAS surfactant on the surface. The addition of sodium silicate resulted in a noticeable reduction in intensities. This was expected since this alters the chemical composition of the surface. However, the lowest intensity was observed when the initial water content of the slurries was increased to 63 wt%.

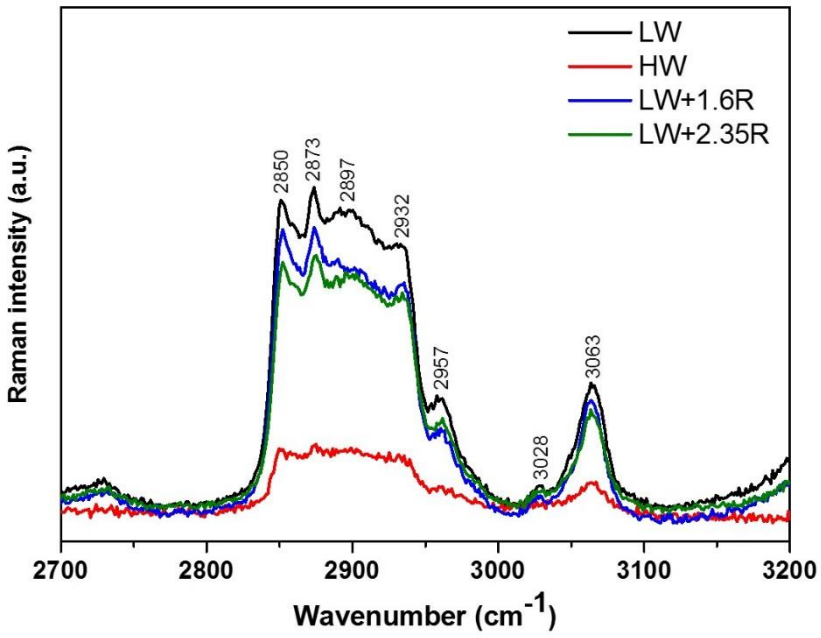

Figure 6.10 Raman spectra (2700-3200 cm-1) of spray-dried powders as a function of detergent formulation. Notes: (LW) low-water content slurry; (HW) high-water content slurry; (LW+1.6 R) low-water content slurry containing 1.6 SiO_2:Na_2O R.

Returning to the composition of the detergent slurries, presented in Chapter 3, although high-water and low-water content slurries, in the absence of sodium silicates, differ in initial NaLAS concentration, they are estimated to have identical chemical composition upon removal of water. However, according to the Raman results, the surface of detergent powders produced from low-water content slurries appears to be richer in NaLAS. The reason for this can be explained by the difference in matrix composition. The matrix can be defined as a solid continues phase excluding

the undissolved sodium sulphate, in which the nano-sized crystals of inorganic salts along with lamellar liquid crystalline phases of NaLAS are dispersed. It was earlier shown that the matrix composition and microstructure of the detergent powders can be largely determined by the initial water content of slurries. The higher the concentration of water, the greater are the quantities of dissolved sodium sulphate within the slurry matrix. This consequently increases the ratio of dissolved sodium sulphate to NaLAS "active matter" within the matrix of the resulting powders. Therefore, it is the increased dissolved sodium sulphate within the matrix that is mainly responsible for the observed reduction in the aliphatic C-H stretching intensity. This view can be better elucidated by examining the 3-D XRT images of detergent granules. Figure **6.11**b shows the spatial distribution along with the number-weighted mean diameter distribution of remaining undissolved sodium sulphate within a typical detergent granule produced from low-water content slurries. It can be seen that the main number of the crystalline particles are distributed in the range of ~5-30 µm and a secondary population can be observed in a range of 30-70 µm. Also, a small number of considerably large particles is noticeable around ~120 µm. The increased water content in detergent slurries, however; significantly reduced the size of remaining particles. From Figure **6.11**d it can be noticed that the particles are only distributed in a limited range of ~5-40 µm, suggesting the increased quantity of dissolved sodium sulphate within the matrix. The influence of the initial water content on the matrix composition was also manifested in the surface microstructure where a crystalline surface was observed for the resulting powders (Figure **6.11**c) as compared with those produced from low-water content slurries. The microscopic observations of the latter case (Figure **6.11**a) became of significant interest as viewed in conjunction with the results of confocal Raman microscopy indicating the highest intensity in the C-H aliphatic stretching region as the consequence of a greater LAS concentration. It has been reported that LAS powders are intrinsically sticky and are less free flowing (Zoller, 2004). This can potentially explain the relatively higher HR value (1.14) for these samples. Therefore, the effect of LAS on the flow behaviour of the detergent powders can be two folds. On one hand the presence of LAS on the granule surface increases the stickiness of the powders. On the other hand their higher ratio

to dissolved sodium sulphate within the granule matrix may result in softer surface contacts between the powder particles which consequently increases the cohesion within the powder bed.

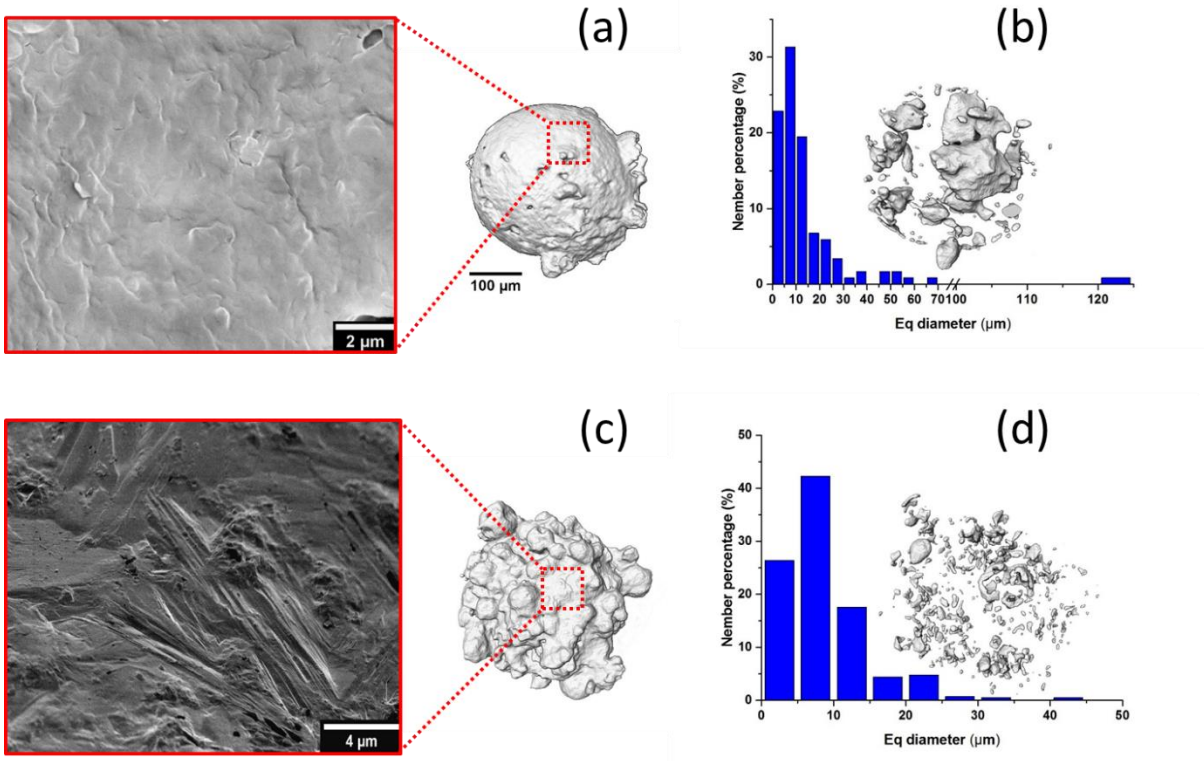

Figure 6.11 3D XRT reconstruction (voxel size: 1.76 µm) of a detergent granule (equivalent dimeter: 304.97 µm) produced from low-water content slurries (a) along with a typical SEM micrograph illustrating the surface microstructure of these powders and, 3D view of the undissolved sodium sulphate particles (b) as well as the corresponding number-weighted size distribution. (c) and (d) Show typical surface morphology of a detergent granule (equivalent dimeter: 326.90 µm) produced from high-water content slurries and its spatial distribution of remaining sodium sulphate crystals respectively.

6.2.4 Mechanical properties

The different parameters obtained from the uniaxial compression tests on spray-dried detergent powders are presented in Table **6.4**. For the single particle compression tests, free-silicate samples produced from low-water content slurries, showed the lowest mean rupture strength. This can potentially explain the consolidation behaviour of these powders during the pre-shearing stage of shear cell test measurements (Figure **6.7**). A noticeably large displacement, which is a measure of the extent of strain within the powder bed, was partially attributed to plastic deformation. In

general, the softer the particle contacts, the greater are the plastic deformation around the contacts and, hence, the poorer is the powder flow (Tomas, 2004b). Therefore, it was a relatively weaker particle strength that was responsible for the poor powder flow behaviour. The increased water content of the detergent slurries, however; considerably increased the mechanical strength of the resulting granules. This can be attributed to greater quantities of dissolved sodium sulphate within the matrix, which therefore alters the matrix composition. Evidence for this can be found in Figure **6.11**d showing the presence of relatively small sodium sulphate particles, mainly, in the range ~ 5-25 µm, when compared with its counterpart in Figure **6.11**b. The poor mechanical strength of the powders was also remarkably improved by the addition of sodium silicates to the detergent slurries. This was expected since concentrated sodium silicate solutions are known to possess unique binding properties due to having unique plasticising effect along with, high activity and strong hygroscopicity, which enable them to serve as binders in many applications (Goberis and Stonis, 2004, Yang et al., 2008b). Commercially available sodium silicate solutions are described as colloidal dispersions of monomeric and polymeric anions. Upon drying, the removal of water from the interstitial spaces causes aggregates to come into close proximity until they form a rigid glass (Roggendorf et al., 2015). The formation of this glassy binder can therefore impart a rigid characteristic on the granule microstructure. The addition of sodium silicate with SiO_2:Na_2O molar ratio of 1.6, remarkably increased the mean rupture strength of the granules. However, the largest mean rupture strength was observed once the molar ratio was increased to 2.35. This can be explained by the fact that with SiO_2:Na_2O molar ratio > 2, sodium silicate solutions mainly contain polymerized silicates which act as effective rigid particles (Böschel et al., 2003, Yang et al., 2008b).

Table 6.4 Average values with standard deviations for the parameters of bulk compression model, and the granule rupture strength derived from the single compression test.

Sample	Single particle compression	Kawakita and Lüdman	
	σ_r, *kPa*	*a*	*1/b, kPa*
LW	27.29±9.42	2.69±0.06	135±27
HW	72.75±25.28	3.37±0.56	264±59
LW+1.6 R	239.44±83.51	2.68±0.03	576±31
LW+2.35 R	262.34±77.50	2.80±0.04	674±64

While the uniaxial single compression test directly measures the apparent strength of the single granules, the fitting of the experimental bulk compression data into Kawakita model provides a good understanding of the consolidation mechanisms, e.g., particle rearrangement and plastic deformation, as well as overall mechanical properties, e.g., yield strength, of the powders. Typical Kawakita plots for spray-dried powers are presented in Figure **6.12**. In all cases the plots show a curved profile at initial compressive pressures, and a linear region can be observed at larger compacting pressures. In general, the initial curved region is mainly attributed to granule sliding and rearrangment at the beginning of compaction process. For the silicate-free samples produced from low-water content slurries, this non-linear region is limited to a noticeably small compressive pressure range (P < 25 kPa), which suggests that compaction of theses powders mainly occurs through plastic deformation (Arifvianto et al., 2015).

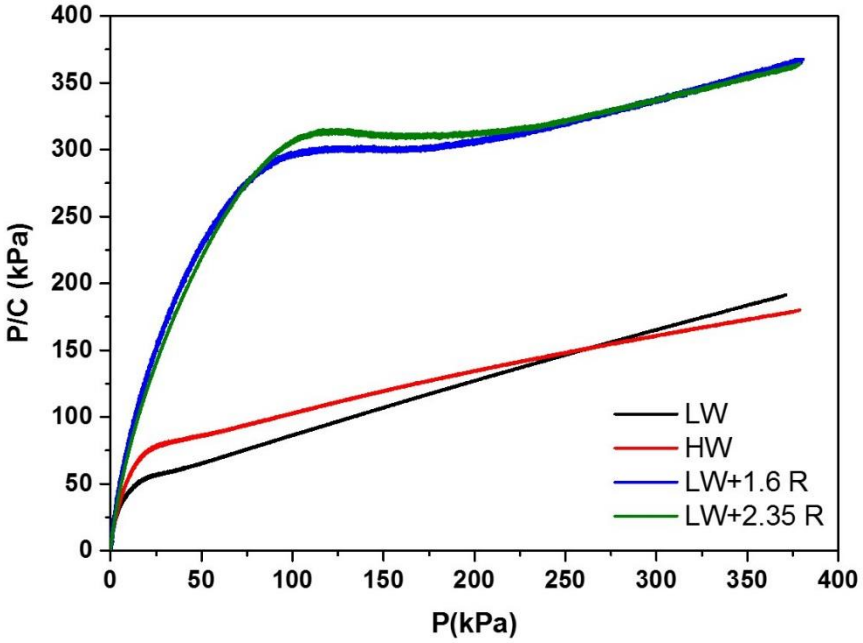

Figure 6.12 Typical kawakita plots for the bulk compression of spray-dried detergent powders.

From Table **6.4** the lowest value of Kwakita parameter 1/b indicates that these powders possess the least resistence against compression. With increasing the water content of the detergent slurries, the Kawakita plots of the resulting powders tend to bend at a slightly larger compressive pressure around ~ 50 kPa, suggessting a relatively stronger powder bed structure against compression. However, the addition of sodium silicate resulted in the plots having a more pronounced curve in a larger range of pressure up to ~125 kPa, which suggests that particle rearrangement plays a significant role in consolidation behaviour of these powders. This yielded larger 1/b values comparing to silicate-free samples. Regarding the Kawakita parameter *a*, the values were alsmost similar for the samples produced from low-water content slurries. However, detergent powders produced from high-water content slurries showed the largest values of physical constant *a*, indicating a greater ability of these powders to compress at the infinit compression pressure (Nordström et al., 2009). The reason for this can be explained by the internal structure of these powders. It was previously demonstrated that the increased water content of the slurries results in the formation of low density foam powders. From Figure **6.8** it

can be seen that these powders possess the lowest loose bulk density (ρ_{loose}=0.24 g.cm^3), which therefore increases the compressibility of the powder bed.

6.3 Conclusions

In this Chapter the influence of initial slurry water content and binder, SiO_2:Na_2O molar ratio of sodium silicate, on the powder flowability was investigated. The initial water content of the detergent slurry was found to play a crucial role in flow behaviour of the resulting powders. The greater the water content of the slurry, the lesser is the remaining undissolved sodium sulphate within detergent granules. The increased dissolved sodium sulphate was evident in SEM micrographs showing a more crystalline surfaces. Therefore, this increases the sodium sulphate-to-LAS ratio within the matrix, and hence improves the mechanical strength of the granules. The microscopic observations were also in good agreement with the spectra obtained from confocal Raman microscopy which showed a lower surface concentration of surfactant in detergent granules produced from high-water content slurries. A reduction in volume fraction of a soft or waxy solid phase not increases the granule strength, but also decreases particle stickiness. The reason that detergent powders produced from low-water content slurries were classified as "medium flowing" according to the classification of Hayes, even though they already showed a poor flow behaviour as measured by Schulze Ring Shear Tester, can be attributed the plastic deformation of granules during the shearing in shear cell tester. Nevertheless, the 3D visualization of interstitial spaces within the powder bed revealed that these granules are very cohesive even in the absence of shearing force. These granules tend to form open structures upon pouring into a container, which are not readily collapse by tapping, leading to a lower bulk density. The addition of sodium silicate with SiO_2:Na_2O molar ratio of 1.6 noticeably improved the flow behaviour, though they are still classified as cohesive materials according to the Jenike's classification. This improved flow behaviour was attributed to the increased granule strength. The detergent

powders became free-flowing ($ff_c < 10$) once the SiO_2:Na_2O molar ratio of sodium silicate was increased to 2.3, while their mechanical strength was slightly higher than those containing silicate with SiO_2:Na_2O molar ratio of 1.6. This can be explained by this fact that sodium silicates show different characteristics as the molar SiO_2:Na_2O changes. Sodium silicates with SiO_2:Na_2O molar ratio > 2, mainly contain polymerized silicates which in turn show different viscoelastic properties. The presence of glassy polymeric films on the granule surface is thought to cause granules to easily rearrange and slide over each other.

Chapter 7 Overall conclusions and future work

7.1 Conclusions

In this thesis, the multiscale structure of spray dried detergent granules was characterized using a complementary range of techniques. A complex composite structure was revealed due to the multiphase nature of the starting slurry and its evolution during the drying process. The structure revealed can be viewed as a solid multi-component colloidal system where sub-micron crystals of inorganic salts along with lamellar liquid crystals of LAS are dispersed within a porous matrix saturated with inorganic salts. The 3-dimensional x-ray tomography provided detailed information on the internal structure of spray-dried detergent powders. The crystals of sodium sulphate are initially undissolved in the slurry and are consequently reduced in number in the product made from higher water content slurry. In general, the higher the water content, the lower is the quantity of remaining undissolved sodium sulphate within the granules. Air is also dispersed in this matrix at two length scales, large vacuoles, driven by 'puffing' *i.e.* water boiling, and micro-scale porosity which evolved during the crystallisation of the drying matrix. The remaining undissolved sodium sulphate particles are either non-homogeneously dispersed around the central vacuole or occupy most of the internal space of the granules as a big particle depending on the detergent granule size. The addition of binders gave rise to the formation of a large number of macro-pores within the granule matrix. This was attributed to the skin forming properties of sodium silicates. For spray-dried detergent powders produced from high-water content slurries central vacuole is not a commonly encountered characteristic. In these granules, the internal structure was a more "foam-like" structure.

The slurry water content also plays a crucial role in governing the granule size and morphological properties of the detergent powders. The increased water content resulted in the formation of irregular granules with rough edges. However, the low-water content slurries have a tendency to produce nearly spherical granules, though a number of adhered fine particles on the granule surface can be observed in the presence of sodium silicate. The mean size of the detergent granules

was found to increase with increasing the water content, which was attributed to the increased build-up of gas pressure, leading to the particle ballooning and puffing. Surface characteristics were also seen to change with the high initial water content producing more crystalline surface.

At the nano-scale, changes in the initial water content or binder, are seen to change both the sulphate polymorphs present and the *d*-spacing of the LAS phase. The increased water content or addition of sodium silicate resulted in the formation of metastable phase of sodium sulphate (phase III). In the absence of sodium silicate, several sets of lamellae were detected in spray-dried detergent powders. This can be explained by the intrinsic polydispersity of LAS molecules, leading to the formation of domain of different composition which are subsequently dehydrated to different extent. The exposure of the detergent granules to a higher relative humidity (70% RH) decreased the population of coexisting lamellar polymorphs. The lamellar *d*-spacing was seen to decrease.

This study reports for the first time a detailed structural analysis of the self-assembled structures of LAS molecules in detergent powders. From the analysis of electron density profiles, it was shown that the water layer thickness (d_W) of lamellar phases increases, while the bilayer thickness (d_{HH}) decreases with increasing the RH value. This reduction in d_{HH} value was accompanied by a transition from *tran*s to *gauche* conformation in hydrocarbon chains. Therefore, with increasing the relative humidity, the existence of domains with large lamellar *d*-spacing consisting of *trans* conformers are not favoured. Interestingly, the spray-dried detergent powders containing sodium silicate showed fewer number of coexisting lamellar polymorphs at the same relative humidity (33% RH). This was due to the hygroscopic characteristics of the sodium silicate which results in a greater equilibrium moisture content as compared with those silicate-free samples. The greater degree of swelling of lamellar phases might be due to an interaction between silicate species and surfactant head groups through direct hydrogen bonding, leading to the separation of head groups. However, at a higher relative humidity (75% RH), the behaviour of lamellar phases was complex in the presence of sodium silicate. Surprisingly, the water layer thickness decreased and this was concomitant with an increase in bilayer thicknesses. The behaviour was explained by the

kosmotropic nature of sodium silicate by which the osmotic pressure is regulated. It was hypothesized that a transition from the glassy to rubbery state at such humid conditions may have resulted in the exposure of a greater number of buried silanol groups whereby a larger osmotic gradient is established and thus extruding water from the bilayers. In other words, while at low relative humidity the hydrogen bonding properties of sodium silicate might have been of significant importance, their kosmotropic effect become predominant at higher RH values.

For the first time, the moisture sorption characteristics of spray-dried detergent powders were related directly to the microstructure and slurry formulation. The morphology was shown to have a significant effect on the water sorption characteristics. In the absence of sodium silicate, the samples produced from high-water content slurries, having a more porous structure and rough surfaces, showed a larger moisture uptake. This larger moisture uptake was attributed to their greater effective surface area. However, the largest equilibrium moisture content at any given relative humidity was observed in detergent powders containing sodium silicate due to their hygroscopic nature. The experimental data were analysed with the mathematical equations. For the nil-silicate samples the mathematical models, *i.e.*, BET, GAB and Oswin described the experimental data well. However, in the presence of sodium silicate, the GAB and Oswin models failed to predict the equilibrium moisture contents obtained from the adsorption process. This was due to a sudden change in moisture sorption behaviour of detergent powders which is not accounted for in these equations. The kinetic of water sorption was suggested to be dominated by the solid state of sodium silicate. A transition from a glassy to rubbery state in sodium silicate, as the consequence of water plasticisation, can considerably increase the water sorption capacity by exposing a greater number of hydrophilic groups. Indeed, in this study a new method based on a gravimetric vapour sorption and ATR-FTIR was developed to assess the glass transition humidity of amorphous materials in spray-dried detergent powders.

The flow behaviour of these powders was affected by both the slurry water content and the addition of binding materials. The results suggest that the surface properties, and mechanical robustness, were more important to the flowability than the shape. In the absence of

sodium silicate, the increased water content significantly improved the flow behaviour which was mainly attributed to the increased mechanical strength of the granules. As it was previously shown earlier in Chapter 3, the initial water content is an important factor determining the matrix composition and hence surface microstructure. This can potentially alter the mechanical properties. In Chapter 6 the combination of confocal Raman microscopy and x-ray micro-CT allowed for a good understanding of the role of slurry water content on the matrix and surface composition. The increased water content resulted in a greater ratio of inorganic salts to LAS within the matrix as it was evident in SEM micrographs as well as the Raman spectra obtained from confocal Raman microscopy. The increased dissolution of sodium sulphate also resulted in the form of small remaining undissolved crystallites in 3D XRT reconstruction of single detergent granules. The greater the ratio of inorganic salts to soft and waxy solid phase, *i.e.*, LAS, within the matrix, the greater is the mechanical strength, and hence the greater the resistance against plastic deformation. The SiO_2:Na_2O molar ratio of sodium silicate on the powder flowability was also investigated. The addition of sodium silicate with a molar-ratio of 1.6 to the low-water content slurries resulted in a considerable increase in the mean rupture strength of the granules and improved the powder flowability, though they were still classified as "cohesive" according to the Jenike's classification. The largest mean rupture strength was observed once the molar ratio was increased to 2.35. This was explained by the fact that concentrated sodium silicate solutions adopt different characteristics, *e.g.*, rheological and binding characteristics, depending on the SiO_2:Na_2O molar ratio. A higher molar ratio increases the concentration of polymerised silicates. This is thought to form a glassy film on the surface upon drying, which causes the granules to easily rearrange and slide over each other.

7.2 Future work

This thesis provided a fundamental understanding of the structure of spray-dried detergent powders using four simple model formulations. Typically, the role of water as a key versatile ingredient, was particularly highlighted in the structure, matrix composition and functional properties. Changes in the matrix composition were seen to change both the flowability and mechanical properties of the detergent powders. The findings of this study, however; can be applied to a wider formulation space. For example the role of remaining undissolved inorganic salts in the structure and functional properties can be elucidated by increasing the amount of undissolved solids within a fixed matrix. Furthermore, for a better selection of process variables, the slurry formulations of the current study can be investigated at different process conditions.

However, from the technological point of view, the large scale equipment required to make representative granules, limit the formula space that can be studied. Additionally, assessing the relationship between matrix composition and their intrinsic properties is sometimes fraught with difficulties due to convolution with geometry, heterogeneity, and porosity effects. Consequently, a system for producing repeatable dried detergent matrix formulations with controlled, reproducible geometry is required. One approach can be producing a thin film of detergent slurry. Spin coating is one of the most commonly used technique for depositing thin films to substrates. The thickness of the dried coated film can be typically controlled by rotation speed, feed concentration and drying temperatures. The resulting films are almost pore free with a smooth surface. Therefore, this system can also be ideal for characterization of mechanical and surface properties for atomic force microscopy (AFM) and nano-indentation test. The surface provides an excellent substrate for investigating wetting, coating and dissolution of matrix materials. Also, such a system can typically overcome the problems encountered in the microscopic observation of liquid –crystalline phases of surfactant molecules in detergent powders. Transmission electron microscopy (TEM) is a typical and commonly used technique for the visualisation of these self-assembled structures. This requires preparing ultra-thin specimens, less than 100 nm thick, on a TEM grid which allows for a good observation. Several preparation techniques have been

developed to prepare thin specimens, including focused ion beam (FIB) and microtome sectioning. In the current work, an attempt was made to produce thin slices using the microtome sectioning technique. However, the main disadvantage of this technique is that water-soluble components are readily dissolved upon floating the thin slices on the top of aqueous solutions of a microtome bath. An alternative approach can be depositing a thin film of detergent slurries on TEM grids.

References

.

AGUILERA, J., DEL VALLE, J. & KAREL, M. 1995. Caking phenomena in amorphous food powders. *Trends in Food Science & Technology,* 6**,** 149-155.

AHLNECK, C. & ZOGRAFI, G. 1990. The molecular basis of moisture effects on the physical and chemical stability of drugs in the solid state. *International Journal of Pharmaceutics,* 62**,** 87-95.

ALEXANDRIDIS, P., OLSSON, U. & LINDMAN, B. 1998. A Record Nine Different Phases (Four Cubic, Two Hexagonal, and One Lamellar Lyotropic Liquid Crystalline and Two Micellar Solutions) in a Ternary Isothermal System of an Amphiphilic Block Copolymer and Selective Solvents (Water and Oil). *Langmuir,* 14**,** 2627-2638.

ALSOP, R. J., SCHOBER, R. M. & RHEINSTÄDTER, M. C. 2016. Swelling of phospholipid membranes by divalent metal ions depends on the location of the ions in the bilayers. *Soft Matter,* 12**,** 6737-6748.

ANDERSEN, H. D., WANG, C., ARLETH, L., PETERS, G. H. & WESTH, P. 2011. Reconciliation of opposing views on membrane–sugar interactions. *Proceedings of the National Academy of Sciences,* 108**,** 1874-1878.

ANDERSON, P. R. & BENJAMIN, M. M. 1985. Effect of silicon on the crystallization and adsorption properties of ferric oxides. *Environmental Science & Technology,* 19**,** 1048-1053.

ANSARI, M. A. & STEPANEK, F. 2008. The effect of granule microstructure on dissolution rate. *Powder Technology,* 181**,** 104-114.

ARANOVICH, G. & DONOHUE, M. 1998. Analysis of Adsorption Isotherms: Lattice Theory Predictions, Classification of Isotherms for Gas–Solid Equilibria, and Similarities in Gas and Liquid Adsorption Behavior. *Journal of Colloid and Interface Science,* 200**,** 273-290.

ARIFVIANTO, B., LEEFLANG, M. A. & ZHOU, J. 2015. The compression behaviors of titanium/carbamide powder mixtures in the preparation of biomedical titanium scaffolds with the space holder method. *Powder Technology,* 284**,** 112-121.

ARTHUR, E., TULLER, M., MOLDRUP, P. & DE JONGE, L. W. 2016. Evaluation of theoretical and empirical water vapor sorption isotherm models for soils. *Water Resources Research,* 52**,** 190-205.

ASAY, D. B. & KIM, S. H. 2005. Evolution of the Adsorbed Water Layer Structure on Silicon Oxide at Room Temperature. *The Journal of Physical Chemistry B,* 109**,** 16760-16763.

ATZENI, C., CABIDDU, M. G., MASSIDDA, L. & SANNA, U. 1995. Crystallization of sodium sulphate in polymer impregnated plasters. *Cement and Concrete Composites,* 17**,** 3-8.

BAJPAI, D. & TYAGI, V. K. 2007. Laundry Detergents: An Overview. *Journal of Oleo Science,* 56**,** 327-340.

BARNETTE, A. L., ASAY, D. B. & KIM, S. H. 2008. Average molecular orientations in the adsorbed water layers on silicon oxide in ambient conditions. *Physical Chemistry Chemical Physics,* 10**,** 4981-4986.

BARRERA-MEDRANO, D., SALMAN, A. D., REYNOLDS, G. K. & HOUNSLOW, M. J. 2007. Chapter 25 Granule structure. *In:* SALMAN, A. D., HOUNSLOW, M. J. & SEVILLE, J. P. K. (eds.) *Handbook of Powder Technology.* Elsevier Science B.V.

BASU, S., SHIVHARE, U. S. & MUJUMDAR, A. S. 2006. Models for Sorption Isotherms for Foods: A Review. *Drying Technology,* 24**,** 917-930.

BEN ABDELHAMID, M., MIHOUBI, D., SGHAIER, J. & BELLAGI, A. 2016. Water Sorption Isotherms and Thermodynamic Characteristics of Hardened Cement Paste and Mortar. *Transport in Porous Media,* 113**,** 283-301.

BEN MABROUK, K., KAUFFMANN, T. H., AROUI, H. & FONTANA, M. D. 2013. Raman study of cation effect on sulfate vibration modes in solid state and in aqueous solutions. *Journal of Raman Spectroscopy,* 44**,** 1603-1608.

BLAHOVEC, J. 2004. Sorption isotherms in materials of biological origin mathematical and physical approach. *Journal of Food Engineering,* 65**,** 489-495.

BOEREFIJN, R., DONTULA, P.-R. & KOHLUS, R. 2007a. Chapter 14 Detergent granulation. *Handbook of Powder Technology,* 11**,** 673-703.

BOEREFIJN, R., DONTULA, P.-R. & KOHLUS, R. 2007b. Chapter 14 Detergent granulation. *In:* A.D. SALMAN, M. J. H. & SEVILLE, J. P. K. (eds.) *Handbook of Powder Technology.* Elsevier Science B.V.

BOISSIÈRE, C., BRUBACH, J. B., MERMET, A., DE MARZI, G., BOURGAUX, C., PROUZET, E. & ROY, P. 2002. Water Confined in Lamellar Structures of AOT Surfactants: An Infrared Investigation. *The Journal of Physical Chemistry B,* 106**,** 1032-1035.

BOLZE, J., FUJISAWA, T., NAGAO, T., NORISADA, K., SAITÔ, H. & NAITO, A. 2000. Small angle X-ray scattering and 31P NMR studies on the phase behavior of phospholipid bilayered mixed micelles. *Chemical Physics Letters,* 329**,** 215-220.

BONCHEVA, M., DAMIEN, F. & NORMAND, V. 2008. Molecular organization of the lipid matrix in intact Stratum corneum using ATR-FTIR spectroscopy. *Biochimica et Biophysica Acta (BBA) - Biomembranes,* 1778**,** 1344-1355.

BONILLA, E., AZUARA, E., BERISTAIN, C. I. & VERNON-CARTER, E. J. 2010. Predicting suitable storage conditions for spray-dried microcapsules formed with different biopolymer matrices. *Food Hydrocolloids,* 24**,** 633-640.

BONNER, I. J. & KENNEY, K. L. 2013. Moisture sorption characteristics and modeling of energy sorghum (Sorghum bicolor (L.) Moench). *Journal of Stored Products Research,* 52**,** 128-136.

BÖSCHEL, D., JANICH, M. & ROGGENDORF, H. 2003. Size distribution of colloidal silica in sodium silicate solutions investigated by dynamic light scattering and viscosity measurements. *Journal of Colloid and Interface Science,* 267**,** 360-368.

BOTH, E. M., KARLINA, A. M., BOOM, R. M. & SCHUTYSER, M. A. I. 2018. Morphology development during sessile single droplet drying of mixed maltodextrin and whey protein solutions. *Food Hydrocolloids,* 75**,** 202-210.

BRUNAUER, S., DEMING, L. S., DEMING, W. E. & TELLER, E. 1940. On a Theory of the van der Waals Adsorption of Gases. *Journal of the American Chemical Society,* 62**,** 1723-1732.

BRYANT, G. & WOLFE, J. 1989. Can hydration forces induce lateral phase separations in lamellar phases? *European Biophysics Journal,* 16**,** 369-374.

CADDEN, A.-M. 1988. Moisture Sorption Characteristics of Several Food Fibers. *Journal of Food Science,* 53**,** 1150-1155.

CARMIGNATO, S., DEWULF, W. & LEACH, R. 2018. *Industrial X-ray computed tomography*, Springer.

CARTER, B. P. & SCHMIDT, S. J. 2012. Developments in glass transition determination in foods using moisture sorption isotherms. *Food Chemistry,* 132**,** 1693-1698.

CONBOY, J. C., MESSMER, M. C. & RICHMOND, G. L. 1997. Dependence of Alkyl Chain Conformation of Simple Ionic Surfactants on Head Group Functionality As Studied by Vibrational Sum-Frequency Spectroscopy. *The Journal of Physical Chemistry B,* 101**,** 6724-6733.

DISALVO, E. A., LAIRION, F., MARTINI, F., TYMCZYSZYN, E., FRÍAS, M., ALMALECK, H. & GORDILLO, G. J. 2008. Structural and functional properties of hydration and confined water in membrane interfaces. *Biochimica et Biophysica Acta (BBA) - Biomembranes,* 1778**,** 2655-2670.

DRASLER, B., DROBNE, D., SADEGHPOUR, A. & RAPPOLT, M. 2015. Fullerene up-take alters bilayer structure and elasticity: A small angle X-ray study. *Chemistry and Physics of Lipids,* 188**,** 46-53.

DURIE, R. A. & MILNE, J. W. 1978. Infrared spectra of anhydrous alkali metal sulphates. *Spectrochimica Acta Part A: Molecular Spectroscopy,* 34**,** 215-220.

EVANSON, K. W. & URBAN, M. W. 1991. Surface and interfacial FTIR spectroscopic studies of latexes. I. Surfactant–copolymer interactions. *Journal of Applied Polymer Science,* 42**,** 2287-2296.

FARBER, L., TARDOS, G. & MICHAELS, J. N. 2003. Use of X-ray tomography to study the porosity and morphology of granules. *Powder Technology,* 132**,** 57-63.

FITZPATRICK, J. 2013. 12 - Powder properties in food production systems. *Handbook of Food Powders.* Woodhead Publishing.

FITZPATRICK, J. J., BARRINGER, S. A. & IQBAL, T. 2004. Flow property measurement of food powders and sensitivity of Jenike's hopper design methodology to the measured values. *Journal of Food Engineering,* 61**,** 399-405.

FORNY, L., MARABI, A. & PALZER, S. 2011. Wetting, disintegration and dissolution of agglomerated water soluble powders. *Powder Technology,* 206**,** 72-78.

FRANCIA, V., MARTÍN, L., BAYLY, A. E. & SIMMONS, M. J. H. 2016a. Agglomeration in counter-current spray drying towers. Part A: Particle growth and the effect of nozzle height. *Powder Technology,* 301**,** 1330-1343.

FRANCIA, V., MARTÍN, L., BAYLY, A. E. & SIMMONS, M. J. H. 2016b. Agglomeration in counter-current spray drying towers. Part B: Interaction between multiple spraying levels. *Powder Technology,* 301**,** 1344-1358.

GAL, A., WEINER, S. & ADDADI, L. 2010. The Stabilizing Effect of Silicate on Biogenic and Synthetic Amorphous Calcium Carbonate. *Journal of the American Chemical Society,* 132**,** 13208-13211.

GALANTE, D. C. & DILLAN, K. W. 1981. Heavy-duty laundry detergents. *Journal of the American Oil Chemists Society,* 58**,** 356A-362A.

GAMBLE, J. F., TERADA, M., HOLZNER, C., LAVERY, L., NICHOLSON, S. J., TIMMINS, P. & TOBYN, M. 2016. Application of X-ray microtomography for the characterisation of hollow polymer-stabilised spray dried amorphous dispersion particles. *International Journal of Pharmaceutics,* 510**,** 1-8.

GARIDEL, P., KACONIS, Y., HEINBOCKEL, L., WULF, M., GERBER, S., MUNK, A., VILL, V. & BRANDENBURG, K. 2015. Self-Organisation, Thermotropic and Lyotropic Properties of Glycolipids Related to their Biological Implications. *The Open Biochemistry Journal,* 9**,** 49-72.

GOBERIS, S. & STONIS, R. 2004. Advantageous features of sodium silicate as the plasticizer for low-cement refractory castables. *Refractories and Industrial Ceramics,* 45**,** 446-449.

GOULA, A. M. & ADAMOPOULOS, K. G. 2008. Effect of Maltodextrin Addition during Spray Drying of Tomato Pulp in Dehumidified Air: II. Powder Properties. *Drying Technology,* 26**,** 726-737.

HAMILTON, A. & MENZIES, R. I. 2010. Raman spectra of mirabilite, Na2SO4·10H2O and the rediscovered metastable heptahydrate, Na2SO4·7H2O. *Journal of Raman Spectroscopy,* 41**,** 1014-1020.

HAYES, G. D. 1987. *Food engineering data handbook,* Harlow, Longman Scientific & Technical.

HERMAN DE GROOT, W., ADAMI, I. & MORETTI, G. F. 1995. *The manufacture of modern detergent powders,* Wassenaar, the Netherlands, Herman de Groot Academic Publisher.

HILL, C. A. S., NORTON, A. & NEWMAN, G. 2009. The water vapor sorption behavior of natural fibers. *Journal of Applied Polymer Science,* 112**,** 1524-1537.

HILL, C. A. S., NORTON, A. J. & NEWMAN, G. 2010. The water vapour sorption properties of Sitka spruce determined using a dynamic vapour sorption apparatus. *Wood Science and Technology,* 44**,** 497-514.

HINTZ, W., ANTONYUK, S., SCHUBERT, W., EBENAU, B., HAACK, A. & TOMAS, J. 2008. Determination of Physical Properties of Fine Particles, Nanoparticles and Particle Beds. *Modern Drying Technology.* Wiley-VCH Verlag GmbH & Co. KGaA.

HO, S. T. & HUTMACHER, D. W. 2006. A comparison of micro CT with other techniques used in the characterization of scaffolds. *Biomaterials,* 27**,** 1362-1376.

HUANG, T., TORAYA, H., BLANTON, T. & WU, Y. 1993. X‐ray powder diffraction analysis of silver behenate, a possible low‐angle diffraction standard. *Journal of applied crystallography,* 26**,** 180-184.

HUNTINGTON, D. H. 2004. The Influence of the Spray Drying Process on Product Properties. *Drying Technology,* 22**,** 1261-1287.

ISRAELACHVILI, J. N. 2011. *Intermolecular and surface forces: revised third edition*, Academic press.

JAKOBI, G. & LÖHR, A. 1987. *Detergents and textile washing: principles and practice*, VCH Publishers.

JAMESON, J. R. 2014. *Characterization of bone material properties and microstructure in osteogenesis Imperfecta/Brittle bone disease.* Marquette University.

JENIKE, A. W. 1967. Quantitative design of mass-flow bins. *Powder Technology,* 1**,** 237-244.

JENSEN, E. 2012. Types of Imaging, Part 1: Electron Microscopy. *The Anatomical Record,* 295**,** 716-721.

JERRAM, D. A. & HIGGINS, M. D. 2007. 3D analysis of rock textures: quantifying igneous microstructures. *Elements,* 3**,** 239-245.

JUPPO, A. M. & YLIRUUSI, J. 1994. Effect of amount of granulation liquid on total pore volume and pore size distribution of lactose, glucose and mannitol granules. *European journal of pharmaceutics and biopharmaceutics,* 40**,** 299-309.

KATSARAS, J. 1998. Adsorbed to a Rigid Substrate, Dimyristoylphosphatidylcholine Multibilayers Attain Full Hydration in All Mesophases. *Biophysical Journal,* 75**,** 2157-2162.

KAWAKITA, K. & LÜDDE, K.-H. 1971. Some considerations on powder compression equations. *Powder Technology,* 4**,** 61-68.

KAYMAK-ERTEKIN, F. & GEDIK, A. 2004. Sorption isotherms and isosteric heat of sorption for grapes, apricots, apples and potatoes. *LWT - Food Science and Technology,* 37**,** 429-438.

KEELEY, C. T. 1983. Sodium silicate: The key ingredient in detergent agglomeration. *Journal of the American Oil Chemists' Society,* 60**,** 1370-1372.

KELKAR, S., BOUSHEY, C. J. & OKOS, M. 2015. A method to determine the density of foods using X-ray imaging. *Journal of Food Engineering,* 159**,** 36-41.

KELLERMEIER, M., GLAAB, F., KLEIN, R., MELERO-GARCIA, E., KUNZ, W. & GARCIA-RUIZ, J. M. 2013. The effect of silica on polymorphic precipitation of calcium carbonate: an on-line energy-dispersive X-ray diffraction (EDXRD) study. *Nanoscale,* 5**,** 7054-7065.

KELLY, G. M., O'MAHONY, J. A., KELLY, A. L. & O'CALLAGHAN, D. J. 2016. Water sorption and diffusion properties of spray-dried dairy powders containing intact and hydrolysed whey protein. *LWT - Food Science and Technology,* 68**,** 119-126.

KHOMANE, K. S., MORE, P. K., RAGHAVENDRA, G. & BANSAL, A. K. 2013. Molecular Understanding of the Compaction Behavior of Indomethacin Polymorphs. *Molecular Pharmaceutics,* 10**,** 631-639.

KRANENBURG, M., VLAAR, M. & SMIT, B. 2004. Simulating Induced Interdigitation in Membranes. *Biophysical Journal,* 87**,** 1596-1605.

KUDELSKI, A. 2008. Analytical applications of Raman spectroscopy. *Talanta,* 76**,** 1-8.

KULKARNI, C. V., WACHTER, W., IGLESIAS-SALTO, G., ENGELSKIRCHEN, S. & AHUALLI, S. 2011. Monoolein: a magic lipid? *Physical Chemistry Chemical Physics,* 13**,** 3004-3021.

LABUZA, T. P. & ALTUNAKAR, B. 2007. Water activity prediction and moisture sorption isotherms. *Water activity in foods: fundamentals and applications,* 109**,** 154.

LEE, C. W. B., DAS GUPTA, S. K., MATTAI, J., SHIPLEY, G. G., ABDEL-MAGEED, O. H., MAKRIYANNIS, A. & GRIFFIN, R. G. 1989. Characterization of the L.lambda. phase in trehalose-stabilized dry membranes by solid-state NMR and x-ray diffraction. *Biochemistry,* 28**,** 5000-5009.

LEROCH, S. & WENDLAND, M. 2012. Simulation of Forces between Humid Amorphous Silica Surfaces: A Comparison of Empirical Atomistic Force Fields. *The Journal of Physical Chemistry C,* 116**,** 26247-26261.

LEWICKI, P. P. 2009. Data and models of water activity. II: Solid foods. *Food properties handbook***,** 68-143.

LEWIS, R. N. & MCELHANEY, R. N. 1993. Studies of mixed-chain diacyl phosphatidylcholines with highly asymmetric acyl chains: a Fourier transform infrared spectroscopic study of interfacial hydration and hydrocarbon chain packing in the mixed interdigitated gel phase. *Biophysical Journal,* 65**,** 1866-1877.

LEWIS, R. N. A. H. & MCELHANEY, R. N. 2007. Fourier Transform Infrared Spectroscopy in the Study of Lipid Phase Transitions in Model and

Biological Membranes. *In:* DOPICO, A. M. (ed.) *Methods in Membrane Lipids.* Totowa, NJ: Humana Press.

LEWIS, R. N. A. H. & MCELHANEY, R. N. 2013. Membrane lipid phase transitions and phase organization studied by Fourier transform infrared spectroscopy. *Biochimica et Biophysica Acta (BBA) - Biomembranes,* 1828**,** 2347-2358.

LEWIS, R. N. A. H., WINTER, I., KRIECHBAUM, M., LOHNER, K. & MCELHANEY, R. N. 2001. Studies of the Structure and Organization of Cationic Lipid Bilayer Membranes: Calorimetric, Spectroscopic, and X-Ray Diffraction Studies of Linear Saturated P-O-Ethyl Phosphatidylcholines. *Biophysical Journal,* 80**,** 1329-1342.

LI, L., MIZUHATA, M. & DEKI, S. 2005. Preparation and characterization of alkyl sulfate and alkylbenzene sulfonate surfactants/TiO2 hybrid thin films by the liquid phase deposition (LPD) method. *Applied Surface Science,* 239**,** 292-301.

LI, Q., RUDOLPH, V., WEIGL, B. & EARL, A. 2004a. Interparticle van der Waals force in powder flowability and compactibility. *International Journal of Pharmaceutics,* 280**,** 77-93.

LI, Q., RUDOLPH, V., WEIGL, B. & EARL, A. 2004b. Interparticle van der Waals force in powder flowability and compactibility. *International Journal of Pharmaceutics,* 280**,** 77-93.

LI, R. F., PENCHEV, R., RAMACHANDRAN, V., ROBERTS, K. J., WANG, X. Z., TWEEDIE, R. J., PRIOR, A., GERRITSEN, J. W. & HUGEN, F. M. 2008. Particle Shape Characterisation via Image Analysis: from Laboratory Studies to In-process Measurements Using an in Situ Particle Viewer System. *Organic Process Research & Development,* 12**,** 837-849.

LIAW, M. S., MACKLEY, M. R., BRIDGWATER, J., MOGGRIDGE, G. D. & BAYLY, A. E. 2003. Multilamellar vesicles in a commercial surfactant system. *AIChE Journal,* 49**,** 2966-2973.

LINNOW, K., ZEUNERT, A. & STEIGER, M. 2006. Investigation of Sodium Sulfate Phase Transitions in a Porous Material Using Humidity- and Temperature-Controlled X-ray Diffraction. *Analytical Chemistry,* 78**,** 4683-4689.

LIU, L. X., MARZIANO, I., BENTHAM, A. C., LITSTER, J. D., E.T.WHITE & HOWES, T. 2008a. Effect of particle properties on the flowability of ibuprofen powders. *International Journal of Pharmaceutics,* 362**,** 109-117.

LIU, L. X., MARZIANO, I., BENTHAM, A. C., LITSTER, J. D., E.T.WHITE & HOWES, T. 2008b. Effect of particle properties on the flowability of ibuprofen powders. *International Journal of Pharmaceutics,* 362**,** 109-117.

MA, J.-G., BOYD, B. J. & DRUMMOND, C. J. 2006. Positional Isomers of Linear Sodium Dodecyl Benzene Sulfonate: Solubility, Self-Assembly, and Air/Water Interfacial Activity. *Langmuir,* 22**,** 8646-8654.

MA, Y., GHOSH, S. K., BERA, S., JIANG, Z., TRISTRAM-NAGLE, S., LURIO, L. B. & SINHA, S. K. 2015. Accurate calibration and control of relative humidity close to 100% by X-raying a DOPC multilayer. *Physical Chemistry Chemical Physics,* 17**,** 3570-3576.

MACALUSO, R. T., WELLS, B., WANGELINE, C., COCHRAN, K. & GREVE, B. K. 2016. Powder X-ray diffraction and electron microscopy studies of polycrystalline Au2PrIn. *Polyhedron,* 114**,** 313-316.

MAHER, P. G., ROOS, Y. H. & FENELON, M. A. 2014. Physicochemical properties of spray dried nanoemulsions with varying final water and sugar contents. *Journal of Food Engineering,* 126**,** 113-119.

MARSHALL, C. P. & OLCOTT MARSHALL, A. 2013. Raman hyperspectral imaging of microfossils: potential pitfalls. *Astrobiology,* 13**,** 920-931.

MEHROTRA, B. N. 1981. The crystal structure of Na_2SO_4 III. *Zeitschrift für Kristallographie - Crystalline Materials,* 155**,** 159-163.

MORAGA, G., MARTíNEZ-NAVARRETE, N. & CHIRALT, A. 2004. Water sorption isotherms and glass transition in strawberries: influence of pretreatment. *Journal of Food Engineering,* 62**,** 315-321.

MUIR, D. D. 2007. Encapsulated and Powdered Foods. *International Journal of Dairy Technology,* 60**,** 61-61.

NAGLE, J. F. & TRISTRAM-NAGLE, S. 2000. Structure of lipid bilayers. *Biochimica et Biophysica Acta (BBA) - Reviews on Biomembranes,* 1469**,** 159-195.

NORDSTRÖM, J. & ALDERBORN, G. 2011. Degree of compression as a potential process control tool of tablet tensile strength. *Pharmaceutical Development and Technology,* 16**,** 599-608.

NORDSTRÖM, J., KLEVAN, I. & ALDERBORN, G. 2009. A particle rearrangement index based on the Kawakita powder compression equation. *Journal of Pharmaceutical Sciences,* 98**,** 1053-1063.

OCKELFORD, J., TIMIMI, B. A., NARAYAN, K. S. & TIDDY, G. J. T. 1993. An upper critical point in a lamellar liquid crystalline phase. *The Journal of Physical Chemistry,* 97**,** 6767-6769.

OHNO, K., FUKUDA, M., YOSHIDA, H., TAMAOKI, H. & MATSUURA, H. 2000. Vibrational spectroscopic and theoretical calculation studies on conformational behavior of simple sodium 1-alkanesulfonates. *Journal of Molecular Structure,* 553**,** 49-59.

OKORAFOR, O. C. 1999. Solubility and Density Isotherms for the Sodium Sulfate−Water−Methanol System. *Journal of Chemical & Engineering Data,* 44**,** 488-490.

ONIDA, B., CAMAROTA, B., UGLIENGO, P., GOTO, Y., INAGAKI, S. & GARRONE, E. 2005. Mesoporous Benzene−Silica Hybrid Materials with a Different Degree of Order in the Wall Structure: An IR Comparative Study. *The Journal of Physical Chemistry B,* 109**,** 21732-21736.

OPALIŃSKI, I., CHUTKOWSKI, M. & STASIAK, M. 2012. Characterizing moist food-powder flowability using a Jenike shear-tester. *Journal of Food Engineering,* 108**,** 51-58.

OUYANG, J., WANG, J., WANG, Y., YIN, Q. & HAO, H. 2015. Thermodynamic study on dynamic water and organic vapor sorption on amorphous valnemulin hydrochloride. *Frontiers of Chemical Science and Engineering,* 9**,** 94-104.

PABST, G., HODZIC, A., ŠTRANCAR, J., DANNER, S., RAPPOLT, M. & LAGGNER, P. 2007. Rigidification of Neutral Lipid Bilayers in the Presence of Salts. *Biophysical Journal,* 93**,** 2688-2696.

PALZER, S. 2005. The effect of glass transition on the desired and undesired agglomeration of amorphous food powders. *Chemical Engineering Science,* 60**,** 3959-3968.

PARIKH, A. N., GILLMOR, S. D., BEERS, J. D., BEARDMORE, K. M., CUTTS, R. W. & SWANSON, B. I. 1999. Characterization of Chain Molecular Assemblies in Long-Chain, Layered Silver Thiolates: A Joint Infrared Spectroscopy and X-ray Diffraction Study. *The Journal of Physical Chemistry B,* 103**,** 2850-2861.

PARIKH, D. M. 2009. *Handbook of pharmaceutical granulation technology*, CRC Press.

PAUCHARD, L. & ALLAIN, C. 2003. Buckling instability induced by polymer solution drying. *EPL (Europhysics Letters),* 62**,** 897.

PELEG, M. 1977. FLOWABILITY OF FOOD POWDERS AND METHODS FOR ITS EVALUATION — A REVIEW. *Journal of Food Process Engineering,* 1**,** 303-328.

PENG, G., CHEN, X., WU, W. & JIANG, X. 2007. Modeling of water sorption isotherm for corn starch. *Journal of Food Engineering,* 80**,** 562-567.

PÉREZ-ALONSO, C., BERISTAIN, C. I., LOBATO-CALLEROS, C., RODRÍGUEZ-HUEZO, M. E. & VERNON-CARTER, E. J. 2006. Thermodynamic analysis of the sorption isotherms of pure and blended carbohydrate polymers. *Journal of Food Engineering,* 77**,** 753-760.

PETRACHE, H. I., TRISTRAM-NAGLE, S., HARRIES, D., KUČERKA, N., NAGLE, J. F. & PARSEGIAN, V. A. 2006. Swelling of phospholipids by monovalent salt. *Journal of lipid research,* 47**,** 302-309.

PODGORNIK, R. & PARSEGIAN, V. A. 1992. Thermal-mechanical fluctuations of fluid membranes in confined geometries: the case of soft confinement. *Langmuir,* 8**,** 557-562.

POSZYTEK, K. 2005. *Wheat flour flowability as affected by water activity, storage time and consolidation*, Institute of Agrophysics.

POULOS, A. S., NANIA, M., LAPHAM, P., MILLER, R. M., SMITH, A. J., TANTAWY, H., CARAGAY, J., GUMMEL, J., CES, O., ROBLES, E. S. J. & CABRAL, J. T. 2016. Microfluidic SAXS Study of Lamellar and Multilamellar Vesicle Phases of Linear Sodium Alkylbenzenesulfonate Surfactant with Intrinsic Isomeric Distribution. *Langmuir,* 32**,** 5852-5861.

QUIRIJNS, E. J., VAN BOXTEL, A. J. B., VAN LOON, W. K. P. & VAN STRATEN, G. 2005. Sorption isotherms, GAB parameters and isosteric heat of sorption. *Journal of the Science of Food and Agriculture,* 85**,** 1805-1814.

RASMUSSEN, S. E., JORGENSEN, J.-E. & LUNDTOFT, B. 1996. Structures and Phase Transitions of Na2SO4. *Journal of Applied Crystallography,* 29**,** 42-47.

RICHARDS, C., MOHAMMADI, M. S. & TIDDY, G. J. T. 2009. Formulating liquid detergents with naturally derived surfactants—Phase behaviour, crystallisation and rheo-stability of primary alkyl sulphates based on coconut oil. *Colloids and Surfaces A: Physicochemical and Engineering Aspects,* 338**,** 119-128.

RICHARDS, C., TIDDY, G. J. T. & CASEY, S. 2007. Lateral Phase Separation Gives Multiple Lamellar Phases in a “Binary” Surfactant/Water System: The Phase Behavior of Sodium Alkyl Benzene Sulfonate/Water Mixtures. *Langmuir,* 23**,** 467-474.

RODRIGUEZ-NAVARRO, C., DOEHNE, E. & SEBASTIAN, E. 2000. How does sodium sulfate crystallize? Implications for the decay and testing of building materials. *Cement and Concrete Research,* 30**,** 1527-1534.

ROGGENDORF, H., BÖSCHEL, D. & TREMPLER, J. 2001. Structural evolution of sodium silicate solutions dried to amorphous solids. *Journal of Non-Crystalline Solids,* 293-295**,** 752-757.

ROGGENDORF, H., FISCHER, M., ROTH, R. & GODEHARDT, R. 2015. Influence of Temperature and Water Vapour Pressure on Drying Kinetics and Colloidal Microstructure of Dried Sodium Water Glass. *Advances in Chemical Engineering and Science,* Vol.05No.01**,** 11.

ROUQUEROL, F., ROUQUEROL, J. & SING, K. 1999. CHAPTER 1 - Introduction. *Adsorption by Powders and Porous Solids.* London: Academic Press.

ROY, A., DUTTA, R., KUNDU, N., BANIK, D. & SARKAR, N. 2016. A Comparative Study of the Influence of Sugars Sucrose, Trehalose, and Maltose on the Hydration and Diffusion of DMPC Lipid Bilayer at Complete Hydration: Investigation of Structural and Spectroscopic Aspect of Lipid–Sugar Interaction. *Langmuir,* 32**,** 5124-5134.

RUIZ-AGUDO, E., RODRIGUEZ-NAVARRO, C. & SEBASTIÁN-PARDO, E. 2006. Sodium Sulfate Crystallization in the Presence of Phosphonates: Implications in Ornamental Stone Conservation. *Crystal Growth & Design,* 6**,** 1575-1583.

SADEK, C., TABUTEAU, H., SCHUCK, P., FALLOURD, Y., PRADEAU, N., LE FLOCH-FOUÉRÉ, C. & JEANTET, R. 2013. Shape, Shell, and Vacuole Formation during the Drying of a Single Concentrated Whey Protein Droplet. *Langmuir,* 29**,** 15606-15613.

SAMIMI, A., HASSANPOUR, A. & GHADIRI, M. 2005. Single and bulk compressions of soft granules: Experimental study and DEM evaluation. *Chemical Engineering Science,* 60**,** 3993-4004.

SATO, K. 2018. *Crystallization of Lipids: Fundamentals and Applications in Food, Cosmetics and Pharmaceuticals*, John Wiley & Sons.

SCHIFFTER, H. & LEE, G. 2007. Single-droplet evaporation kinetics and particle formation in an acoustic levitator. Part 2: Drying kinetics and particle formation from microdroplets of aqueous mannitol, trehalose, or catalase. *Journal of Pharmaceutical Sciences,* 96**,** 2284-2295.

SCHUBERT, H. 1987. Food particle technology. Part I: Properties of particles and particulate food systems. *Journal of Food Engineering,* 6**,** 1-32.

SCHULZE, D. 2007. *Powders and bulk solids: behavior, characterization, storage and flow*, Springer Science & Business Media.

SCOUTARIS, N., VITHANI, K., SLIPPER, I., CHOWDHRY, B. & DOUROUMIS, D. 2014. SEM/EDX and confocal Raman microscopy as complementary tools for the characterization of pharmaceutical tablets. *International Journal of Pharmaceutics,* 470**,** 88-98.

SEARS, W. M. 2001. Isosteric Heat of Adsorption of Water Vapor on Bismuth Iron Molybdate Measured by the Method of Constant Surface Conductance. *Langmuir,* 17**,** 5237-5244.

SHIMIZU, S. & MATUBAYASI, N. 2014. Gelation: The Role of Sugars and Polyols on Gelatin and Agarose. *The Journal of Physical Chemistry B,* 118**,** 13210-13216.

SHRESTHA, A. K., HOWES, T., ADHIKARI, B. P. & BHANDARI, B. R. 2007. Water sorption and glass transition properties of spray dried lactose hydrolysed skim milk powder. *LWT - Food Science and Technology,* 40**,** 1593-1600.

SMITH, S. E. 1947. The Sorption of Water Vapor by High Polymers. *Journal of the American Chemical Society,* 69**,** 646-651.

SMULDERS, E. & RÄHSE, W. 2000. Laundry Detergents, 3. Production, Testing and Economic Aspects. *Ullmann's Encyclopedia of Industrial Chemistry.* Wiley-VCH Verlag GmbH & Co. KGaA.

SORNETTE, D. & OSTROWSKY, N. 1984. Repulsive steric interaction between membranes of finite size. *J. Phys. France,* 45**,** 265-271.

STEWART, J. A., SAIANI, A., BAYLY, A. & TIDDY, G. J. T. 2009. The phase behaviour of lyotropic liquid crystals in linear alkylbenzene sulphonate (LAS) systems. *Colloids and Surfaces A: Physicochemical and Engineering Aspects,* 338**,** 155-161.

STEWART, J. A., SAIANI, A., BAYLY, A. & TIDDY, G. J. T. 2011. Phase Behavior of Lyotropic Liquid Crystals in Linear Alkylbenzene Sulphonate (LAS) Systems in the Presence of Dilute and Concentrated Electrolyte. *Journal of Dispersion Science and Technology,* 32**,** 1700-1710.

THAKUR, S. C., AHMADIAN, H., SUN, J. & OOI, J. Y. 2014. An experimental and numerical study of packing, compression, and caking behaviour of detergent powders. *Particuology,* 12**,** 2-12.

TIMMERMANN, E. O., CHIRIFE, J. & IGLESIAS, H. A. 2001. Water sorption isotherms of foods and foodstuffs: BET or GAB parameters? *Journal of Food Engineering,* 48**,** 19-31.

TOGNONVI, M. T., MASSIOT, D., LECOMTE, A., ROSSIGNOL, S. & BONNET, J.-P. 2010. Identification of solvated species present in concentrated and dilute sodium silicate solutions by combined 29Si NMR and SAXS studies. *Journal of Colloid and Interface Science,* 352**,** 309-315.

TOMAS, J. 2004a. Fundamentals of cohesive powder consolidation and flow. *Granular Matter,* 6**,** 75-86.

TOMAS, J. 2004b. Product Design of Cohesive Powders – Mechanical Properties, Compression and Flow Behavior. *Chemical Engineering & Technology,* 27**,** 605-618.

TSOTSAS, E. & MUJUMDAR, A. S. 2011. *Modern drying technology: Volume 3, Product quality and formulation,* Weinheim; Chichester, Wiley-VCH.

UCHINO, T., SAKKA, T. & IWASAKI, M. 1991. Interpretation of Hydrated States of Sodium Silicate Glasses by Infrared and Raman Analysis. *Journal of the American Ceramic Society,* 74**,** 306-313.

ULUSOY, U. & KURSUN, I. 2011. Comparison of different 2D image analysis measurement techniques for the shape of talc particles produced by different media milling. *Minerals Engineering,* 24**,** 91-97.

VAN DALEN, G., NOOTENBOOM, P. & HEUSSEN, P. C. M. 2011. Correlative microscopy of detergent granules. *Journal of Microscopy,* 241**,** 273-281.

VEGA-GÁLVEZ, A., PALACIOS, M., LEMUS-MONDACA, R. & PASSARO, C. 2008. Moisture sorption isotherms and isosteric heat determination in Chilean papaya (Vasconcellea pubescens). *Química Nova,* 31**,** 1417-1421.

VENKATARAMAN, N. V. & VASUDEVAN, S. 2001. Interdigitation of an Intercalated Surfactant Bilayer. *The Journal of Physical Chemistry B,* 105**,** 7639-7650.

VENUGOPAL, E., BHAT, S. K., VALLOORAN, J. J. & MEZZENGA, R. 2011. Phase Behavior of Lipid–Based Lyotropic Liquid Crystals in Presence of Colloidal Nanoparticles. *Langmuir,* 27**,** 9792-9800.

VICENTE, J., PINTO, J., MENEZES, J. & GASPAR, F. 2013. Fundamental analysis of particle formation in spray drying. *Powder Technology,* 247**,** 1-7.

VIDYA, Y. S. & LAKSHMINARASAPPA, B. N. 2013. Preparation, Characterization, and Luminescence Properties of Orthorhombic Sodium Sulphate. *Physics Research International,* 2013**,** 7.

VISSER, J. 1989. Van der Waals and other cohesive forces affecting powder fluidization. *Powder Technology,* 58**,** 1-10.

WALTON, D. E. 2000. THE MORPHOLOGY OF SPRAY-DRIED PARTICLES A QUALITATIVE VIEW. *Drying Technology,* 18**,** 1943-1986.

WALTON, D. E. 2002. Spray-Dried Particle Morphologies. *Developments in Chemical Engineering and Mineral Processing,* 10**,** 323-348.

WANG, B., ZHANG, H., EVANS, D. G. & DUAN, X. 2005. Surface modification of layered double hydroxides and incorporation of hydrophobic organic compounds. *Materials Chemistry and Physics,* 92**,** 190-196.

WANG, D.-Y., DAS, A., LEUTERITZ, A., MAHALING, R. N., JEHNICHEN, D., WAGENKNECHT, U. & HEINRICH, G. 2012. Structural characteristics and flammability of fire retarding EPDM/layered double hydroxide (LDH) nanocomposites. *RSC Advances,* 2**,** 3927-3933.

WANG, Q., ZHU, Y. & LI, H. 2015. Imaging model for the scintillator and its application to digital radiography image enhancement. *Optics Express,* 23**,** 33753-33776.

WARRING, S. L., BEATTIE, D. A. & MCQUILLAN, A. J. 2016. Surficial Siloxane-to-Silanol Interconversion during Room-Temperature Hydration/Dehydration of Amorphous Silica Films Observed by ATR-IR and TIR-Raman Spectroscopy. *Langmuir,* 32**,** 1568-1576.

WATRY, M. R. & RICHMOND, G. L. 2000. Comparison of the Adsorption of Linear Alkanesulfonate and Linear Alkylbenzenesulfonate Surfactants at Liquid Interfaces. *Journal of the American Chemical Society,* 122**,** 875-883.

WESTH, P. 2008. Glucose, sucrose and trehalose are partially excluded from the interface of hydrated DMPC bilayers. *Physical Chemistry Chemical Physics,* 10**,** 4110-4112.

XU, Z. P. & BRATERMAN, P. S. 2003. High affinity of dodecylbenzene sulfonate for layered double hydroxide and resulting morphological changes. *Journal of Materials Chemistry,* 13**,** 268-273.

YANG, X., ROONASI, P. & HOLMGREN, A. 2008a. A study of sodium silicate in aqueous solution and sorbed by synthetic magnetite using in situ ATR-FTIR spectroscopy. *Journal of Colloid and Interface Science,* 328**,** 41-47.

YANG, X., ZHU, W. & YANG, Q. 2008b. The Viscosity Properties of Sodium Silicate Solutions. *Journal of Solution Chemistry,* 37**,** 73-83.

ZAFAR, U., VIVACQUA, V., CALVERT, G., GHADIRI, M. & CLEAVER, J. A. S. 2017. A review of bulk powder caking. *Powder Technology,* 313**,** 389-401.

ZETTLEMOYER, A. C. 1968. Hydrophobic surfaces. *Journal of Colloid and Interface Science,* 28**,** 343-369.

ZHAO, H. & DARWIN, D. 1990. Quantitative Backscattered Electron Analysis Techniques for Cement-Based Materials. University of Kansas Center for Research, Inc.

ZHOU, D. & QIU, Y. 2010. Understanding material properties in pharmaceutical product development and manufacturing: Powder flow and mechanical properties. *Journal of Validation Technology,* 16**,** 65.

ZOLLER, U. 2004. *Handbook of detergents, Part B: Environmental impact*, CRC Press.

ZOLLER, U. & SOSIS, P. 2008. *Handbook of detergents, part F: Production*, CRC Press.